1971

Slab behavior of a prestressed concrete i-beam bridge -- bartonsville bridge, May 1971

Anton W. Wegmuller

David A. VanHorn

OFFICE
OF
RESEARCH

LEHIGH UNIVERSITY

Prestressed Concrete I-Beam Bridges

Progress Report No. 3

SLAB BEHAVIOR OF A PRESTRESSED CONCRETE I-BEAM BRIDGE

BARTONSVILLE BRIDGE

by
Anton W. Wegmuller
David A. VanHorn

Fritz Engineering Laboratory Report No. 349.3

COMMONWEALTH OF PENNSYLVANIA

Department of Transportation

Bureau of Materials, Testing and Research

Leo D. Sandvig - Director
Wade L. Gramling - Research Engineer
Kenneth L. Heilman - Research Coordinator

Project 67-12: Lateral Distribution of Load for Bridges constructed with Prestressed Concrete I-Beams

SLAB BEHAVIOR

of a

PRESTRESSED CONCRETE I-BEAM BRIDGE

BARTONSVILLE BRIDGE

by

Anton W. Wegmuller
David A. VanHorn

This work was sponsored by the Pennsylvania Department of Transportation; U. S. Department of Transportation, Federal Highway Administration; and the Reinforced Concrete Research Council. The opinions, findings, and conclusions expressed in this publication are those of the authors, and not necessarily those of the sponsors.

LEHIGH UNIVERSITY

Office of Research

Bethlehem, Pennsylvania

May, 1971

Fritz Engineering Laboratory Report No. 349.3

TABLE OF CONTENTS

ABSTRACT

This report describes the field testing of the slab of a beam-slab highway bridge subjected to loading with a test vehicle approximating AASHO HS 20 truck loading. The test structure, located near Bartonsville, Pennsylvania, was a multi-span, simply supported bridge consisting of a cast-in-place concrete slab supported by five precast prestressed concrete I-beams laterally spaced at 8 feet. The test span was 68 feet 6 inches in length. The testing program consisted of the continuous recording of surface strains at various locations on the slab, as the test vehicle was driven over the span at various speeds.

The principal objective was to develop information on the magnitude of slab strains produced by live loads simulated by the test vehicle. The measured strains were used to compute stresses and moments in the slab. It was found that the slab moments derived from the field measurements were substantially smaller than those used in the design of the slab, and that the stresses produced were considerably less than those anticipated in the design.

1. INTRODUCTION

1.1 Background

The proportioning of the slab of a prestressed concrete highway bridge is an important phase of the design of the superstructure. For most highway bridges, the floor system is comprised of a reinforced concrete slab supported by longitudinal prestressed concrete or steel beams. The transmission of loads between beams is accomplished by the slab cast to act compositely with the beams. The interaction of beam and slab presents a challenging problem for the analyst, and as a result, the problem of load distribution has been treated analytically by several authors. However, the most current methods of analysis can still not account for the many variables involved in the structural behavior of the beam-slab assemblage and none is thoroughly verified by test results. Most bridges designed in this country use the design standards of the American Association of State Highway Officials[1]. However, these specifications and design procedures developed for bridge superstructures provide only an approximate prediction of the behavior of bridge slabs under the application of live loads.

In 1967, the need for experimental verification of lateral load distribution formed the basis for the initiation of a research project at Lehigh University, for the purpose of evaluating the structural response of prestressed concrete I-beam

bridges. The primary purpose of this project is to experimentally determine the actual lateral distribution of vehicular live loads for this type of bridge. The secondary purpose of the project is to investigate the behavior of the slab of the same bridge type.

Initial slab tests[17] were conducted on an existing highway bridge supported by prestressed concrete box-beams, near Hazleton, Pennsylvania. These tests served as pilot tests for following slab investigations, and provided valuable insight into the lateral distribution of load and the behavior of the bridge. A vehicle, closely simulating the AASHO HS 20 loading, was driven across the test span at different speeds. Instrumentation was arranged to measure slab strains at different locations on the surface of the slab, and at uncovered slab reinforcing bars. These tests revealed that: (1) all measured strains and computed stresses were small in magnitude, and the applied live load never caused cracking in the slab, (2) the effects of multiple vehicle loads could be evaluated by superimposing single vehicle effects, and (3) large strains and stresses were produced due to local effects caused by concentrated wheel loads.

Similar tests were then planned and executed on the slab of another existing highway bridge, supported by prestressed concrete I-beams, near Bartonsville, Pennsylvania. A detailed description of these tests as well as a presentation and interpretation of the experimental results are given in this report.

1.2 Object and Scope

Under the action of wheel loads, the slab deflects in a shell-like manner, with bending produced both in the transverse and longitudinal directions. Due to interaction with girders, continuity of the slab over supporting beams, and different slab thickness at different points, the analysis of a slab panel for concentrated loads is a difficult problem. Hence, the basic purpose of this investigation was to measure the magnitude and distribution of strains and stresses at different locations of the slab surface, and to determine the local effect caused by concentrated wheel loads.

In the phase of the investigation reported herein, strains produced by live load at different locations in the slab of a prestressed concrete I-beam highway bridge were measured. The strain data allowed the computation of stresses and bending moments at different locations in the slab. These stresses and moments, based on experimental strain data and occurring under actual conditions, could then be compared with design moments using AASHO Standard Specification for Highway Bridges, or available methods of slab analysis. It is the purpose of this report to present and interpret the experimental data.

Field testing was conducted with the U.S. Bureau of Public Roads (now, the Federal Highway Administration) field test unit, consisting of a loading truck and monitoring trailer. Test runs across the bridge were made by directing a truck along

one of several lanes, approximately equally spaced across the width of the bridge deck. The center-line of each of these lanes corresponded either to the center-line of a beam or to a line midway between adjacent beams. Data was obtained from gages located at two slab panels instrumented at the quarter-span section of the bridge.

1.3 Previous Research

A recent literature search and review of existing methods of slab analysis and design of highway girder bridges is given in Ref. 3. Many publications dealing with the analysis of the slab are compiled in this survey as well as in Ref. 16. The present AASHO (1969) Specifications for Highway Bridges are primarily based on theoretical work done by Westergaard[4] and Newmark[5]. These specifications allow a rapid design of the slab, but fail to allow for many important variables associated with the behavior of slabs, such as torsional stiffness of the beams, thickness of the slab, and restraint between beams and slab.

To date, only a few experimental investigations on full scale structures have been made to study the behavior of bridge slabs. Early experimental investigations to determine the effective width of slabs were made by Kelley[6]. The information resulting from these tests served as a basis for one of the earliest methods of slab design. The purpose of later tests made by Richart[7] was to collect information for a more effective

design of bridge slabs. The tests by both Kelley and Richart were made without the aid of advanced experimental equipment in use today. Further tests by Newmark[8] provided a considerable insight into the behavior of slabs of highway bridges and served to verify the AASHO Specifications for Highway Bridges. The subject of a following study by Richart was a theoretical and experimental investigation of the effect of concentrated loads on bridge slabs, and the report[9] provides a state of the art of bridge design up to the year 1948. In the following twenty years, a number of investigations have been made to find the response of slabs under wheel loads, mostly in connection with the problem of lateral distribution of load to the stringers.

In summary the previously conducted tests revealed that: (1) the test strains are in poor agreement with the strains predicted by elastic theory, and test results indicate smaller strains both in the reinforcement and on the slab surface, (2) bending moments in the slab are difficult to determine if the slab is cracked, (3) moments in the slab under concentrated wheel loads are less than predicted by elastic theory, possibly because of redistribution of stresses due to local inelastic behavior, and (4) the controlling moment in the slab is the transverse moment occurring at the center of the slab panel. Despite all of the cited investigations and findings, the specifications have changed but little in the last twenty years.

At Lehigh University, the problem of load distribution

in spread box-beam bridges has been under investigation since 1964. The investigation was initiated by a pilot field study of the Drehersville Bridge[10,11], and continued with field studies of the Berwick[12], Brookville[13], White Haven[14], and Philadelphia[15] Bridges. In 1967, a similar project on lateral distribution of load for bridges constructed with prestressed concrete I-beams was initiated. Two bridges were included in the study, the Bartonsville Bridge (reported herein) and the Lehighton Bridge.

2. TESTING

2.1 Test Bridge

The test bridge, the details of which are shown in Figs. 1 through 5, carries Legislative Route 1002 over the Pocono Creek and L.R. 45033, and is located near Bartonsville, Pennsylvania. The sixth span of the ten-span bridge, as illustrated in Fig. 1, was chosen as the test span. This span is simply supported, and has a length of 68 feet 6 inches, center to center of bearings. The cross-section of the bridge is shown in Fig. 3. Five identical longitudinal AASHO type III I-beams equally spaced at 8 feet, together with a cast-in-place reinforced concrete slab, are the main elements in cross-section of the bridge superstructure. The reinforced concrete slab provides a roadway width of 32 feet, and has a specified minimum thickness of 7-1/2 inches between beams (see Fig. 3). Measurements however, as indicated in Fig. 4, showed that the actual slab thickness of the test section Q ranges from 5.7 to 7.7 inches. The girders and the slab were designed to carry the AASHO HS 20 truck loading.

2.2 Gage Sections and Locations

Two bridge cross-sections, Section M and Section Q, as shown in Fig. 2, were selected for strain gage application. To gather information on the lateral distribution of load to the girders, beams were gaged both at Section M and Q. A detailed

description of the instrumentation for the investigation on lateral distribution of load to the girders is given in Fritz Engineering Laboratory Report No. 349.2[18]. For the slab investigation, summarized in this report, only Section Q was gaged. At this cross-section, as shown in Fig. 5, two slab panels were instrumented. This figure shows the location and designation of all strain gages. As shown in Fig. 5, the response of the slab in the transverse direction was measured by six pairs of single gages mounted on top and bottom surfaces of the slab. Additional transverse gages were placed at the top of beam B and at midspan of the two adjacent slab panels. Gage 44 was the only gage mounted directly on a reinforcing steel bar in the slab.

2.3 Instrumentation

All strain gages used in testing were of the SR-4 electrical resistance type, manufactured by the Baldwin-Lima-Hamilton Corporation. Each gage location was ground and sanded smooth, followed by thorough cleaning with acetone. After mounting, the gage was sealed with SR-4 cement. The gages on the top surface of the slab were waterproofed and covered with tape, for protection against weather and traffic. Each gage was wired into a conventional Wheatstone bridge circuit with three inactive gages placed nearby, such that all gages were at ambient temperature.

Strain data was recorded using a mobile instrument unit

owned by the Federal Highway Administration. The equipment was housed in a trailer; and consisted mainly of an oscillator, 48 gage circuit amplification channels, and three variable speed recording oscillographs. The oscillator transmitted a reference signal to the bank of amplifiers, where each amplifier was connected into a gage circuit as described above. During a test run, the transmitted signal was altered by gage activity, magnified by the amplifier, and transmitted to an oscillograph galvanometer, where the galvanometer movement was permanently recorded on photographic paper.

2.4 Test Vehicle

The vehicle used for testing was a diesel-powered tractor and semi-trailer unit, owned by the Federal Highway Administration. The dimensions of the vehicle closely conform to the AASHO HS 20 design loading[1], measuring 13.0 feet from the front axle to the drive axle, and 20.4 feet from the drive axle to the trailer axle. The trailer, as shown in Fig. 6, was loaded with gravel, distributed to produce axle loads quite close to those of the design vehicle.

2.5 Loading Lanes

The loading lanes, shown in Fig. 7, were laid out on the roadway such that the center-line of the truck was laterally positioned either over the center-line of a girder or over a line midway between girder center-lines. On the Bartonsville Bridge, this scheme led to seven loading lanes, spaced uniformly at

approximately 48 inches. When the vehicle was run in the outside lanes, numbered 1 and 7, the center-line of the outside wheel was 17.5 inches from the curb face.

2.6 Test Runs

A total of 136 runs of the load vehicle were conducted in the field testing of the Bartonsville Bridge. The 35 runs studied in the preparation of this report were of a static nature, with the vehicle moving across the span at a crawl speed of two to three miles per hour. Hand signals were used to guide the vehicle in the desired lateral position during all runs. The remaining 101 runs, consisting of speed runs with speeds varying from 5 mph to 60 mph, and impact runs with a nominal speed of 10 mph, were mainly designed to study the lateral distribution of load to the girders. For impact runs, two wooden ramps were positioned 18 inches from Section Q such that the wheels of the truck had a 2-inch drop and hit the bridge floor at the specified section. Before and after several test runs, the gages were calibrated for zero live load to relate the relationship of the oscillograph traces to the base values. Generally, the time interval between consequent calibrations was not longer than two hours.

2.7 Longitudinal Position and Timing

The position of the load vehicle was indicated on oscillograph records through the use of air hoses placed transversely

across the roadway in the path of the vehicle. These air hoses were placed at Section M, 40 feet east of Section M, and 40 feet west of Section M, respectively. As each axle crossed an air hose, a pressure switch was actuated, causing a sharp offset in a reference trace on the oscillograph records. These offsets were used to correlate the truck position with strain values recorded on the oscillograph. Two additional hoses on each side of Section M were used to determine vehicle speed during speed runs. These hoses served to actuate a digital timing device, which allowed easy computation of average vehicle speed across the span.

3. DATA REDUCTION AND EVALUATION

3.1 Oscillograph Trace Reading

Data reduction began with the identification of the traces for each test run. This identification required the correlation of trace numbers, each of which represented a particular strain gage, with the traces on the test record. The correlation was facilitated by the existence of trace breaks, corresponding to sixteen slab gage traces and two inactive reference traces on each oscillograph record. Following the editing, calibration records were evaluated. Calibration of the galvanometers was required periodically during the testing to ensure accuracy of results. A detailed description of the calibration procedure is given in the investigation on lateral distribution of load for the same bridge[18].

With the completion of editing and the determination of calibration values, the records of test runs could be processed. The vertical excursion of each oscillogram trace from its original position at the start of the run was a measure of the strain produced by the applied live load. By measuring this trace amplitude for a given loading condition, the surface strain at the location of the gage could be computed. In most cases, the maximum amplitude could be located by eye. Typical traces for a crawl and a speed run are shown in Fig. 8. The trace is smooth and without oscillations for all crawl runs, whereas speed run

traces slightly oscillate for most of the runs.

3.2 Evaluation of Oscillograph Data

3.2.1 Calculation of Transverse Strains

Due to the presence of local effects, two characteristic vertical excursions could be taken from the trace representing a particular run; namely vertical excursions V(1) and V(2), together with the corresponding calibration offset. V(1) represents the hypothetical excursion if there were no local effects present caused by concentrated wheel loads, whereas V(2) represents the actual measured overall excursion including these local effects. These two excursions were observed only if a wheel passed directly over the gage or near the gage under consideration.

After the trace amplitudes were measured and tabulated, they were entered as input in a first computer program, written in FORTRAN IV, which instructed the computer to calculate from the two vertical excursions V(1) and V(2) strains $\epsilon_x(1)$ and $\epsilon_x(2)$ occurring in the slab of the test structure. This conversion of vertical excursions (oscillograph trace amplitudes) to strain values, involved multiplication of the measured load trace amplitude by one variable and several constant quantities which were dependent on the electrical circuit for a particular gage. Hence, gage constants (consisting of gage resistance, gage factor, cable length, operation attenuation, and calibration attenuation),

calibration values, and vertical excursions served as program input data.

The program output, consisting of data input and computed strains $\epsilon_x(1)$ and $\epsilon_x(2)$, as well as ratio and difference of the two strain values, was listed separately for each gage and run. In addition, run number, lane number, and speed in mph were printed out on the same record. The computer was then instructed to punch run information and computed strains on data cards for convenient use as input for the subsequent stress computation described in Section 3.2.3.

3.2.2 Calculation of Longitudinal Strains

In the investigation of lateral distribution of load for the same bridge, a computer program was developed to calculate the location of the neutral axis at each girder face, using measured beam strains. A detailed description of this program and the applied statistical approach for the rejection of erroneous strain values is given in Fritz Engineering Laboratory Report No. 349.2[18]. This program could conveniently be used to extrapolate longitudinal strains occurring in the slab from corresponding beam strains. This operation was based on a linear distribution of beam strains extending into the slab. It is believed that the longitudinal strains occurring at the locations of the transverse slab gages near the junctures of beams and slab, could be determined quite accurately, using this procedure.

No longitudinal strains were measured at midspan of the slab panels and therefore a slightly different approach had to be taken. As an approximation, these longitudinal strains were found by linear interpolation of corresponding computed longitudinal slab strains near junctures of beam and slab. The computed longitudinal strains were punched on corresponding data cards mentioned above and completed the data input for the computation of stresses outlined in the next section.

3.2.3 Slab Bending Stresses

A second computer program, written in FORTRAN IV, was developed to calculate transverse and longitudinal stresses in the slab at the location of the transverse slab gages shown in Fig. 5. With transverse strain (ε_x) and longitudinal strain (ε_y) known at a given point, the transverse stress (σ_x) and longitudinal stress (σ_y) could be computed. For a two-dimensional state of stress, theory of elasticity[19] yields:

$$\sigma_x = \frac{E}{1-\nu^2}\left[\varepsilon_x + \nu\,\varepsilon_y\right] = 1.033\ E\left[\varepsilon_x + \nu\,\varepsilon_y\right]$$

$$\sigma_y = \frac{E}{1-\nu^2}\left[\varepsilon_y + \nu\,\varepsilon_x\right] = 1.033\ E\left[\varepsilon_y + \nu\,\varepsilon_x\right]$$

where: ν = Poisson's Ratio (taken as 0.18)

ε_x = Measured strain in transverse direction

ε_y = Measured Strain in longitudinal direction

E = Modulus of elasticity of slab concrete

An assumed average value of E = 5000 ksi was used to compute the stresses. The above mentioned probram instructed the machine to compute transverse stresses $\sigma_x(1)$ based on first trace amplitude, and stresses $\sigma_x(2)$ based on second excursion, as well as the longitudinal stress $\sigma_y(1)$ based on first excursion, and the ratio of transverse stresses. The punched data deck described above, consisting of computed transverse and longitudinal strains served as input. The program output, consisting of data input and computed stresses as well as the run information, was again listed separately for each gage and run. However, principal stresses could not be computed since strains in only two directions had been measured.

3.2.4 Slab Bending Moments

Whenever transverse slab gages were mounted on top and bottom fibers of the slab, at Section Q, bending moments (M_x) producing stresses in the transverse direction, could be computed based on a linear distribution of strain across the slab thickness. The expression for the bending moment due to stresses in the transverse direction is derived in Ref. 19 for a homogenous, elastic material:

$$M_x = -D \frac{\partial^2 w}{\partial x^2} + \nu \frac{\partial^2 w}{\partial y^2} = -\frac{Eh^3}{12(1-\nu^2)} [\Phi_x + \nu \Phi_y]$$

Where: M_x = Transverse bending moment in (ft lb/ft)

D = Plate stiffness (as defined in Ref. 19)

h = Actual thickness of the slab

E = Modulus of elasticity of the slab concrete

ν = Poisson's ratio (taken as 0.18)

Φ_x = Curvature of the slab in transverse direction

Φ_y = Curvature of the slab in longitudinal direction

To apply the above expression, the slab was assumed to be a homogenous, elastic material, and the deck slab reinforcement was neglected. The second term in the expression was neglected since the curvature of the slab in the longitudinal direction is small, and in addition, is multiplied by Poisson's Ratio, making the second term much smaller than the first. After evaluating the transverse strain at the top and bottom fibers of the slab cross-section, the curvature Φ_x could be computed by simply summing these strains and dividing the sum by the actual measured slab thickness, shown in Fig. 4.

An additional subroutine was developed to compute the transverse moments, based on both first and second trace amplitude of transverse strain. In order to calculate these moments directly from strains, an average value of E = 5000 ksi was assumed for the modulus of elasticity of the slab concrete. This assumption was necessary, since there is no definite way of determining the effective value of E from empirical relationships

related to f'_c or from stress-strain information resulting from cylinder tests. The same input data deck was used as in the computation of stresses described above. The program output, consisting of data input and computed transverse moments, as well as the run information, was again listed separately for each pair of gages. The computed transverse bending moments were then compared with design values.

4. PRESENTATION OF TEST RESULTS

4.1 Measured Maximum Slab Strains

Maximum measured transverse compressive and tensile strains (μ in/in) occurring at each gage location are compiled in Table I. These maximum values are given separately for crawl runs and for speed runs, and for strains based on first and second trace amplitudes. Table I shows that for both crawl and speed runs, the measured maximum tensile strain was always below 70 μ in/in, when neglecting local effects, indicating that the slab section was never cracked. Including local effects due to concentrated wheel loads, maximum tensile strains up to 150 μ in/in were recorded, indicating again that the slab section probably was never cracked. The assumption of a homogenous and elastic behavior in computing stresses and bending moments is therefore justified. Maximum measured compressive concrete strains for crawl and speed runs were below 140 μ in/in when neglecting local effects, and below 150 μ in/in considering local effects. All computed longitudinal strains were compressive and the maximum value found was 45 μ in/in, as given in Table I.

In general, the maximum strain values for a particular gage were small and, with a few exceptions, slightly greater for speed runs than for crawl runs. In all tables and figures, a positive sign indicates compression and a negative sign tension at a particular location.

4.2 Computed Maximum Slab Stresses

A summary of maximum computed transverse compressive and tensile stresses occurring at each gage location is given in Table II. Again, all runs were considered and the maximum values are given separately for both crawl and speed runs, and for stresses based on first and second trace amplitude. These maximum stress values were again small and, with a few exceptions, slightly greater for speed runs than for crawl runs. Table II shows that for both crawl and for speed runs, the computed maximum transverse tensile stress was below 170 psi, when local effects are neglected. Considering local effects, transverse tensile stresses up to 400 psi were computed.

Maximum computed compressive concrete stresses for crawl and speed runs were below 230 psi, when neglecting local effects, and below 750 psi considering local effects due to concentrated wheel loads. Computed longitudinal stresses were always of compressive nature and a maximum value of 225 psi was found.

4.3 Influence Lines for Transverse Strains

In Figs. 9 - 24, influence lines for measured transverse strains occurring at different gage locations are presented in graphical form, to show the variation of strain for different load positions. Strains $\epsilon_x(1)$, neglecting local effects and $\epsilon_x(2)$, considering local effects, are plotted in these figures

for a truck centered at each loading lane indicated by numbers at the bottom of the figures. These graphs contain the information gathered from all crawl runs, and are based on average values computed from five crawl runs for each particular loading lane and gage. An examination of the plotted strain information $\epsilon_x(1)$, which excludes local effects, reveals a similarity in shape with corresponding influence lines for a continuous beam. The influence lines for $\epsilon_x(2)$ are similar in shape, with the exception of the region affected by local strains produced by concentrated wheel loads. In this region, a considerable deviation can be recognized, indicating the strong influence of local strains. For the purpose of comparison, the ratio of transverse strains is also shown, giving an indication of the order of magnification of strains produced by the local effects.

Figures 25 - 30 show influence lines for transverse strains, neglecting local effects, for each pair of top and corresponding bottom gages. The purpose of these diagrams is to show the variation of transverse strains across the thickness of the slab, assuming a linear distribution of strain. A variation in the location of the neutral axis for different truck positions can be recognized as well as the occurrence of in-plane strains. Similarly, Figs. 31 - 36 show influence lines for transverse strains $\epsilon_x(2)$ considering local effects.

4.4 Influence Lines For Transverse Stresses

To illustrate the variation of transverse stresses for

different load positions, Figs. 37 - 50 are presented to show combined transverse strains. These strains will be referred to as "reduced transverse stresses". Since the actual value of the modulus of elasticity of the slab is not known, combined strains, rather than actual stresses, are shown. In order to arrive at actual stresses, each given combined strain value must be multiplied by $E/1-\nu^2$. The choice of E and ν is left to the reader. Again, all figures are based on information gathered from crawl runs, and average values computed from five crawl runs are shown for each gage and loading lane. These figures show reduced stresses neglecting local effects as well as reduced stresses considering the local effects due to concentrated wheel loads. The plotted reduced stresses, neglecting local effects, reveal a similarity in shape with the influence lines for transverse strain. The influence lines for reduced stresses, considering local effects, are similar in shape, with the exception of the region affected by local effects. For the purpose of comparison, the ratio of reduced transverse stresses is also shown. Although this ratio is of limited value, it gives an indication of the order of magnitude of local stresses produced in a slab section, Figs. 51 - 56 show influence lines for reduced transverse stresses, neglecting local effects, for each pair of top and bottom gages mounted on the slab. These diagrams show the variation of transverse stresses across the thickness of the slab, assuming a linear distribution of stress. Similarly, Figs. 57 - 62 show

influence lines for reduced transverse stresses considering local effects.

4.5 Influence Lines for Longitudinal Strains

A graphic presentation of measured longitudinal strains, again in the form of influence lines, is given in Figs. 63 - 68. For each pair of top and bottom gages, these figures show the variation of longitudinal strain for different load positions. As outlined in Section 3.2.2, all longitudinal strains occurring in the slab were extrapolated from beam gage data, thus leaving no means of detecting the magnification of longitudinal strains caused by concentrated wheel loads. Therefore, only strains neglecting local effects $\epsilon_y(1)$ are shown in these figures, for a truck centered in each loading lane. Average values based on five crawl runs are shown for each gage and loading lane. These influence lines are relatively smooth and reveal that the slab is always stressed longitudinally in compression. Assuming a linear distribution, the variation of strain across the slab thickness is shown, enabling the visualization of the distribution of in-plane strains for different truck positions.

4.6 Influence Lines for Longitudinal Stresses

Figs. 69 - 74 show, for each pair of top and bottom gages, the variation of reduced longitudinal stresses for different truck positions. In order to arrive at actual stresses, each given combined strain value must again be multiplied by the

factor $E/1-\nu^2$. The figures are based on information gathered from all crawl runs and average values computed from five crawl runs are shown for each gage and loading. The evaluation of strains, as outlined above, permitted only the determination of longitudinal stresses, neglecting local effects. The influence lines show that the slab was in compression for all positions of the truck, and that the top gage locations were stressed slightly higher than the bottom gage locations.

4.7 Influence Lines for Transverse Slab Moments

The following Figs. 75 - 80 show the variation of transverse slab bending moments (in ft lb/ft) occurring in the slab for different truck positions. For this presentation, the modulus of elasticity of the slab concrete was taken as E = 5000 ksi, and a Poisson's ratio of $\nu = 0.18$ was assumed. All influence lines are based on information collected from five crawl runs, and average values are shown for six cross-sections in the slab. The first influence line in a figure shows moments M(1) based on stresses neglecting local effects, whereas the second influence line shows moments M(2) including local effects. All moment computations are based on a linear distribution of strain across the thickness of the slab. The implementation of this assumption will be discussed in Section 5.5. The influence lines for moments considering local effects are again similar in shape to those neglecting local effects except for a region affected by these local effects.

4.8 Effect of Speed

As pointed out in the introduction, it was not possible to study the effect of speed on slab strains, stresses, and moments because only one run per speed for each loading lane was conducted, leaving no means for finding reliable average values. As in a previous slab investigation[17], it was found that the position of the wheel with respect to a gage was of significant influence on the magnitude of strains produced at the location of the gage. Since the driver of the truck had adequate control over the path of the truck for crawl runs only, and since only one run per speed was performed, no reliable average values could be determined. To illustrate this problem the variation of strains $\epsilon_x(1)$ versus speed of the truck at gage 24 is shown in Fig. 81 for three different loading lanes. A study of similar diagrams did not reveal a definite dependency of strain on speed, and based on the present information, no final conclusions can be drawn.

4.9 Effect of Impact

For the impact runs, two wooden ramps were positioned 18 inches from Section Q such that the wheels of the truck had a 2-inch drop, and hit the bridge floor at a specified cross-section. Average values computed from two impact runs are shown as dashed lines in Figs. 25 - 30, and can be compared with average values for strains $\epsilon_x(1)$ computed from five crawl runs, as shown

by solid lines. It can be seen from these figures that the strains produced by impact runs are not significantly greater than the strains produced during the crawl runs. Again, as for speed runs, the position of the wheel with respect to the gage is of great influence on the magnitude of strain produced at the location of the gage. Not too much weight should be given to the computed average values however, since only two impact runs were conducted for each of the lanes 1 through 4. Again, to find reliable average values, additional runs per lane would be necessary.

5. DISCUSSION OF TEST RESULTS

5.1 Maximum Strains and Stresses in the Slab

The summary of maximum measured strains and computed stresses in Table I reveals that recorded strains and stresses were small, and as a result, the slab was probably never cracked due to the applied live load. As will be shown under Section 5.5, the design value used for the transverse moment in the slab was 3400 ft lb/ft. Thus, based on an elastic, homogenous behavior of the slab, fiber stresses of 365 psi would result for a slab of a nominal thickness of 7.5 inches. Considering local effects, maximum measured transverse tensile stresses up to 400 psi were recorded, whereas when neglecting local effects, transverse tensile stresses were below 170 psi. Using a stress analysis based on a cracked section, the design moment of 3400 ft lb/ft (excluding impact) yielded a compressive stress of approximately 700 psi in the concrete, and a maximum tensile stress of approximately 12,000 psi in the reinforcing steel.

5.2 Vehicle Position for Maximum Response

In general, the test structure responded predictably to lateral variation in load vehicle position. Influence lines for transverse strains, stresses, and moments clearly indicate the probable location of the truck for maximum positive and negative response of the slab. At this point, it should be noted that the

influence lines are based on positions of the load vehicle with the center of the truck either directly over one of the beams or at the midpoint of one of the slab spans. Conceivably, maximum effects may have occurred at other locations. However, other positions were not included because of time limitations dictated by the availability of the field test equipment.

In all cases, the largest transverse bending moment in any gaged section occurred when the load vehicle passed the loading lane closest to this section, and the moment decreased as the vehicle was run in lanes at greater lateral distances from the section under consideration. This is also true for longitudinal and transverse strains and stresses.

5.3 Discussion of Local Effects

The problem of evaluating stress distribution in a slab subjected to the action of a concentrated wheel load is of great practical interest, since the stresses produced directly govern the design of a slab. Near the point of application of a concentrated force, a serious local perturbation will occur. Although recognized in earlier studies, the phenomenon of local stresses caused by concentrated wheel loads is still not well understood, and has not been adequately investigated experimentally. One of the objectives of this investigation is to shed some light on this problem, and to actually measure and compute the magnification of stress and strain due to concentrated wheel loads.

From the literature reviewed it appears that no analytical solution for this complex three-dimensional problem exists, considering the actual boundary conditions of the plate. A solution was found by Seewald[19] for the two-dimensional case of a beam loaded by a single concentrated load. This study and other theoretical investigations, show that the local stresses produced by a concentrated wheel load diminish rapidly across the thickness of the slab with increasing distance from the point of application of load. It can be seen from the plotted data shown in this report that the strains produced are mostly greater for the gages located on the top side of the slab than for those on the bottom side. This decrease is also clearly recognizable by comparing the influence lines for strain of gages 43 and 44. As indicated by the plots showing ratios of strain and stress, these ratios are usually between 2 and 6, but can be as high as 11, and are usually smaller for transverse strain than for transverse stress. When judging these results, it must be remembered that these additional local stresses occur only over very small areas at the point of application of load, and therefore are of a purely local nature.

Based on this limited experimental investigation, it is not possible to generalize on the behavior of deck slabs under concentrated wheel loads. However, it would be appropriate to state that the additional stresses produced in the slab in the vicinity of the passing wheel may be redistributed due to possible local inelastic behavior of the slab concrete. Since these

stresses are compressive in nature, it is also possible that no damage will occur due to their occurrence. More theoretical and experimental work, concentrating on establishing possible detrimental effects of such local stresses, should be conducted in order to enable consideration in future slab design procedures.

5.4 Effect of Modulus of Elasticity

As explained in Section 3.2.4, it was necessary to assign a value for the modulus of elasticity of the slab concrete, since there is no definite way of determing the effective value of E from empirical relationships related to f'_c, or from stress-strain information resulting from cylinder tests. There is also no way of determining the effective value of E for the slab concrete from the modulus of elasticity of the beam concrete found in the investigation on lateral distribution of load to the girders of the same bridge.

The ACI Code[2] presents a method for the calculation of the modulus of elasticity based on the formula:

$$E_c = 33\, w^{1.5}\, \sqrt{f'_c} \qquad \text{(psi)}$$

If w, the unit weight of concrete, is taken as 150 lb/ft^3 and f'_c for slab concrete is estimated to be 6000 psi, a value of $E_c = 4750$ ksi is obtained for the modulus of elasticity of the slab concrete. Hence, a value of $E_c = 5000$ ksi was used for all stress and moment computations. As shown previously, all influence

lines for stresses are given in a reduced form, and to arrive at actual stresses, the given reduced values must be multiplied by the factor $E/1-\nu^2$. To convert moment values presented in this report to corresponding values based on a different modulus of elasticity of slab concrete, simple proportion can be applied. However, the assumed value of E in this investigation is in line with the findings reported in connection with the test of a composite beam (steel) and slab (concrete) bridge in California[20]. In this report, values of E were computed from strain distributions in the slab at both midspan and quarter-span locations. Average values of the modulus of elasticity of slab concrete were found to be 5980 ksi and 6670 ksi, respectively.

5.5 Comparison of Design and Experimental Slab Moments

According to the AASHO Standard Specifications for Highway Bridges (1969) the transverse bending moment produced by live load in a bridge slab panel should be calculated using the formula:

$$M = \frac{(S + 2)}{32} P_{20} \qquad [\text{ft lb/ft}]$$

Where: M = Transverse bending moment in slab panel.

S = Effective span length of slab panel in feet.
(S = clear span for slabs cast monolitically with beams)

P_{20} = 16 Kips = Half of the drive or rear axle load of the truck approximating HS 20 AASHO Standard Truck.

With a clear slab span of 6.5 feet, the bending moment for HS 20 loading (excluding impact), is found to be 4250 ft lb per foot of slab width. This value for the slab moment must be multiplied by a factor of 0.8 for a slab continuous over three or more supports, yielding a value of 3400 ft lb/ft. According to the code, this moment value applies to both positive midspan panel moment and negative moment at the supports. The slab is then designed as a rectangular beam of unit width using ordinary reinforced concrete design procedures.

As can be seen from Figs. 75 - 80, representing influence lines for transverse moments for different truck locations, the slab moments M(1) based on stresses neglecting local effects are always below a value of 900 ft lb/ft. The second influence lines, showing moments M(2) including local effects, nowhere indicate a moment value greater than 1900 ft lb/ft. Assuming homogenous behavior, if two trucks are superimposed, a maximum value of 1250 ft lb/ft is obtained when neglecting local effects, and a value of 2500 ft lb/ft when considering local effects. As explained in Section 4.7, all moment computations were based on a linear variation of strain across the slab thickness. This assumption might be perfectly valid for moment computations neglecting local effects, and will thus yield accurate moment values for this case. However, if local effects are to be included, this assumption will provide but a rough approximation for the true moments occurring in the slab, since due to a three-dimensional state of stress

caused by a concentrated wheel load, the strain distribution across the thickness of the slab is no longer linear.

The present investigation shows, as was already experienced in the previous testing of the slab of a box-beam bridge[17], that the experimentally found transverse bending moments are far smaller than the design value based on AASHO Standard Specifications for Highway Bridges (1969). The specifications do not allow for many important variables associated with the behavior of bridge slabs, such as torsional stiffness of the supporting beams, different slab thickness at different points, and the connection between slab and beams. Hence, the present specifications may not lead to the most realistic design of a bridge slab. Although the reported slab tests are not conclusive, the above statement is supported by the test results.

5.6 Effect of Speed and Impact

As mentioned in the introduction, a thorough investigation to study the effect of speed on slab strains was not within the scope of this field test. Since the relative position of the wheel with respect to the recording gage is highly significant, many runs conducted at the same speed would be needed to find and report reliable average values for strains. A study of the effect of speed on the magnitude of strains should be made in a further investigation.

6. SUMMARY AND CONCLUSIONS

6.1 Summary

The main objectives in this report are: (1) the evaluation and presentation of data collected in the field testing of the slab of a prestressed concrete I-beam bridge located near Bartonsville, Pennsylvania, (2) the study of local effects produced in the slab due to concentrated wheel loads, and (3) the comparison of stresses and moments with values predicted by the AASHO Standard Specifications for Highway Bridges (1969). The bridge tested was a beam-slab type structure utilizing five precast, pre-tensioned girders of I-shaped cross-section, topped by a composite reinforced concrete slab.

This investigation was conducted simultaneously with the main investigation on lateral distribution of load to the girders of the same bridge. The instrumentation for the field testing of the slab was devoted to the measurement of fiber strains at two slab panels located at quarter span of the bridge. Six gage positions were located on each panel to evaluate internal transverse strains, stresses, and bending moments produced by the test vehicle. Additional instrumentation placed on the girders allowed an extrapolation of longitudinal strains produced in the slab.

The tests were conducted using a load vehicle closely conforming to AASHO HS 20 truck loading, along with a mobile

instrumentation unit owned by the Federal Highway Administration. Test runs were conducted with the load vehicle moving at crawl speed, and at speeds up to 60 mph, in seven loading lanes established for testing purposes.

Data reduction was done with the aid of a computer, as described in detail in this report. Experimentally found transverse and longitudinal strains occurring in the slab due to the applied live load are presented graphically in the form of influence lines. Similarly, reduced stresses in transverse and longitudinal directions are presented in the form of influence lines.

A comparison of the internal bending moments produced in the slab with those predicted by the AASHO Standard Specifications for Highway Bridges (1969) is presented, as well as a discussion of the local effects caused by concentrated wheel loads. By comparing transverse slab moments to those predicted by the Specifications, it was found that experimental values were far below the Specification-based values. This reduction of moments is partly due to a slightly oversized slab at midspan of the slab, and partly due to the influence of parameters which are not taken into account by the Specifications, but which are important in the behavior of a bridge slab.

6.2 Conclusions

From the testing of the slab of the Bartonsville Bridge, the following conclusions can be drawn:

1. Experimentally found transverse and longitudinal strains and stresses measured at different positions of the slab panel were small, indicating that the slab was not cracked due to the applied live loads.

2. The present investigation shows, as was already verified in a previous test of the slab of a box-beam bridge[17], that experimentally found transverse bending moments are far smaller than the design values based on AASHO Standard Specifications for Highway Bridges (1969).

3. Near the points of application of wheel loads, additional stresses are produced in the slab, resulting in a local perturbation of the present state of stress. Since these stresses often were found to be significantly greater than the stresses computed from unaffected trace amplitudes, it is possible that there may be some inelastic redistribution of stress. The possible detrimental effects of such local stress redistribution should be theoretically and experimentally studied in future investigations in order to enable their consideration in future slab design procedures.

4. In general, the test structure responded predictably to lateral variation in load vehicle position. The location of the truck to produce maximum slab stresses and moments can be determined by making use of influence

lines presented in this report.

5. As long as the slab is not cracked, the superimposing of the results of single truck runs to determine the effects of two truck loading is a valid procedure.

6. Gages applied on the beams allowed an accurate extrapolation of longitudinal strains in the slab at the juncture of beams and slab, but not at midspan of the slab panel. Therefore, in order to find the moments producing longitudinal stresses, longitudinal gages should be placed at these midspan locations in future investigations.

7. The findings from this investigation of slab behavior are the second series reported in the current overall research investigation of beam-slab type bridge behavior conducted at Lehigh University. Therefore, at this time, the results will serve as a representation of the slab behavior at two different transverse slab spans in a typical prestressed concrete I-beam superstructure. Similar results from another I-beam bridge (Lehighton) and a spread box-beam bridge (Hazleton) will form a basis for comparison of field test results, and will provide a useful data base for the future analytical work required to develop possible revisions in specifications and procedures for deck slab design.

7. ACKNOWLEDGMENTS

This study was conducted in the Department of Civil Engineering and Fritz Engineering Laboratory, under the auspices of the Lehigh University Office of Research, as a part of a research investigation sponsored by the Pennsylvania Department of Transportation; the U. S. Department of Transportation, Federal Highway Administration; and the Reinforced Concrete Research Council.

The field test equipment was made available through Mr. C. F. Scheffey, now Director, Office of Research, Federal Highway Administration. The instrumentation of the test structure, and operation of the test equipment, were supervised by Messrs. R. F. Varney and H. Laatz, both from the Federal Highway Administration.

The basic research planning and administrative coordination in this investigation were in cooperation with the following individuals representing the Pennsylvania Department of Transportation: Mr. B. F. Kotalik, Bridge Engineer; Mr. H. P. Koretzky, and Mr. Hans L. Streibel, all from the Bridge Engineering Division; and Messrs. Leo D. Sandvig, Director; Wade L. Gramling, Research Engineer; and Foster C. Sankey and Kenneth L. Heilman, Research Coordinators, all from the Bureau of Materials, Testing and Research.

The following members of the faculty and staff at

Lehigh University made major contributions in the conduct of the field tests and in the reduction and processing of the test data: Dr. C. N. Kostem, Prof. J. O. Liebig, Jr., Felix Barda, Cheng-Shung Lin, Yan-Liang Chen, Chiou-Horng Chen, Daryoush Motarjemi, and Donald Frederickson. The manuscript was typed by Mrs. Ruth Grimes, and the figures were prepared by John M. Gera and Mrs. Sharon Balogh.

8. TABLES

TABLE I: MEASURED MAXIMUM STRAINS

Gage No.	a. Crawl Runs					b. Speed Runs				
	Tens. Strain $\epsilon_x(1)$	Tens. Strain $\epsilon_x(2)$	Compr. Strain $\epsilon_x(1)$	Compr. Strain $\epsilon_x(2)$	Compr. Strain ϵ_y	Tens. Strain $\epsilon_x(1)$	Tens. Strain $\epsilon_x(2)$	Compr. Strain $\epsilon_x(1)$	Compr. Strain $\epsilon_x(2)$	Compr. Strain ϵ_y
34	-15.9	-31.9	9.3	12.4	41.9	-21.5	-42.9	8.0	8.0	42.6
33	-15.8	-29.9	12.7	16.9	30.2	-14.1	-37.8	14.1	28.3	29.8
35	-8.9	-8.9	12.3	40.0	32.1	-9.3	-10.3	9.3	83.1	34.1
37	-22.0	-48.9	5.7	5.7	21.4	-23.6	-72.1	8.7	8.7	21.4
36	-15.9	-27.1	17.6	36.4	22.8	-17.0	-81.8	18.9	27.9	32.8
38	-26.1	-36.5	5.2	8.6	12.7	-31.5	-35.2	11.3	18.4	17.0
43	-18.7	-61.4	13.3	----	27.8	-10.7	-72.5	12.9	19.5	34.0
44	-16.5	-43.6	17.2	6.6	23.8	-22.4	-54.0	15.1	7.5	29.2
26	-15.8	-34.9	17.3	28.2	35.7	-14.3	-35.1	24.9	19.4	40.5
23	-27.7	-50.1	7.6	19.3	25.5	-35.0	-35.0	26.3	39.4	26.8
27	-10.6	-26.5	41.2	65.4	28.3	-28.2	-42.3	45.2	147.8	36.1
24	-17.5	-42.8	4.4	4.4	19.0	-23.0	-61.2	9.2	9.2	22.3
28	-13.2	-41.3	22.0	----	23.5	-16.9	-44.9	19.5	33.4	38.8
25	-25.1	-45.4	16.5	19.6	14.3	-19.9	-25.5	12.0	23.9	21.0
45	-59.4	-148.6	140.7	140.7	----	-66.3	-138.2	28.4	47.4	----
48	-22.3	-44.3	9.1	9.1	----	-33.5	-108.7	10.0	10.0	----

(Units are μ in/in)

TABLE II: MEASURED MAXIMUM STRESSES

Gage No.	a. Crawl Runs					b. Speed Runs				
	Tens. Stress $\sigma_x(1)$	Tens. Stress $\sigma_x(2)$	Compr. Stress $\sigma_x(1)$	Compr. Stress $\sigma_x(2)$	Compr. Stress σ_y	Tens. Stress $\sigma_x(1)$	Tens. Stress $\sigma_x(2)$	Compr. Stress $\sigma_x(1)$	Compr. Stress $\sigma_x(2)$	Compr. Stress σ_y
34	-64	-139	87	130	225	-25	-223	67	67	213
33	-48	-128	89	103	144	-61	-181	79	115	155
35	-34	-34	94	230	177	-36	-44	74	456	181
37	-84	-230	37	37	96	-107	-326	53	53	93
36	-68	-120	111	209	133	-64	-398	117	122	180
38	-125	-151	34	51	13	-152	-166	74	102	17
43	-78	-291	93	6	28	-47	-353	120	132	21
44	-77	-208	107	38	24	-102	-265	93	43	39
26	-69	-158	116	176	36	-66	-168	154	138	41
23	-126	-239	47	119	26	-171	-171	143	211	27
27	-44	-125	231	356	28	-124	-200	252	753	36
24	-74	-208	30	30	20	-106	-308	53	53	22
28	-58	-198	135	13	24	-62	-213	122	202	29
25	-120	-221	95	111	14	-91	-197	72	140	34

(Units are psi)

9. FIGURES

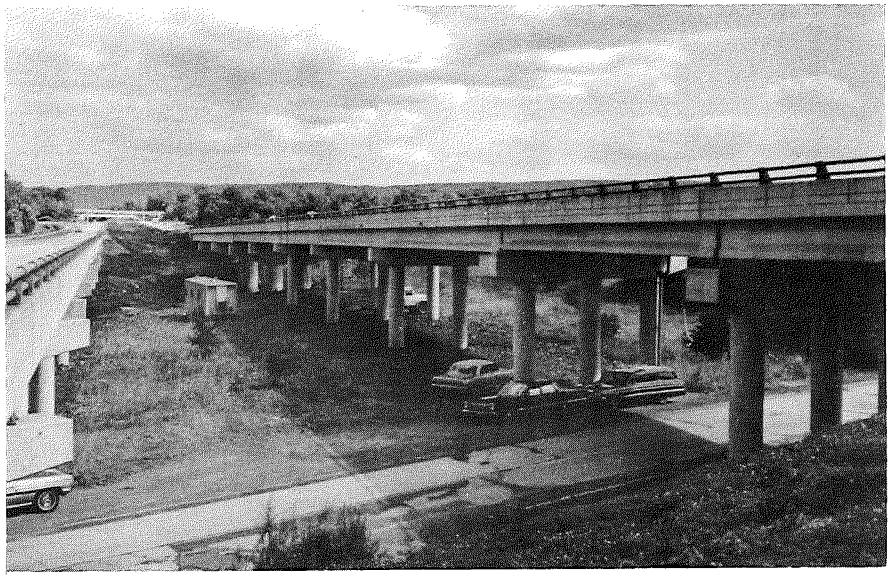

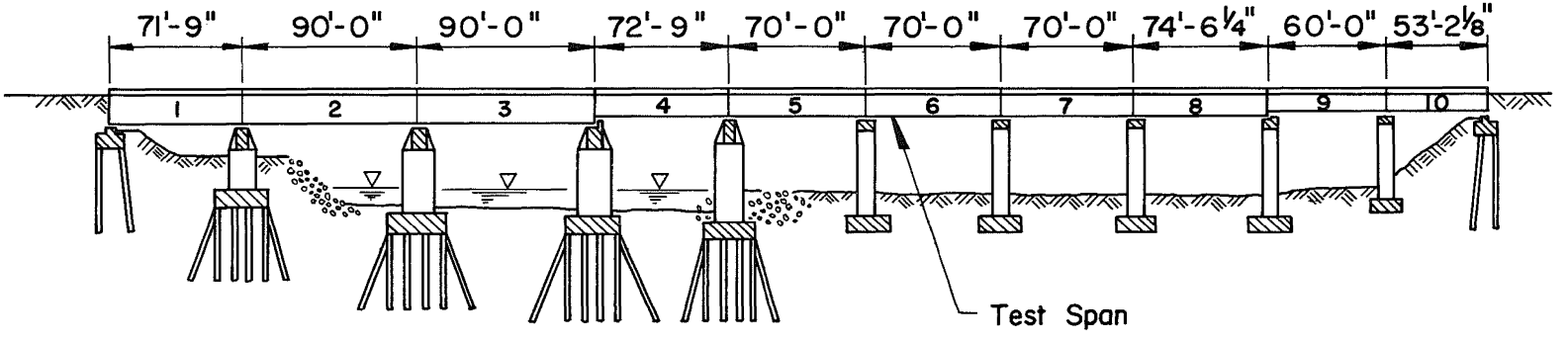

Fig. 1 Elevation of Test Bridge

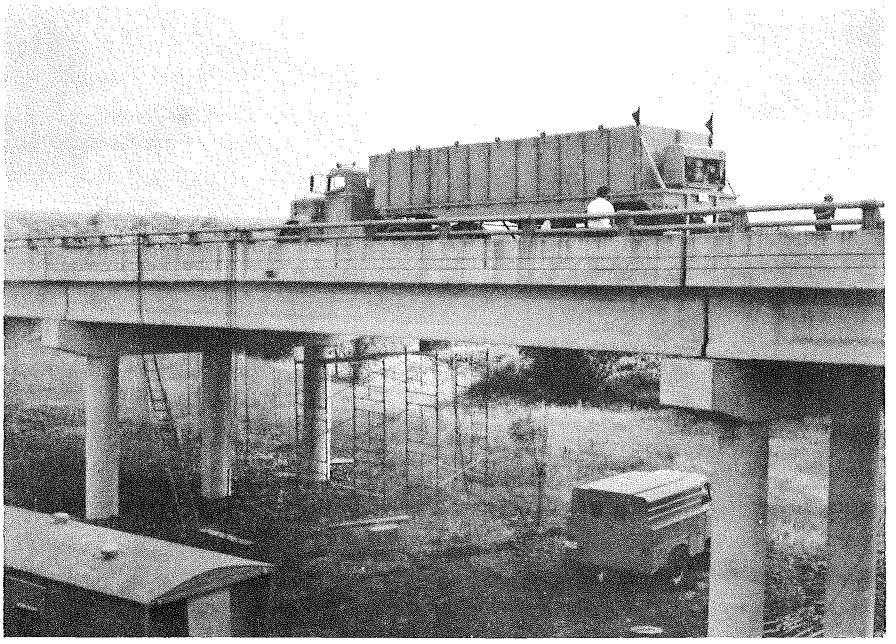

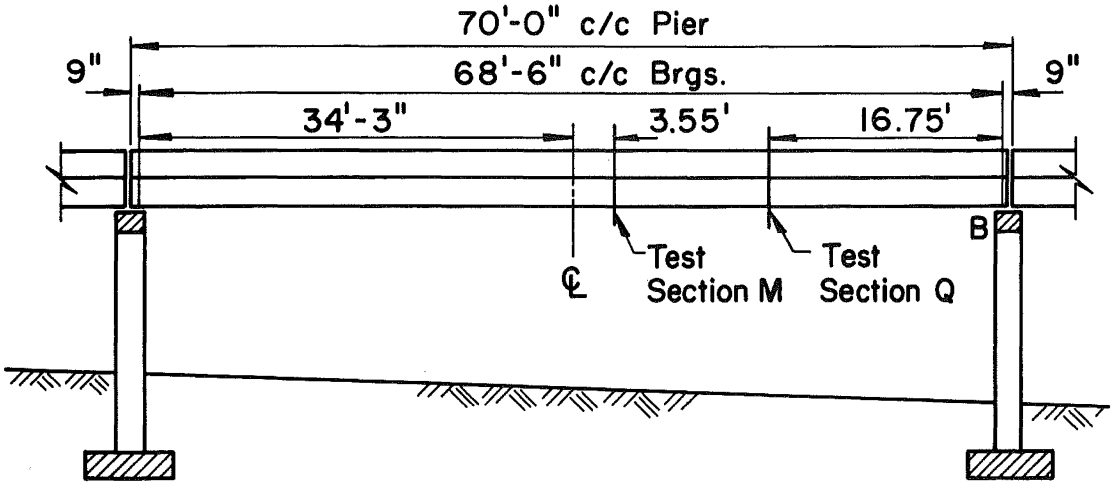

Fig. 2 Elevation of Test Span

DESIGN DIMENSIONS

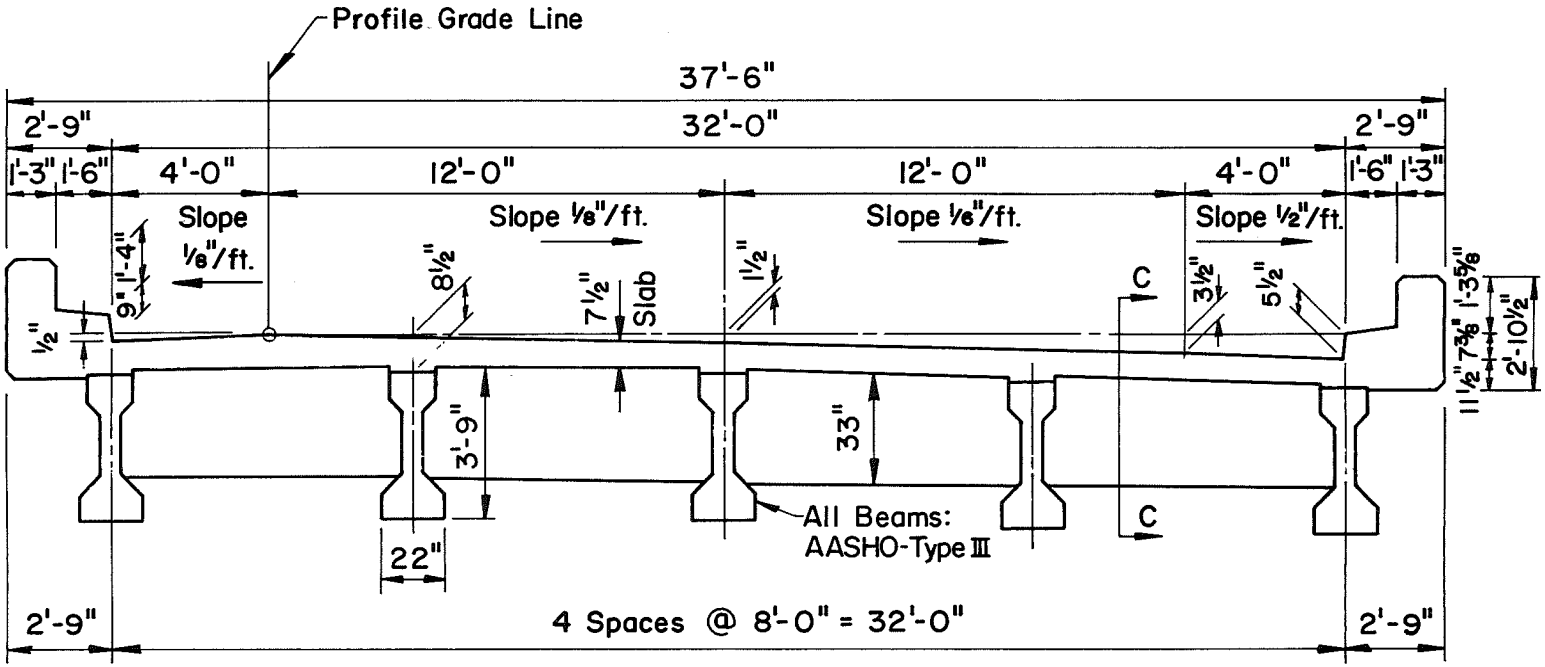

Fig. 3 Cross-Section of Test Bridge

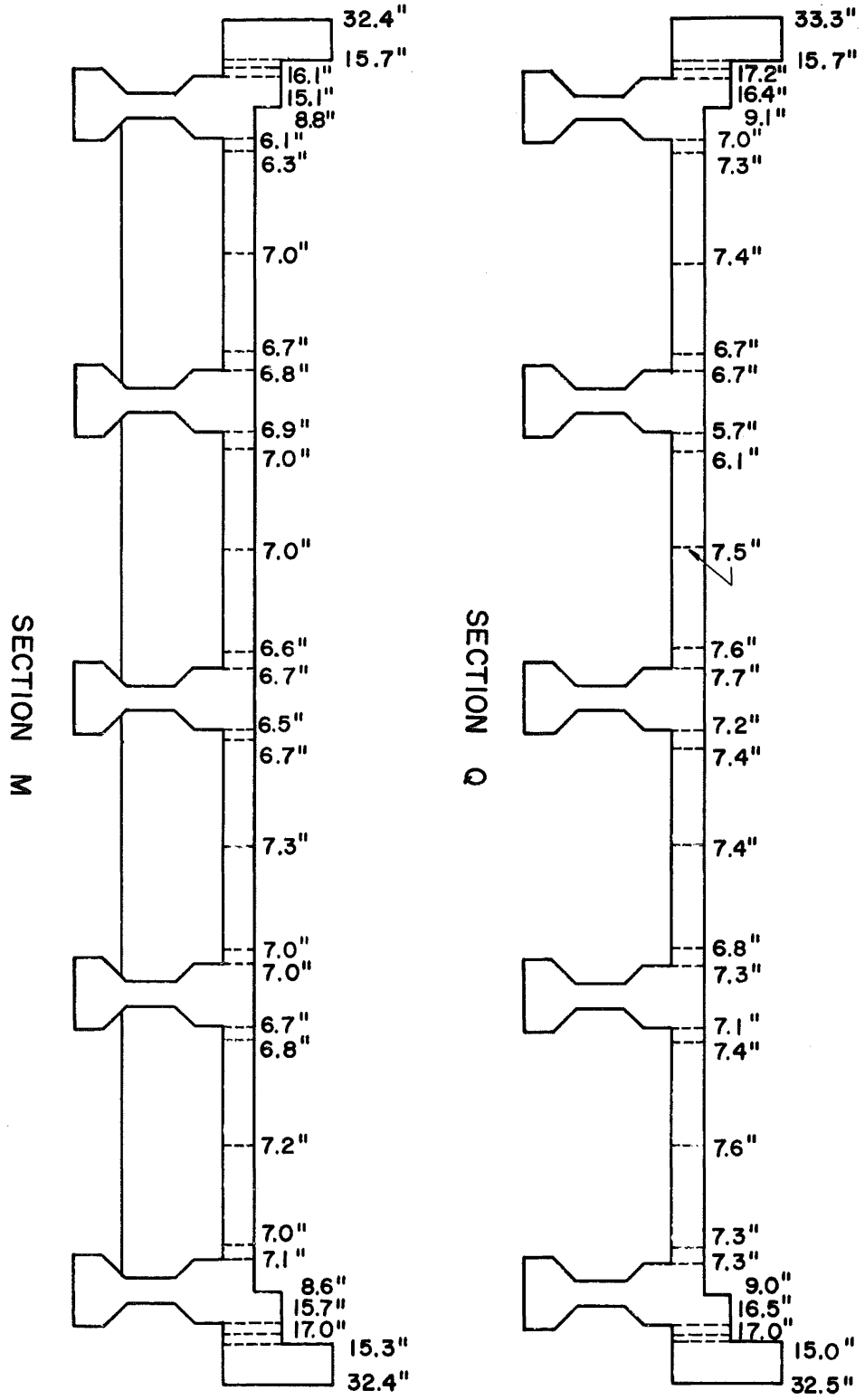

Fig. 4 Measured Thicknesses of Superstructure

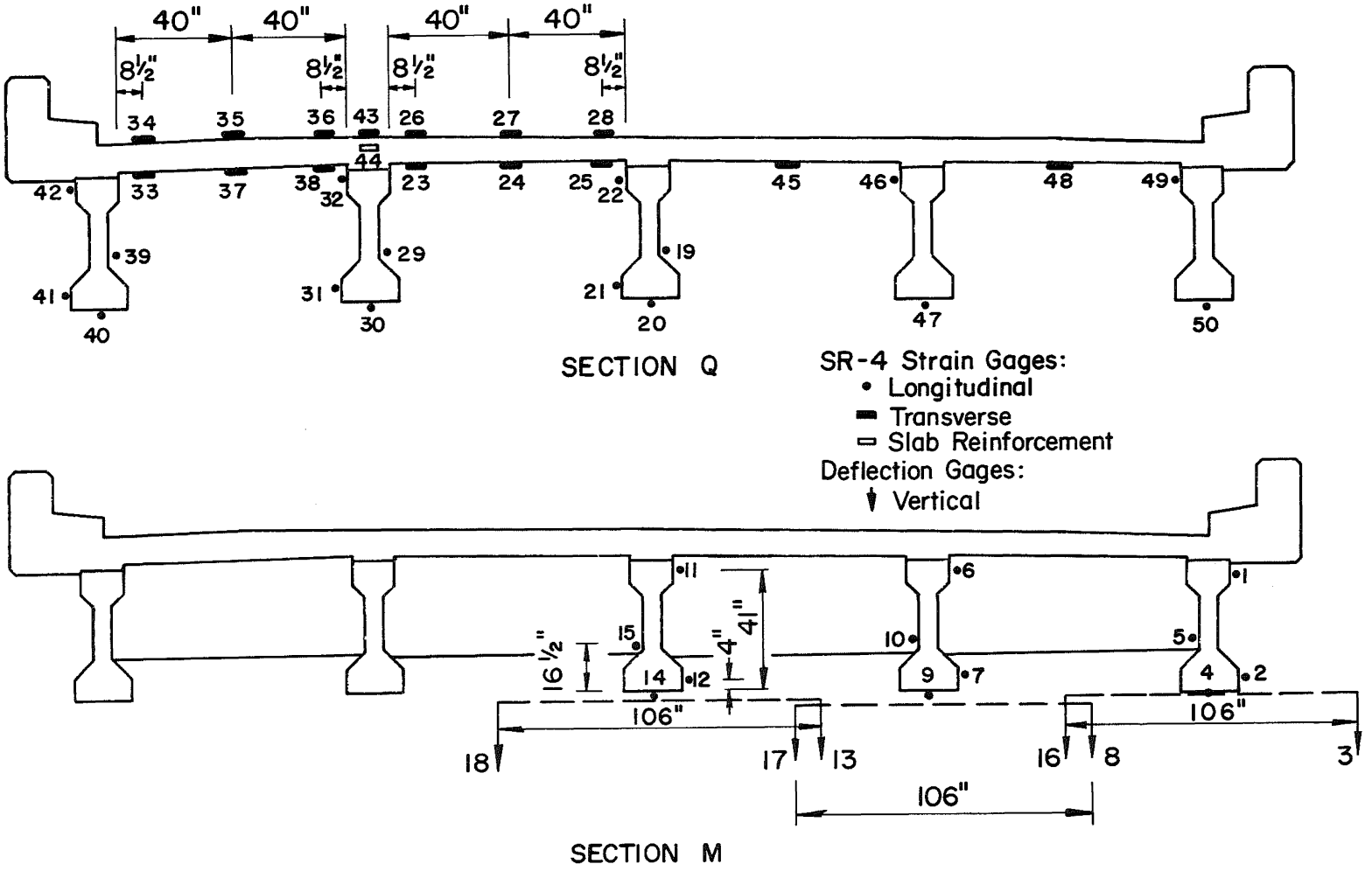

Fig. 5 Location of Gages

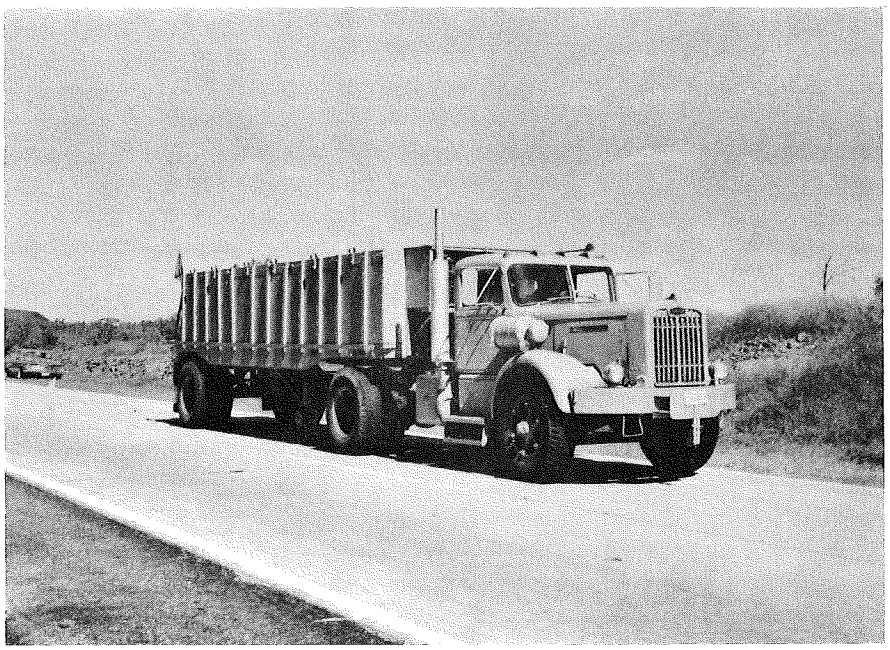

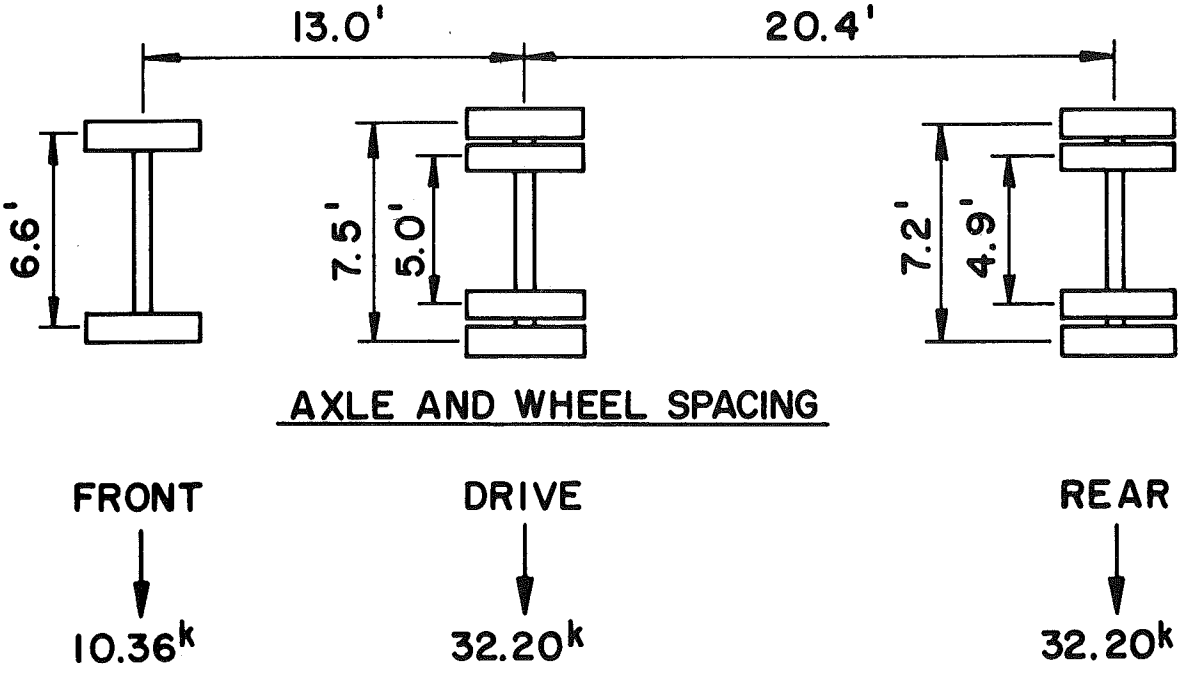

Fig. 6 Test Vehicle

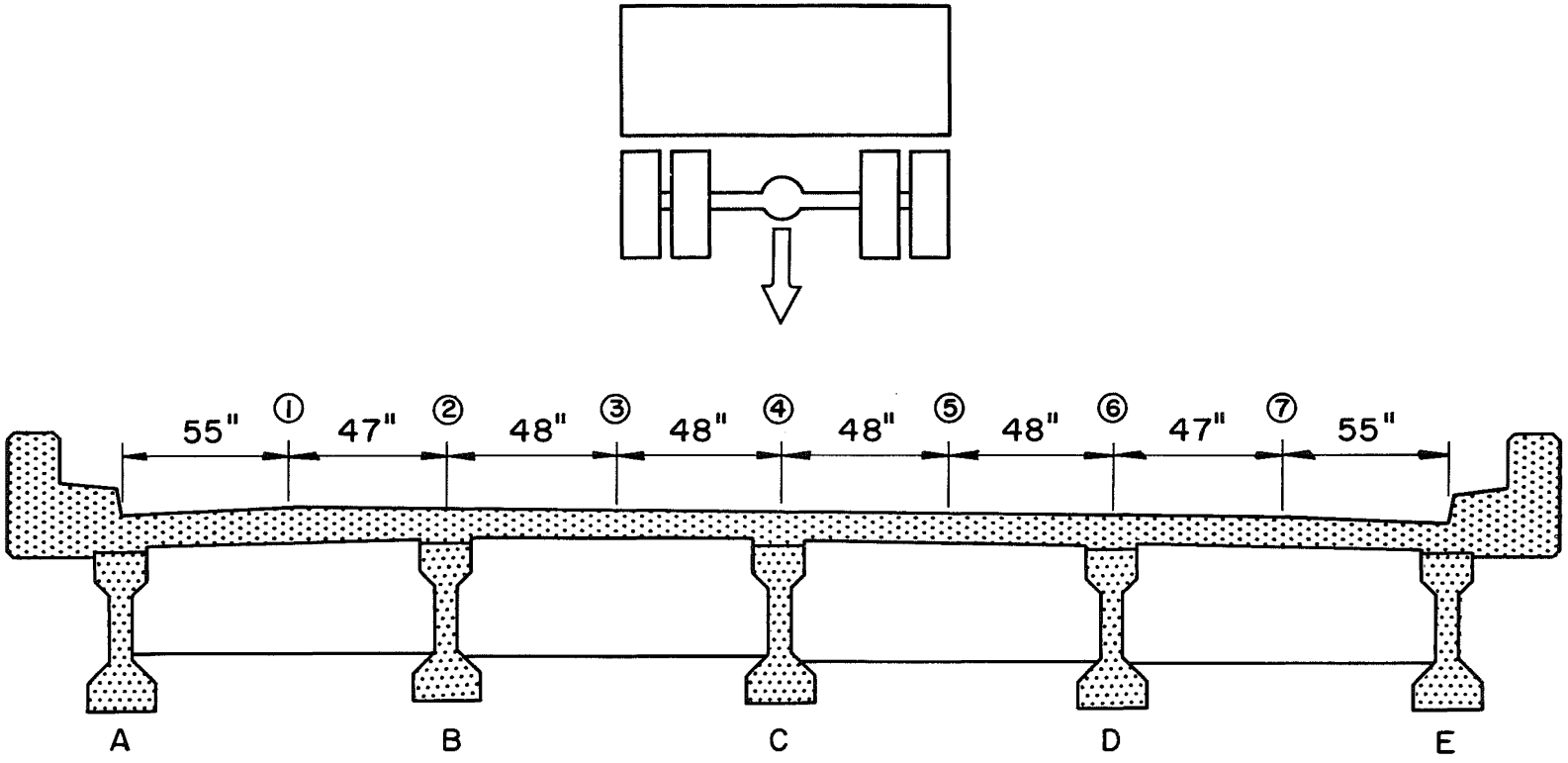

Fig. 7 Loading Lanes

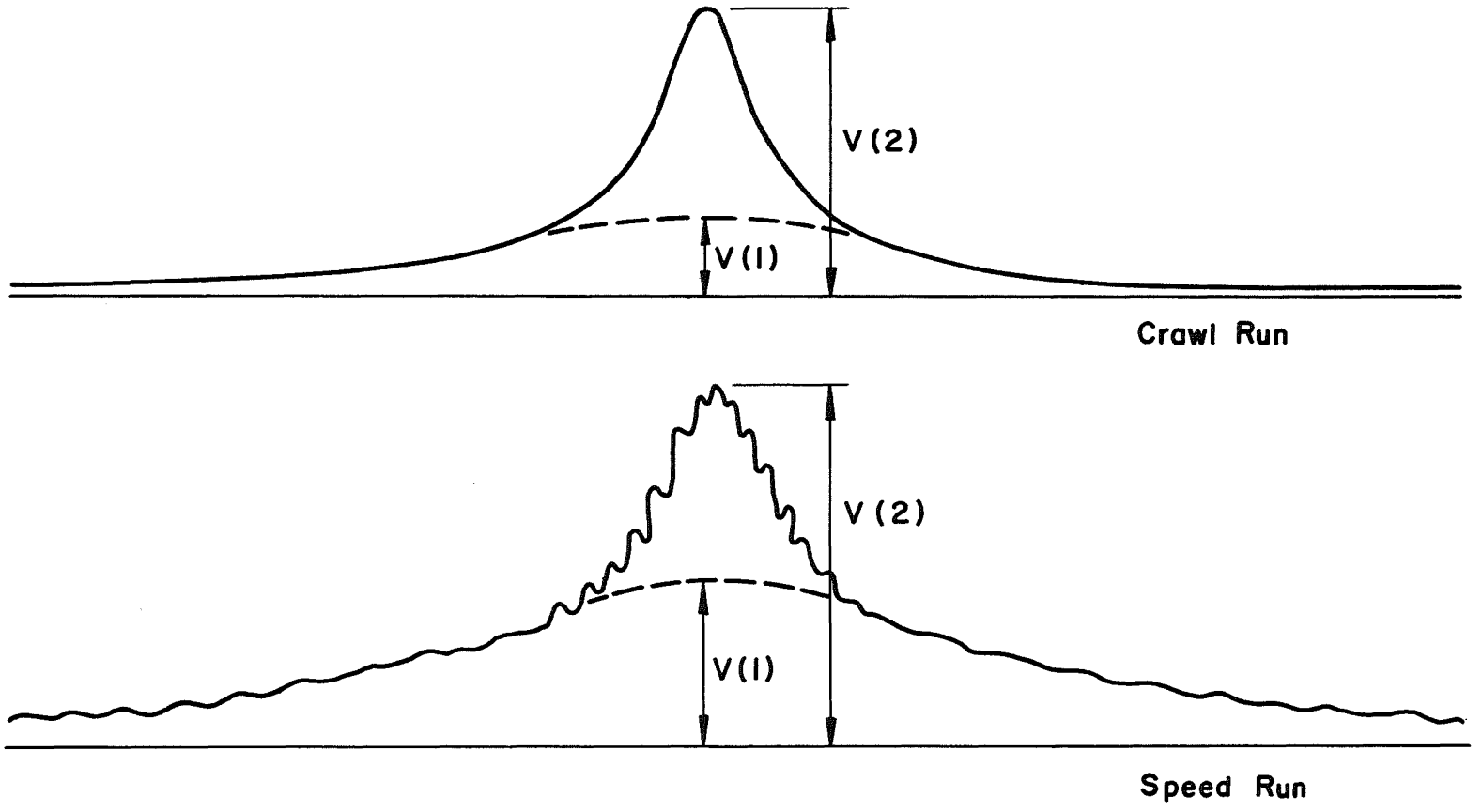

Fig. 8 Typical Traces from Oscillograph

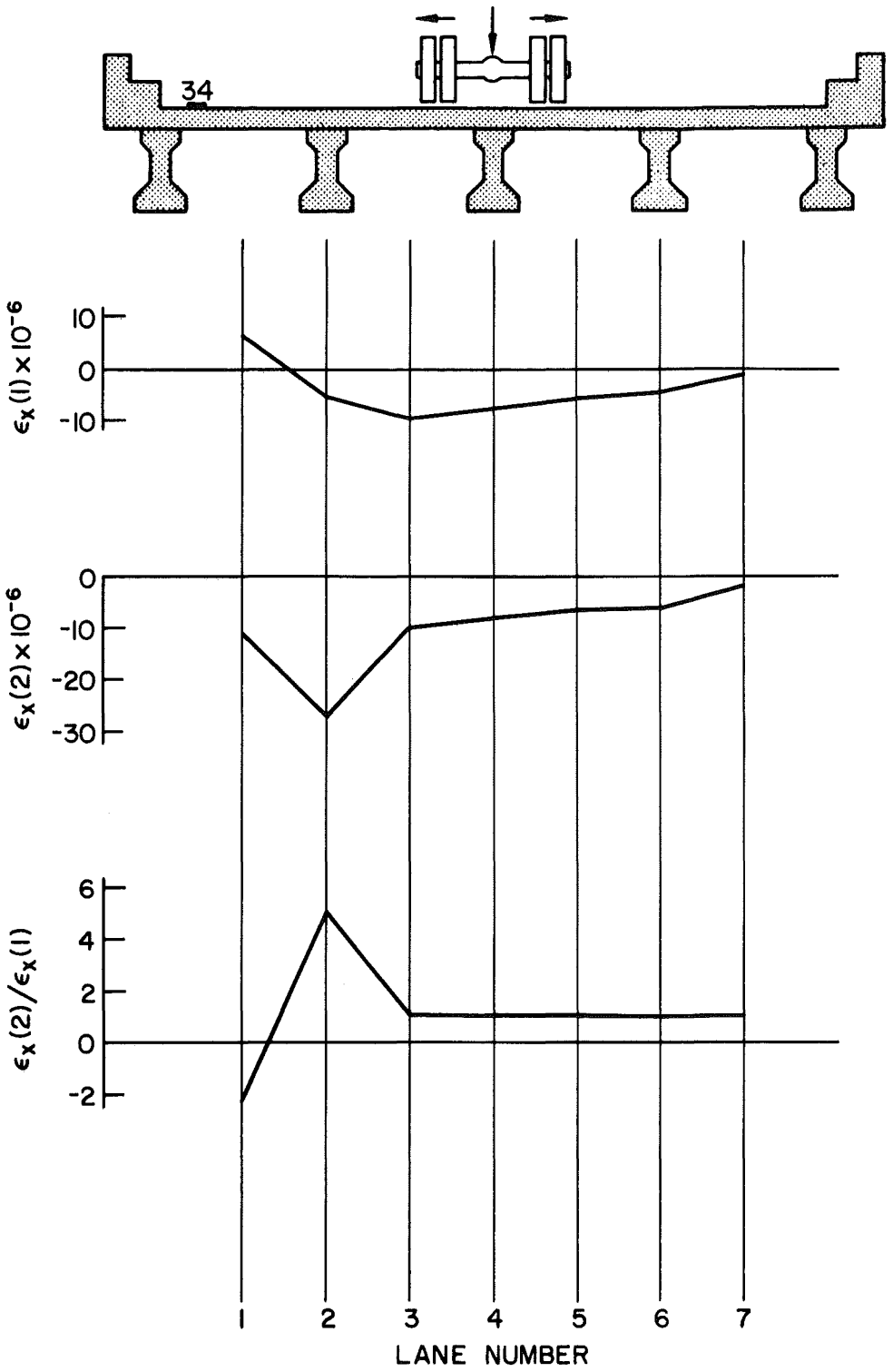

Fig. 9 Influence Lines for Transverse Strains - Crawl Runs
Gage 34

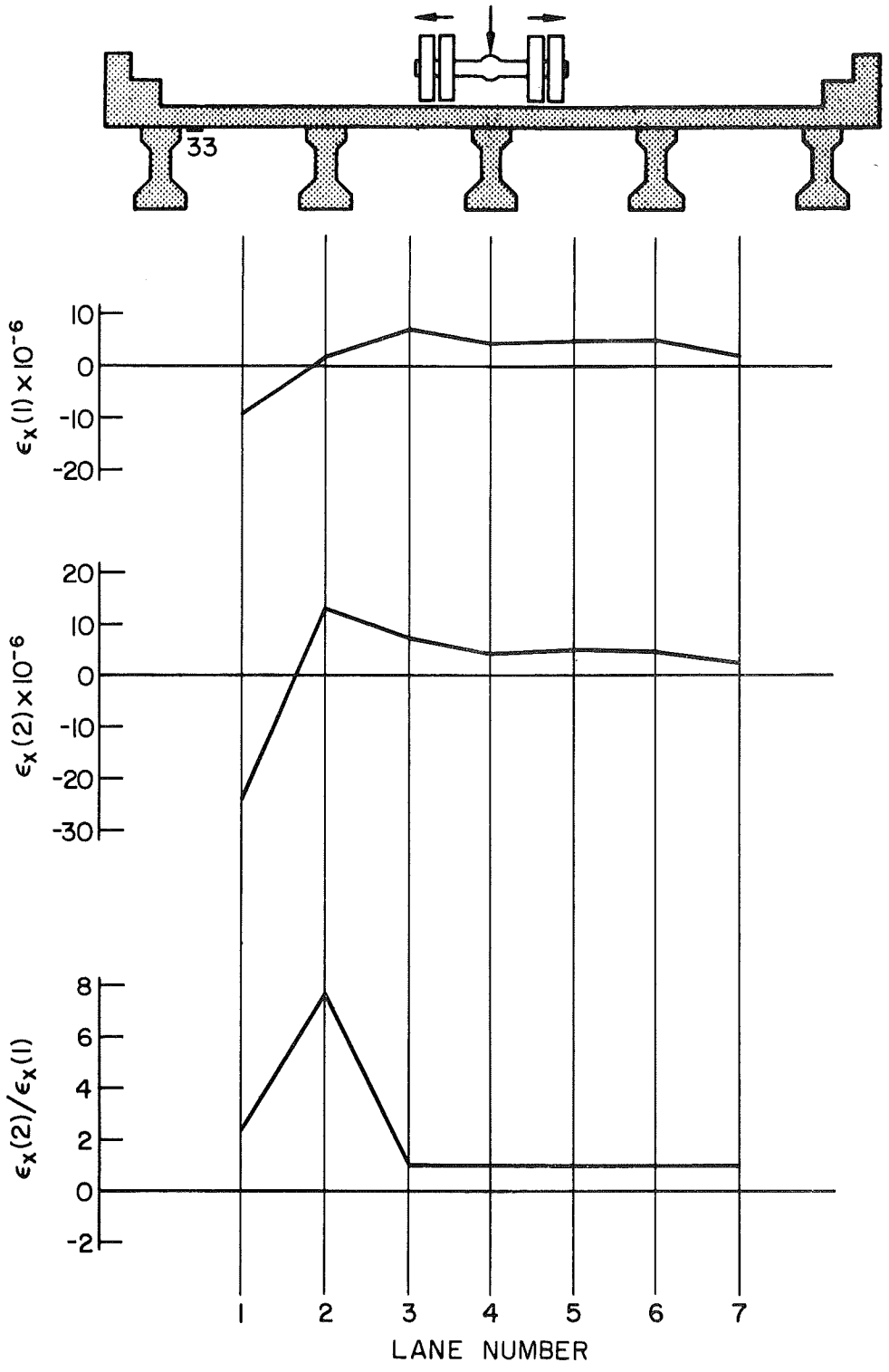

Fig. 10 Influence Lines for Transverse Strains - Crawl Runs
Gage 33

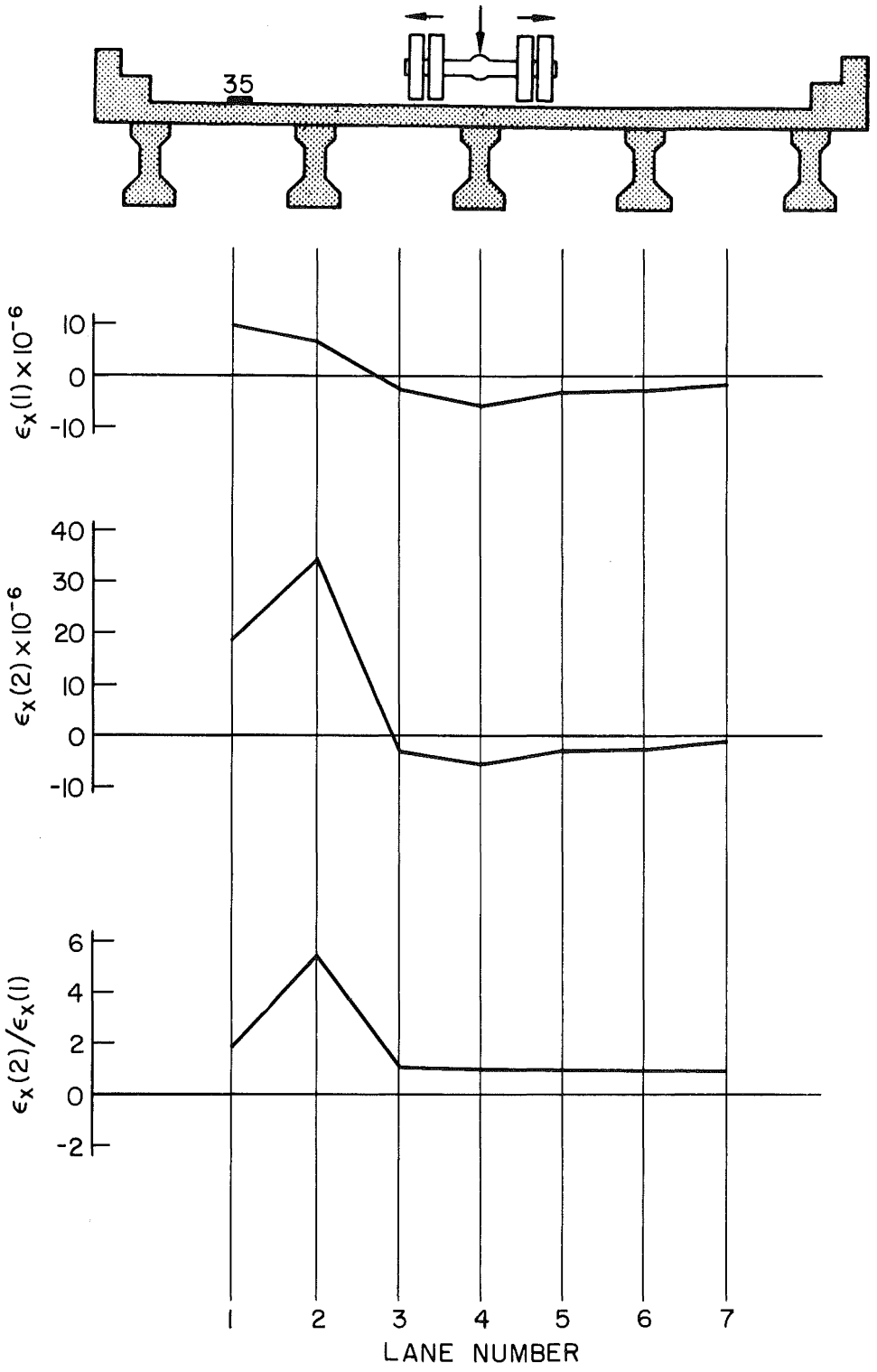

Fig. 11 Influence Lines for Transverse Strains - Crawl Runs
Gage 35

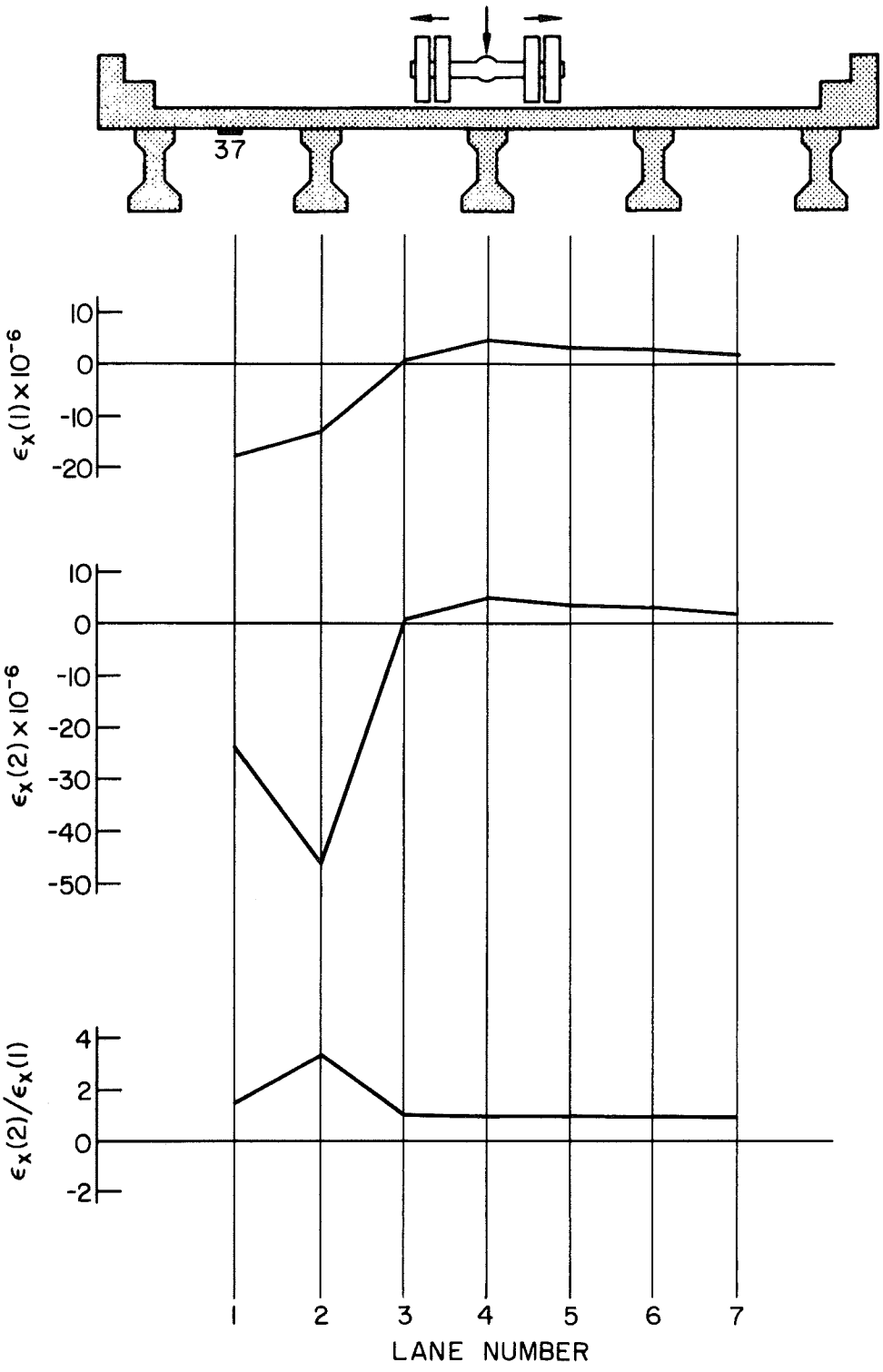

Fig. 12 Influence Lines for Transverse Strains - Crawl Runs
Gage 37

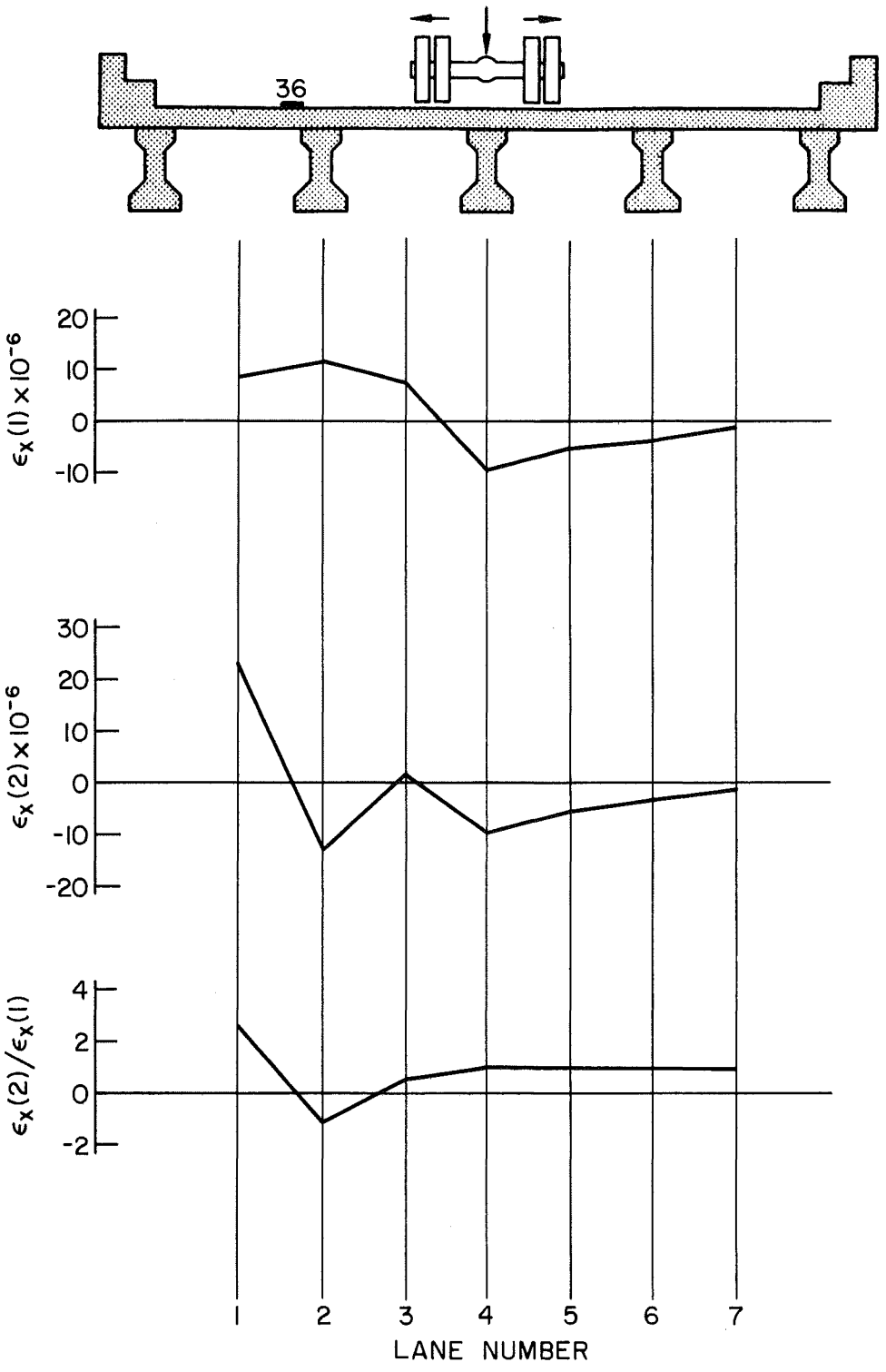

Fig. 13 Influence Lines for Transverse Strains - Crawl Runs
Gage 36

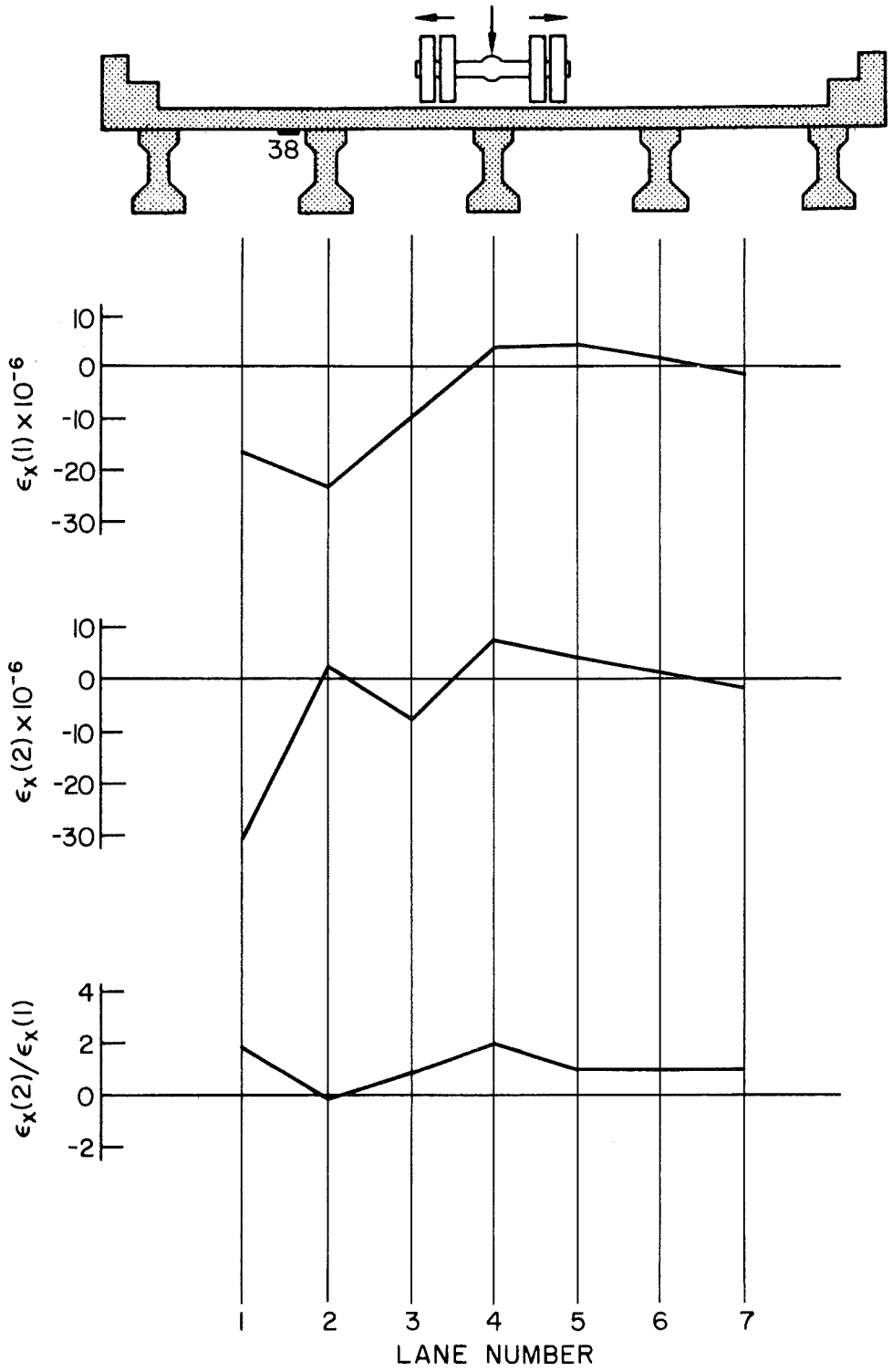

Fig. 14 Influence Lines for Transverse Strains - Crawl Runs
Gage 38

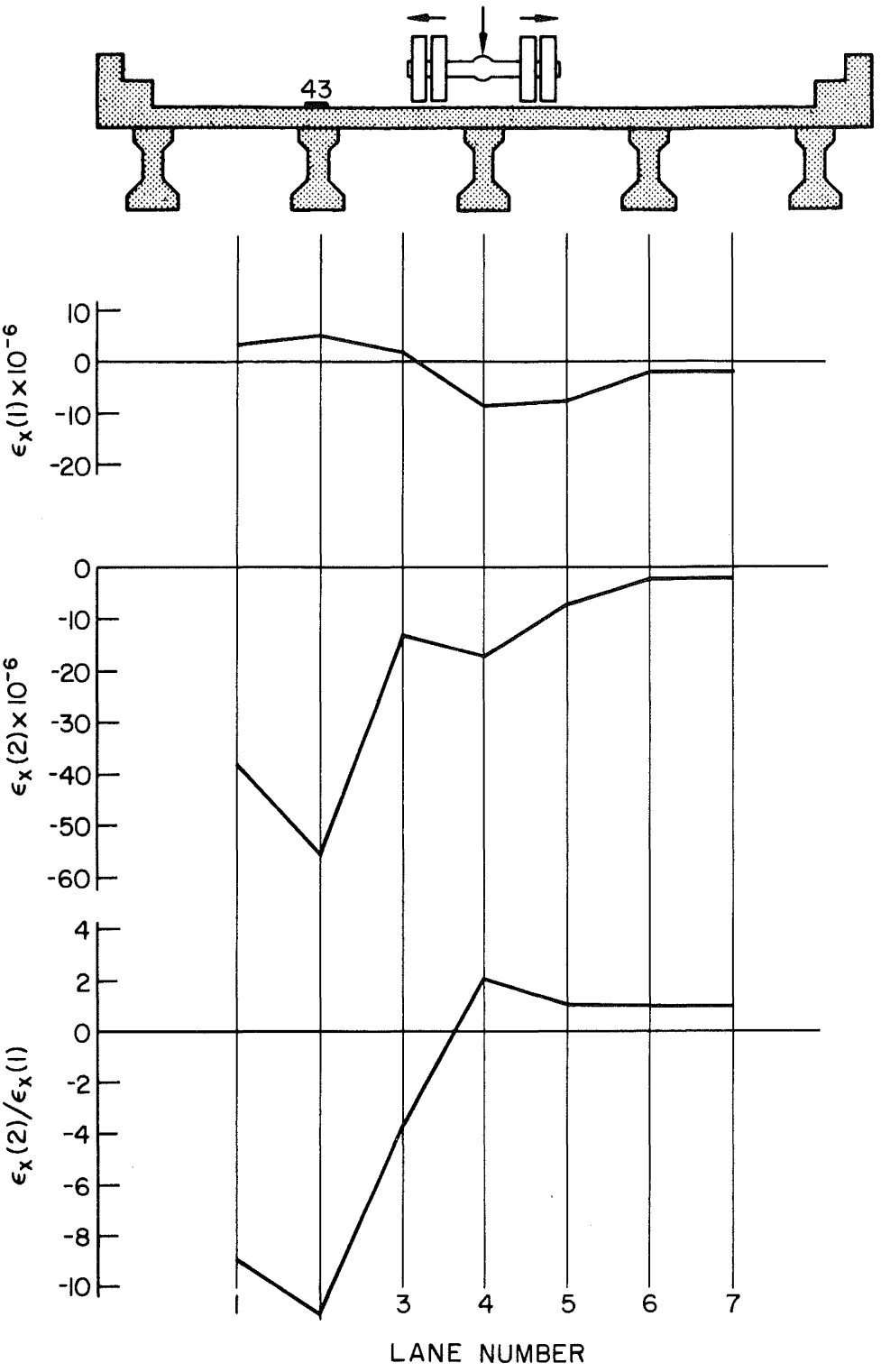

Fig. 15 Influence Lines for Transverse Strains - Crawl Runs
Gage 43

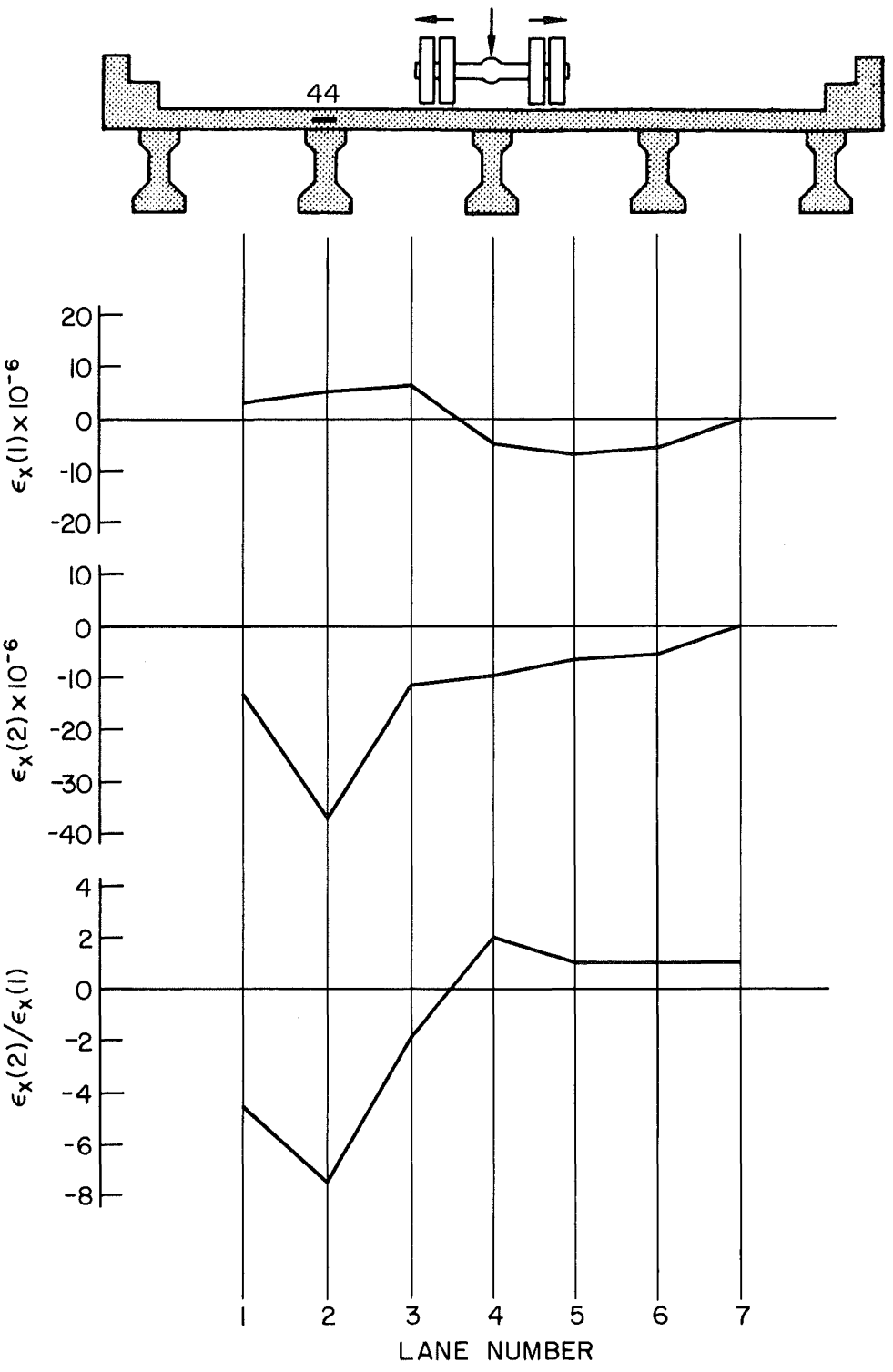

Fig. 16 Influence Lines for Transverse Strains - Crawl Runs
Gage 44

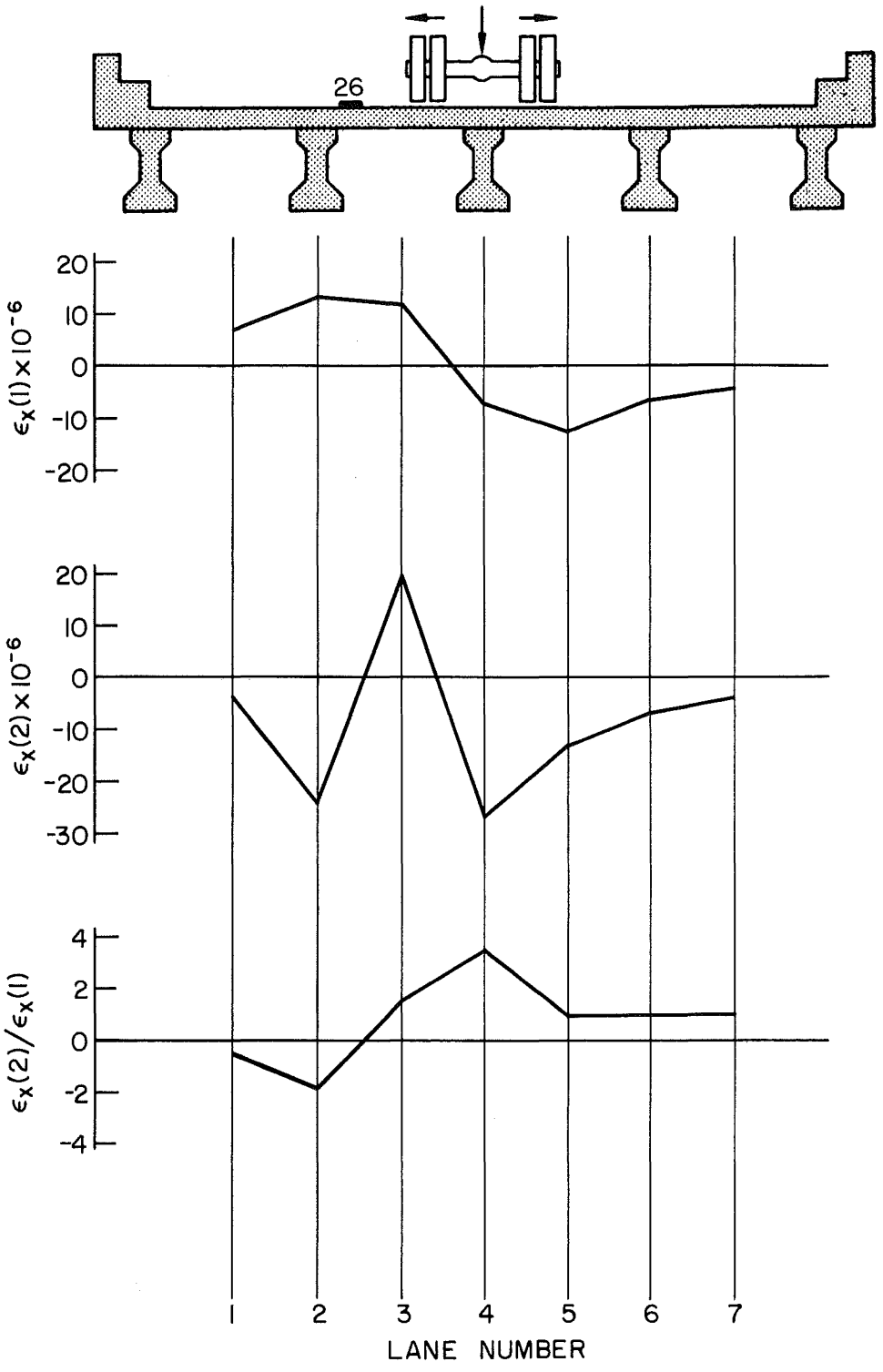

Fig. 17 Influence Lines for Transverse Strains - Crawl Runs
Gage 26

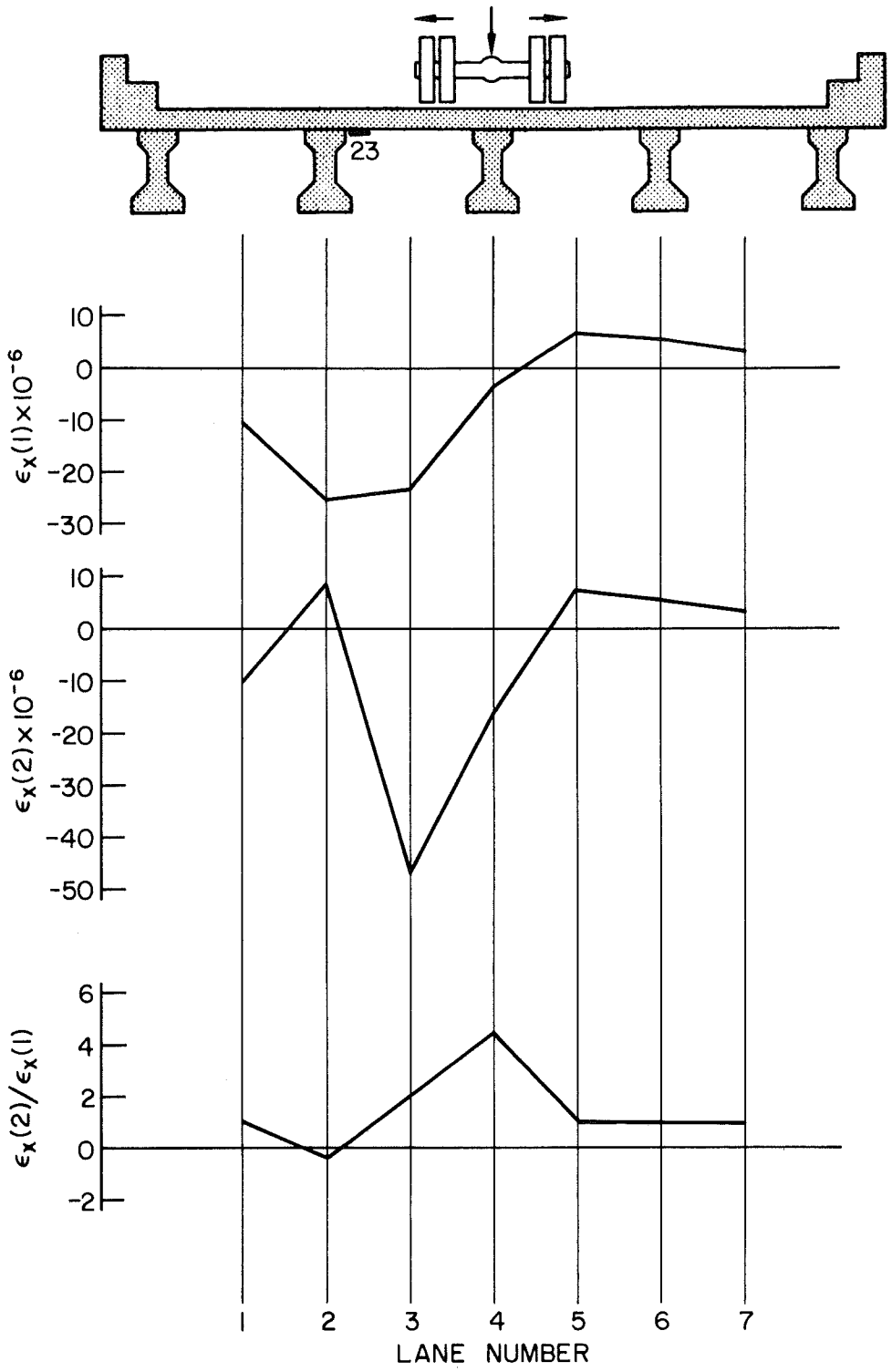

Fig. 18 Influence Lines for Transverse Strains - Crawl Runs
Gage 23

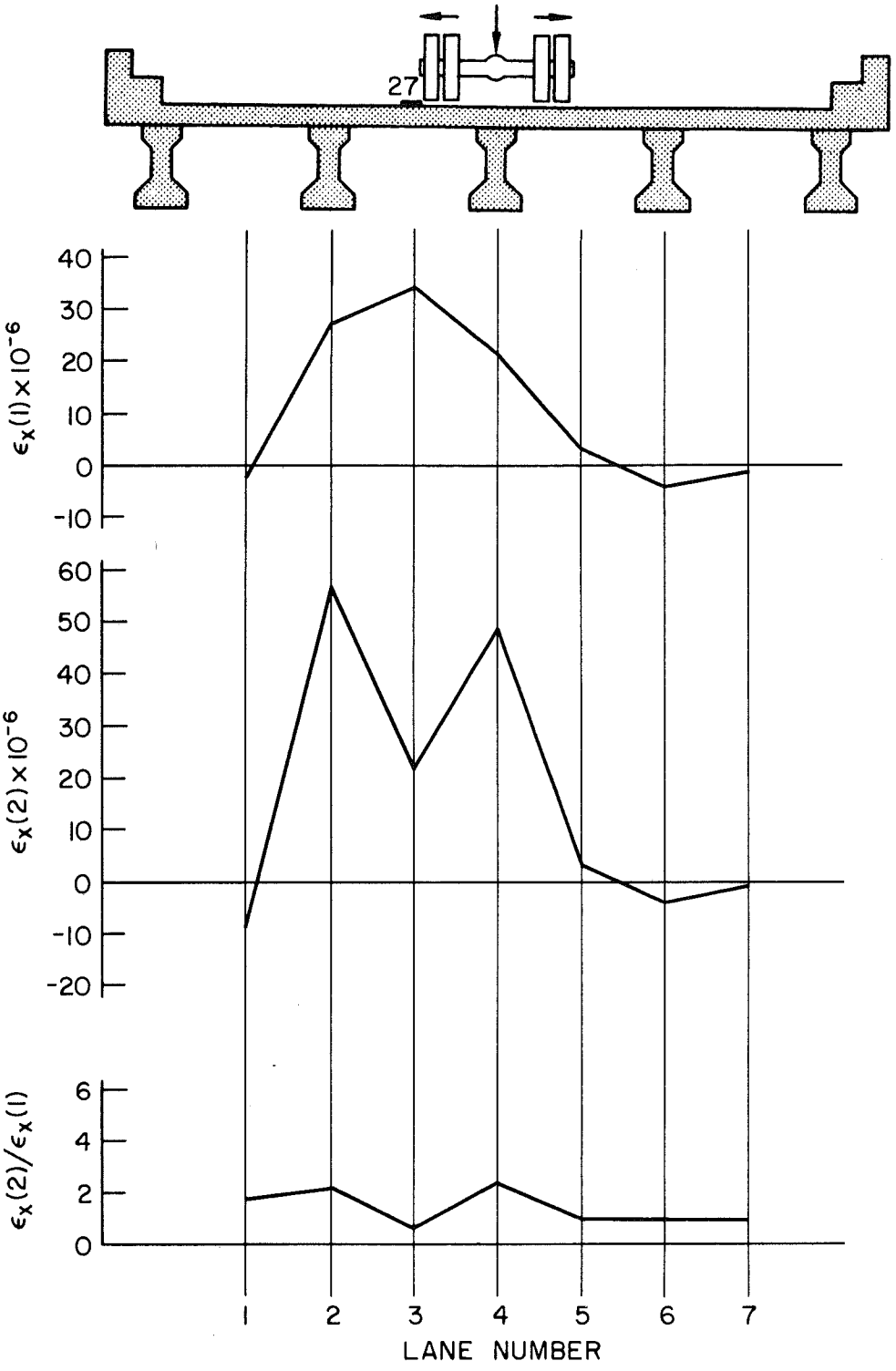

Fig. 19 Influence Lines for Transverse Strains - Crawl Runs
Gage 27

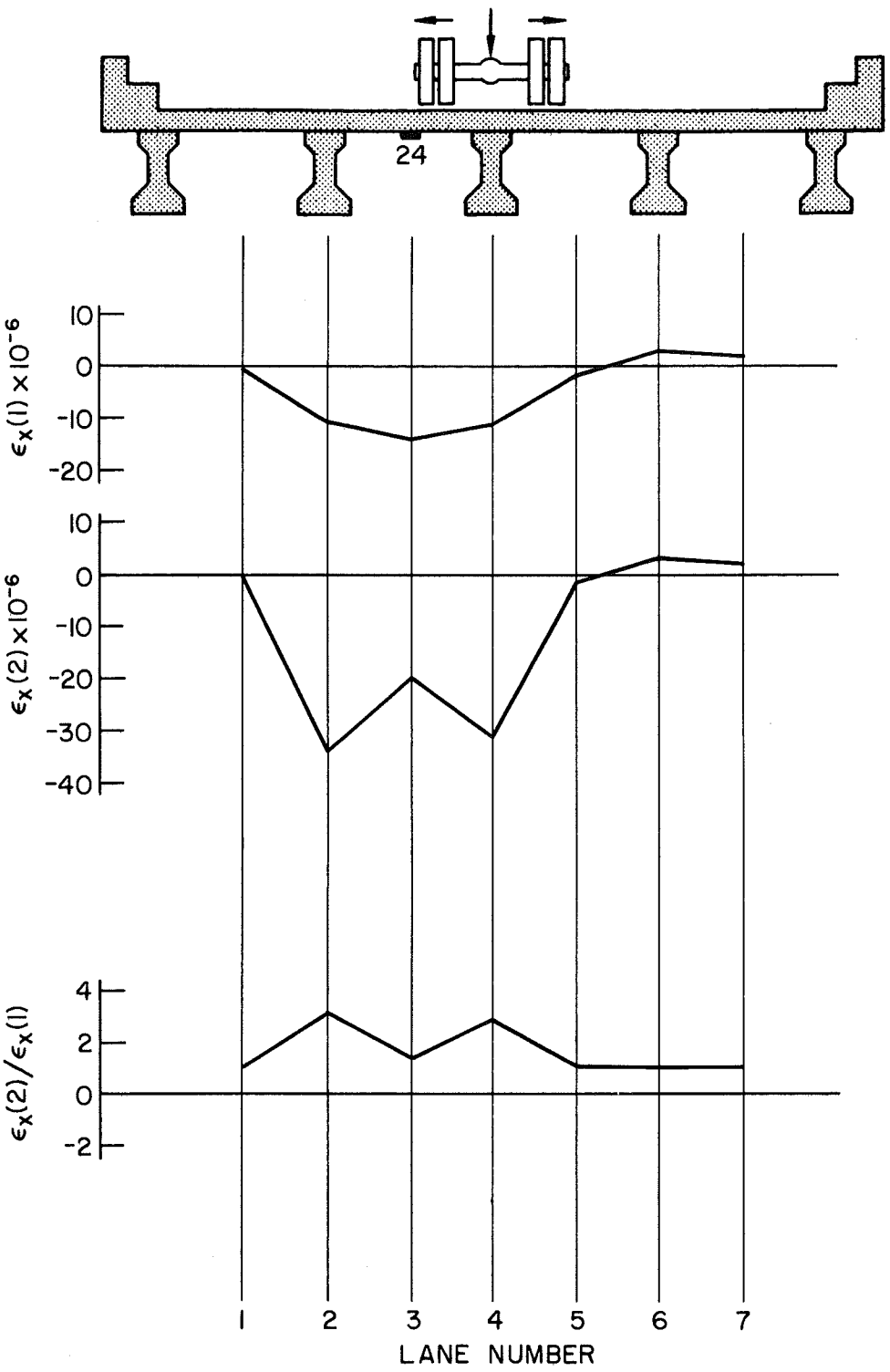

Fig. 20 Influence Lines for Transverse Strains - Crawl Runs
Gage 24

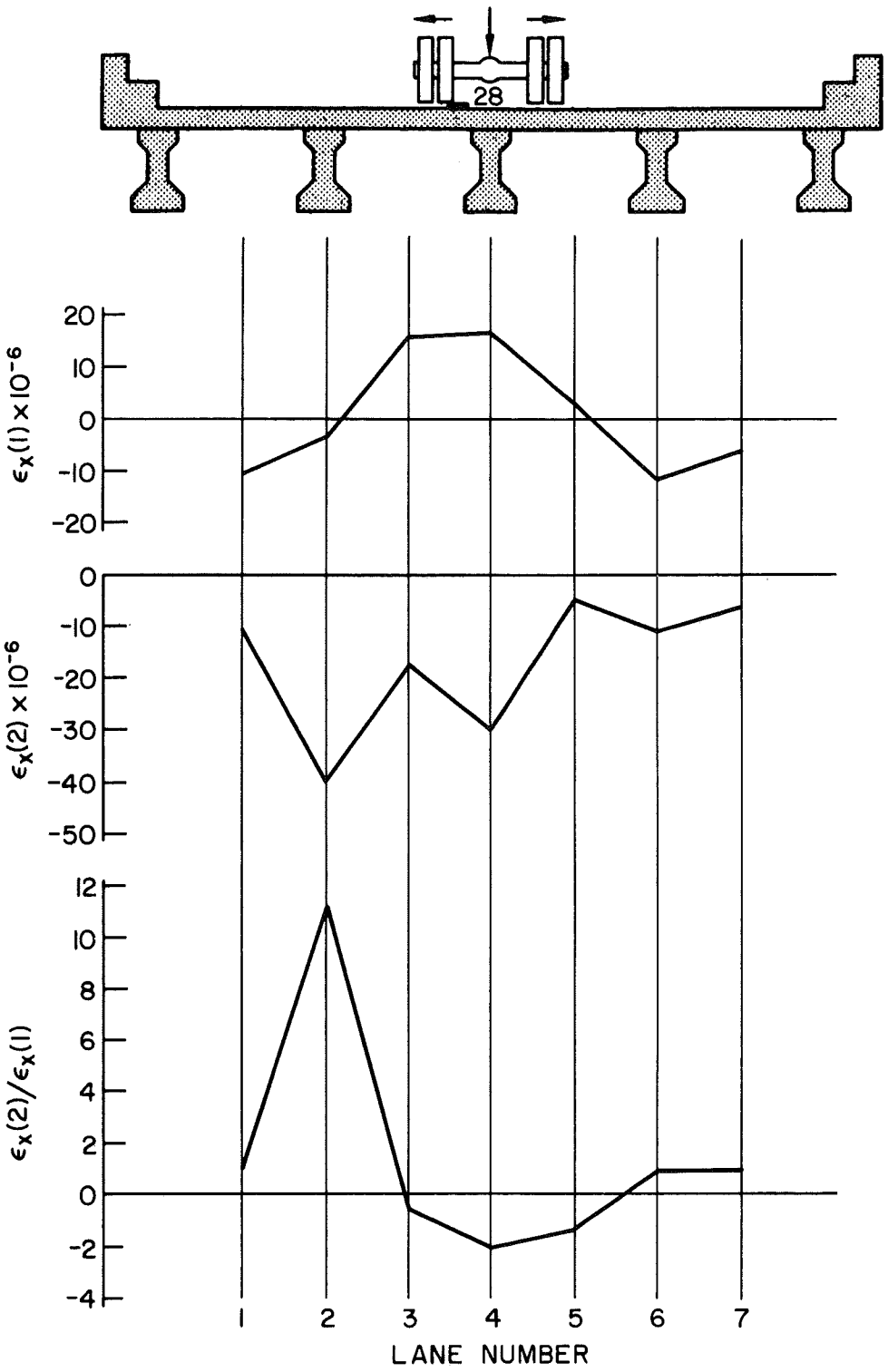

Fig. 21 Influence Lines for Transverse Strains - Crawl Runs
Gage 28

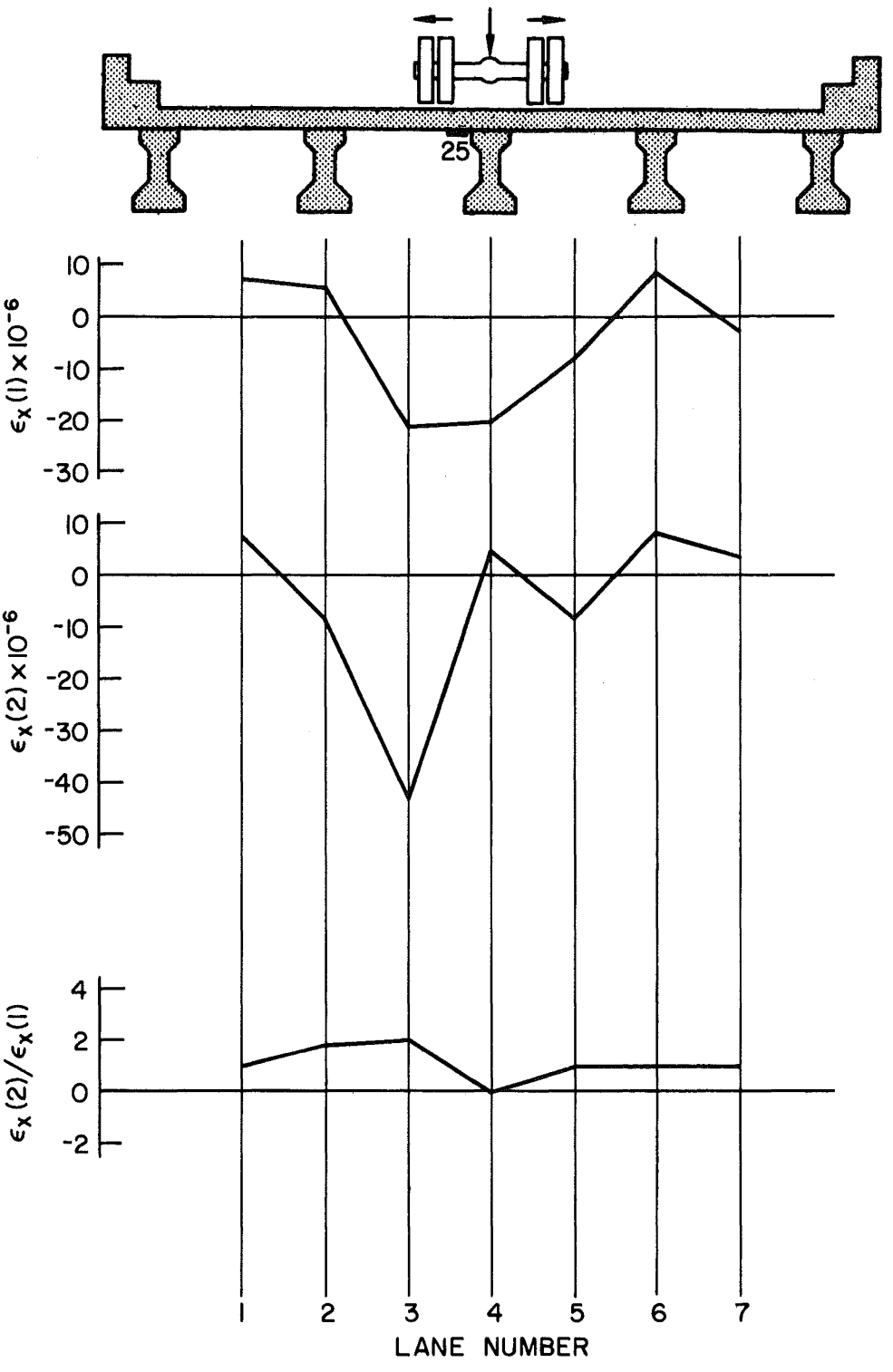

Fig. 22 Influence Lines for Transverse Strains - Crawl Runs
Gage 25

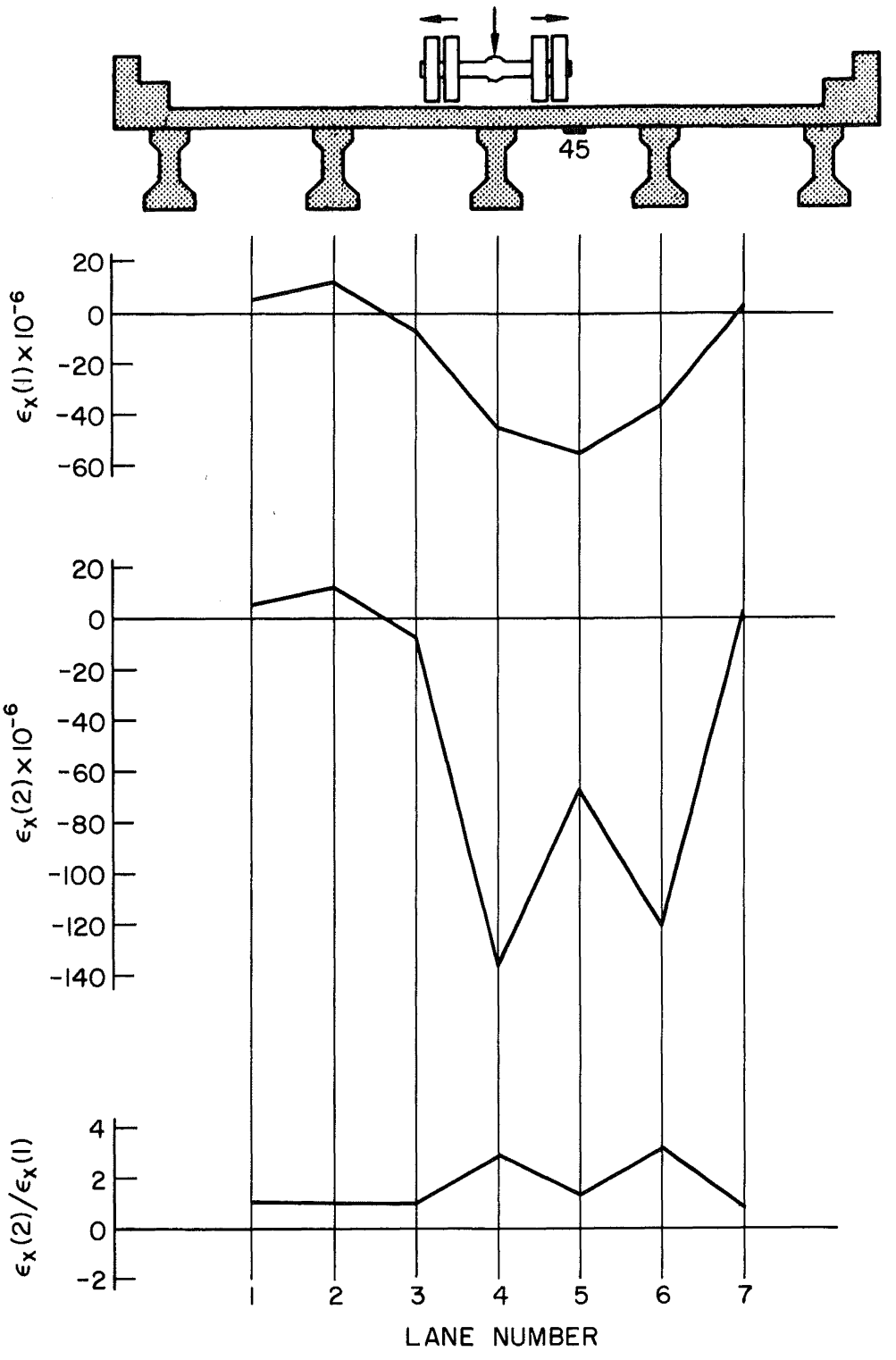

Fig. 23 Influence Lines for Transverse Strains - Crawl Runs
Gage 45

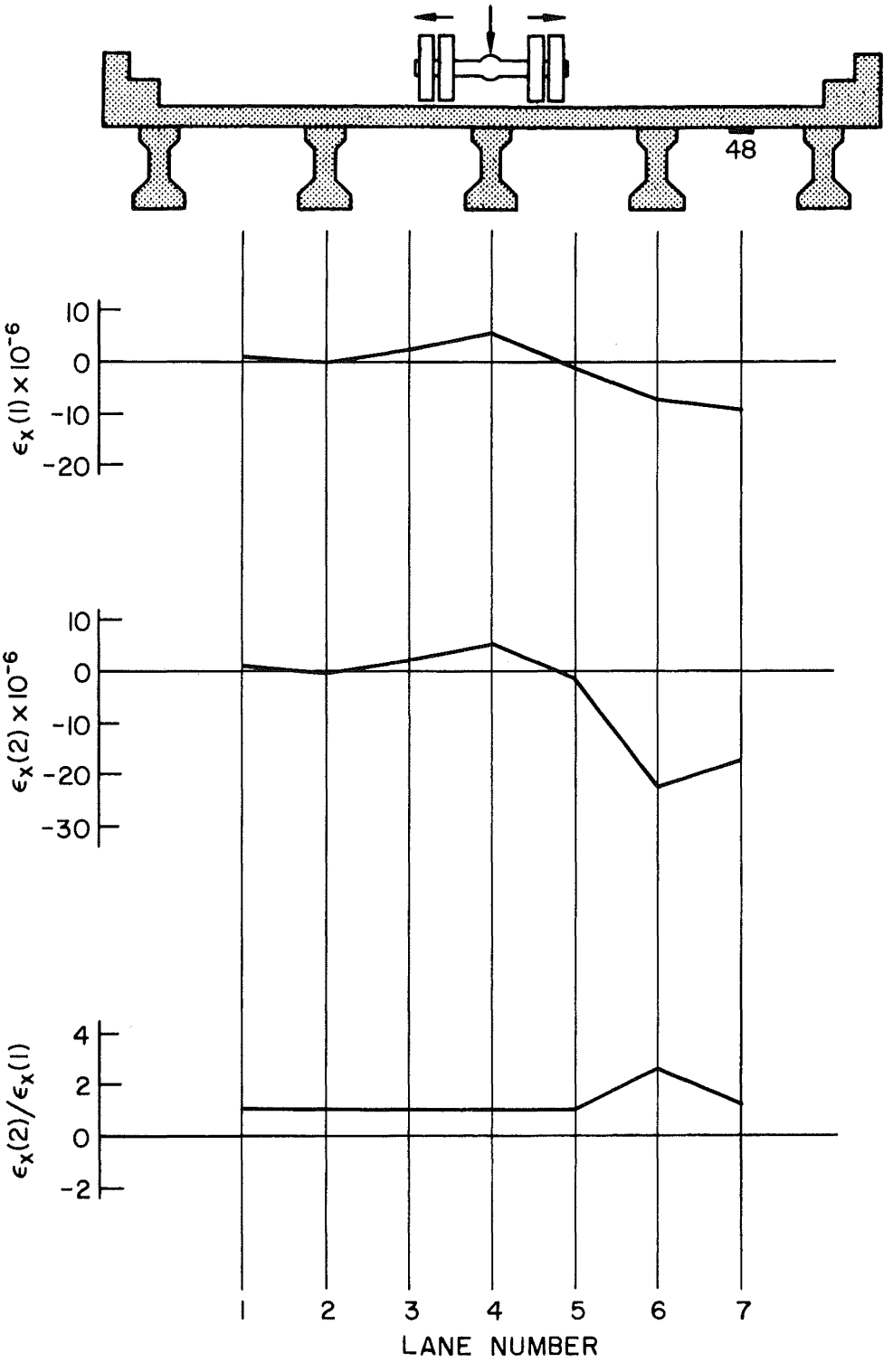

Fig. 24 Influence Lines for Transverse Strains - Crawl Runs
Gage 48

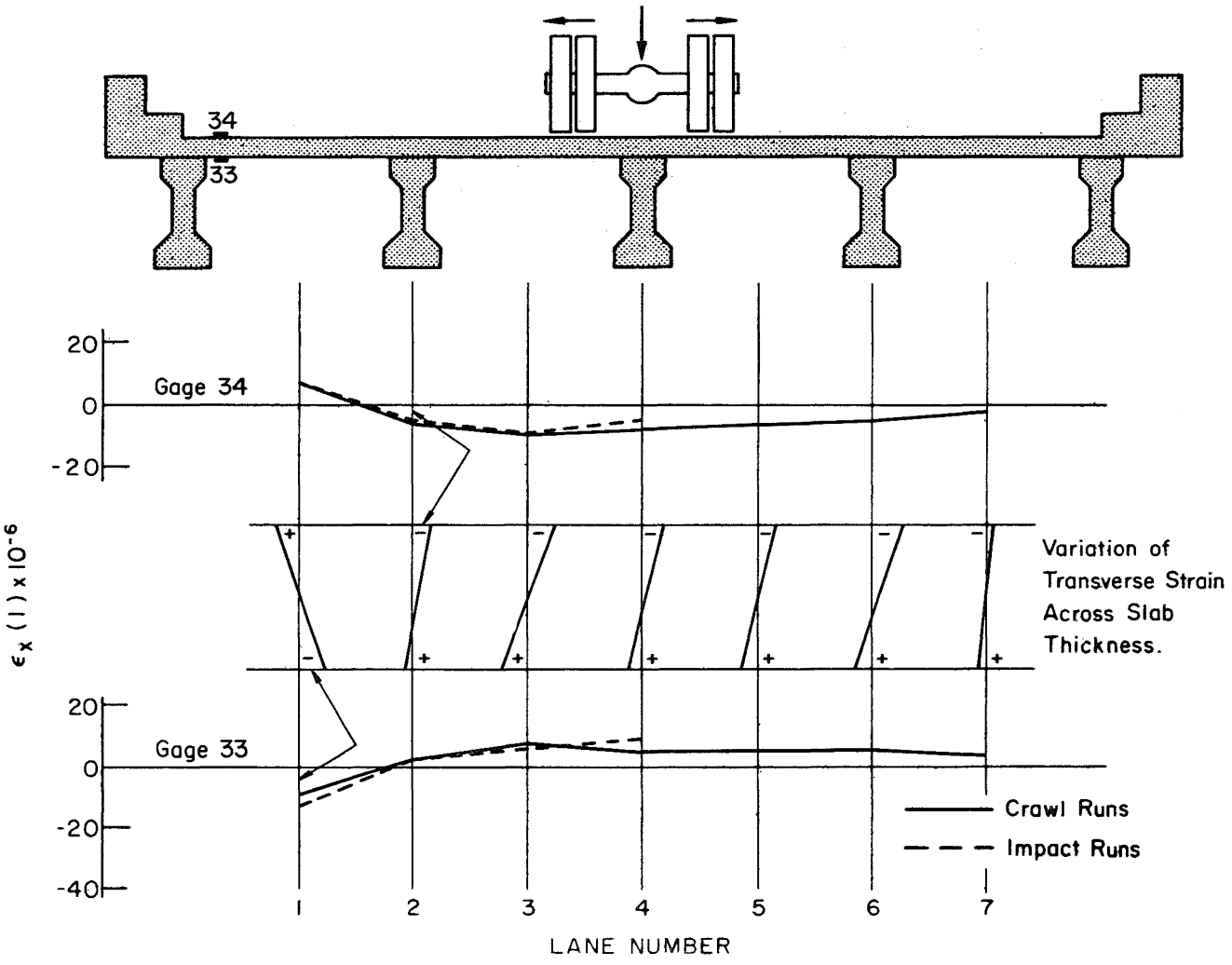

Fig. 25 Variation of Transverse Strain ϵ_x(1) Across Slab Thickness
Gages 34 and 33

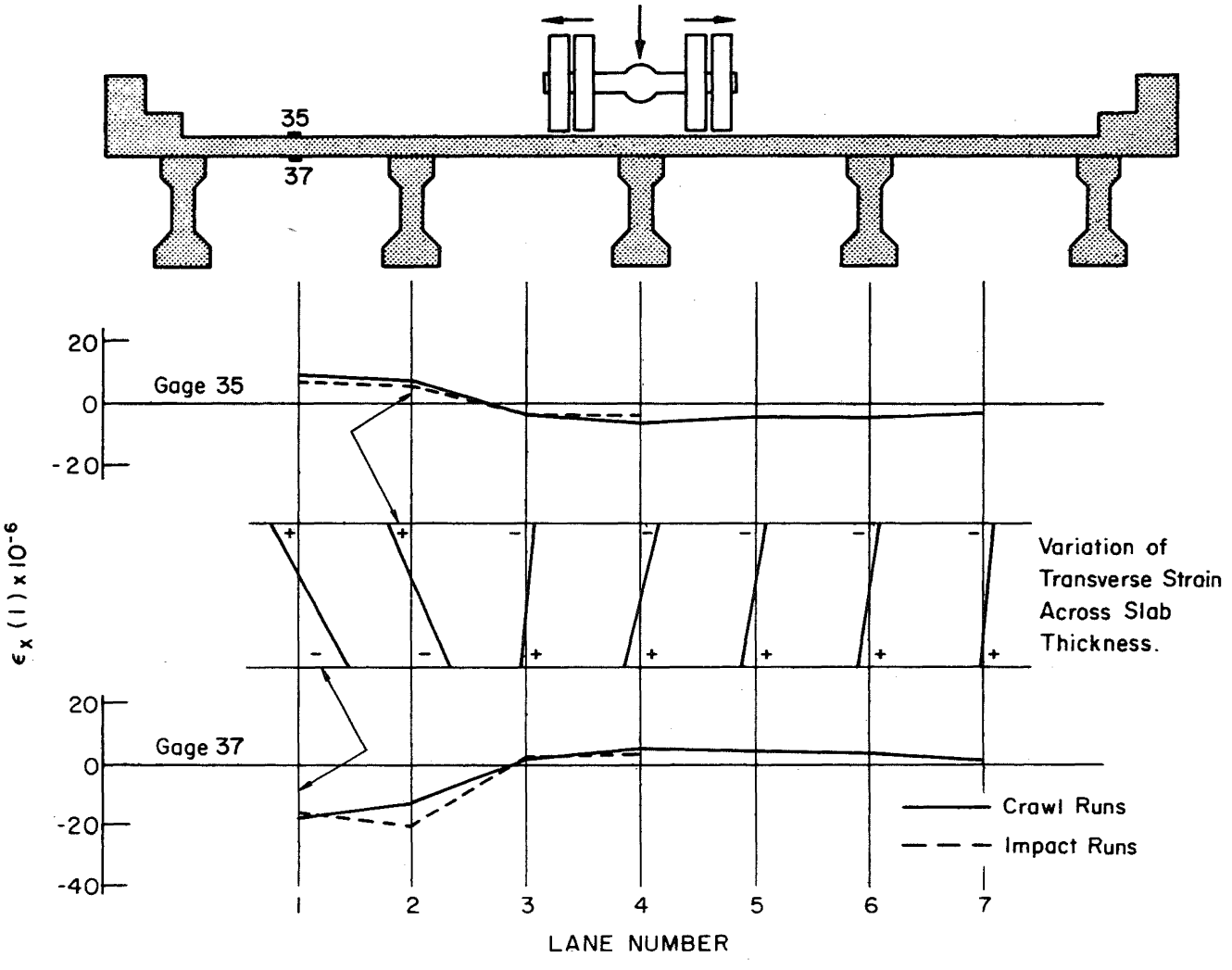

Fig. 26 Variation of Transverse Strain $\epsilon_x(1)$ Across Slab Thickness
Gages 35 and 37

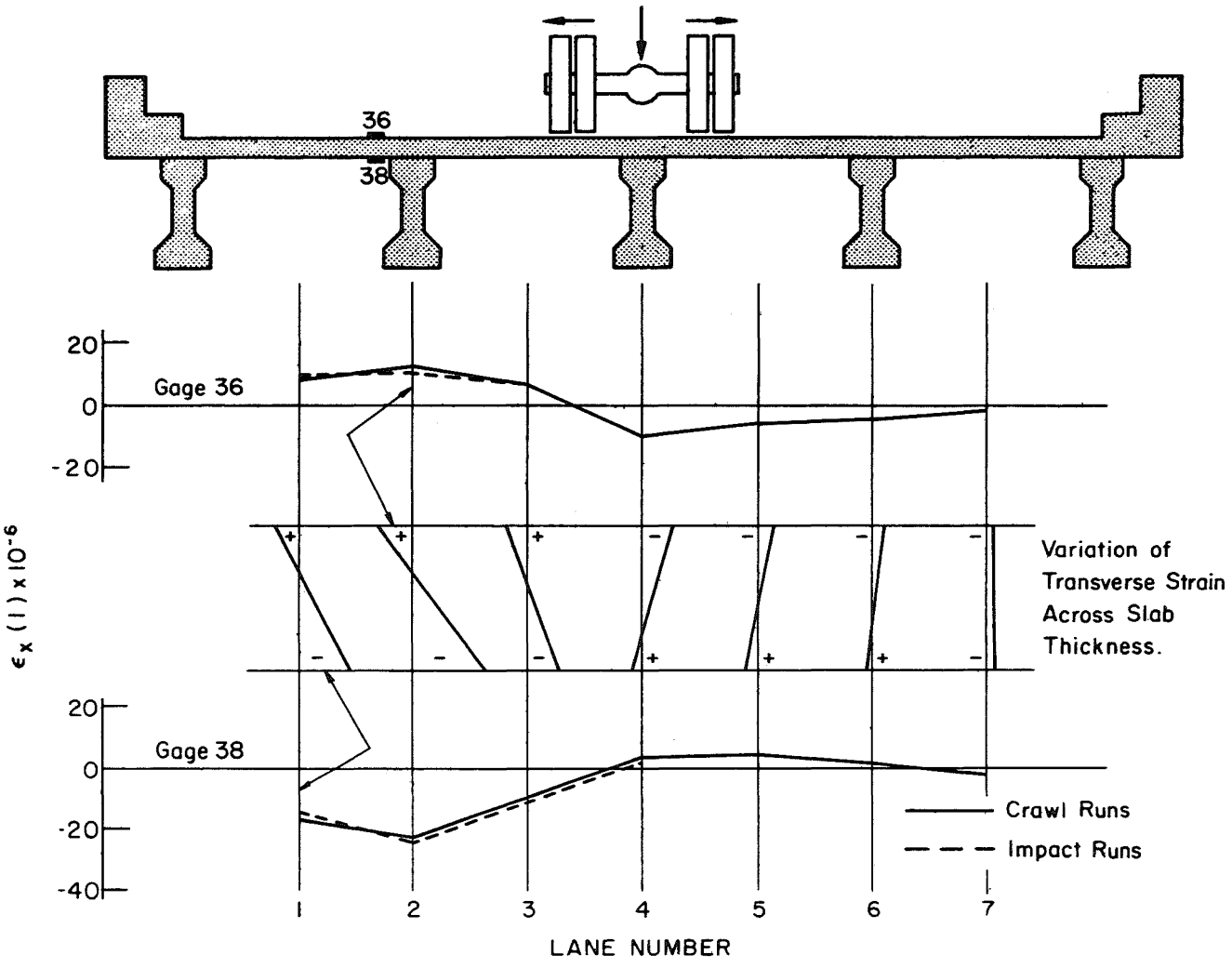

Fig. 27 Variation of Transverse Strain $\epsilon_x(1)$ Across Slab Thickness Gages 36 and 38

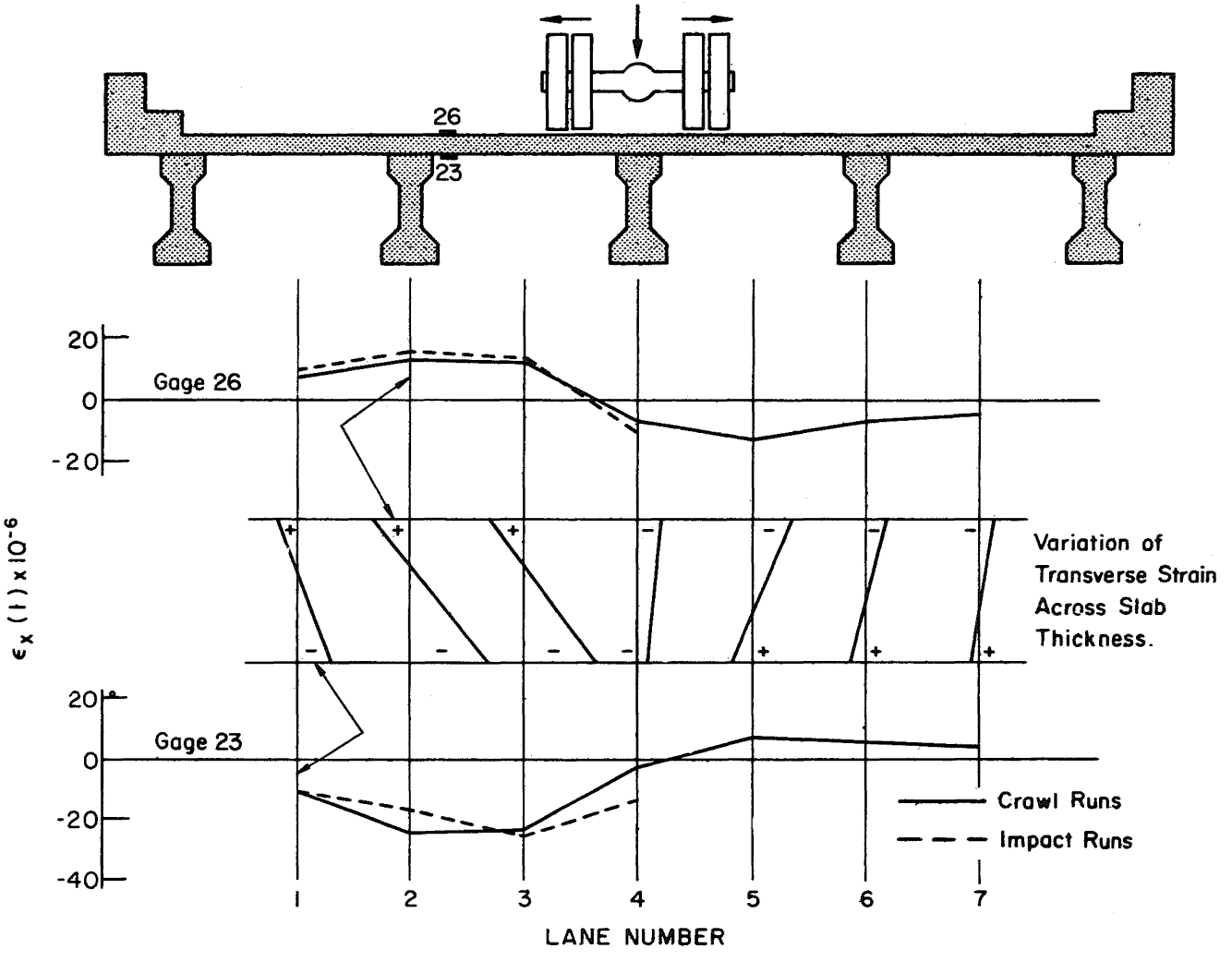

Fig. 28 Variation of Transverse Strain $\epsilon_x(1)$ Across Slab Thickness
Gages 26 and 23

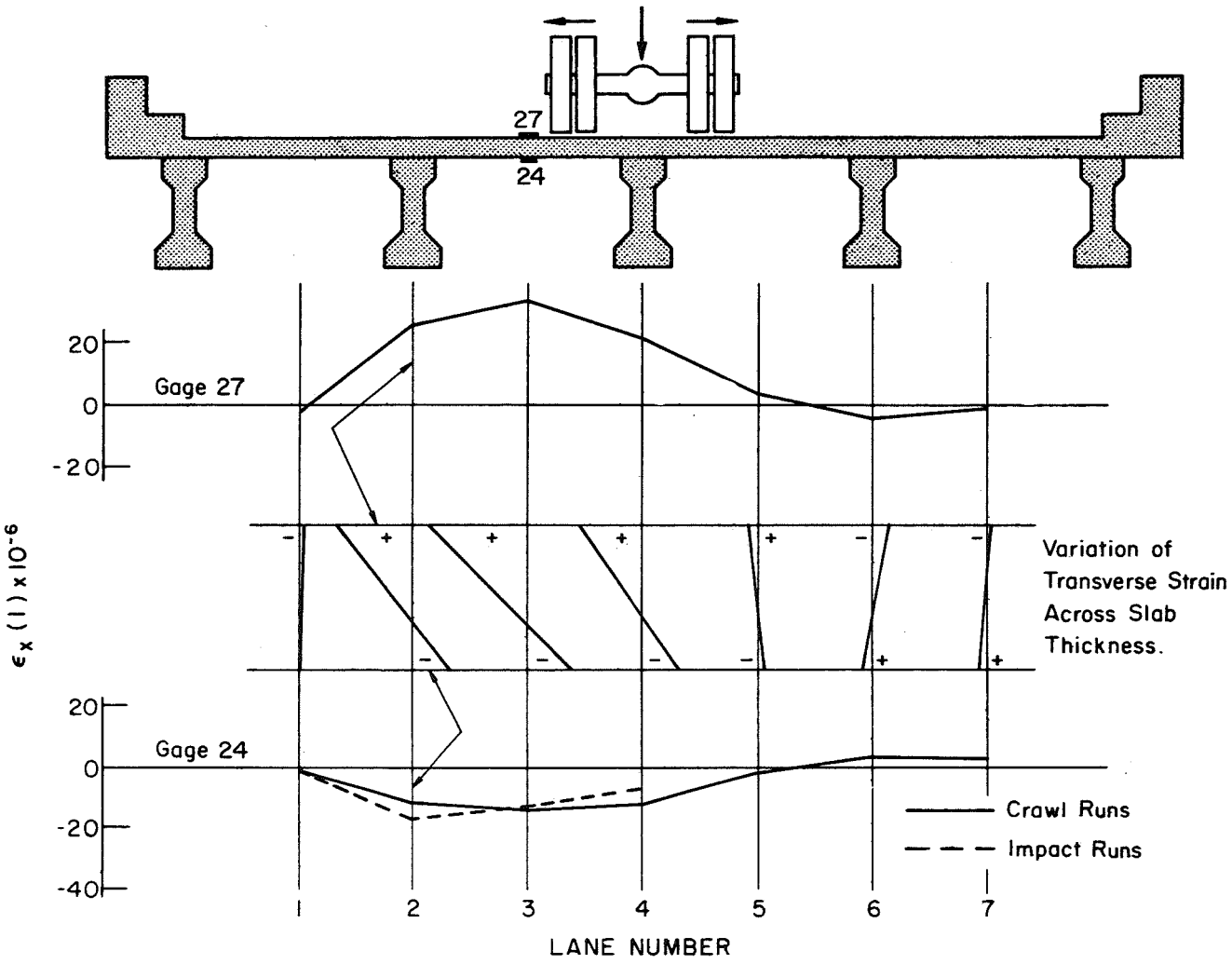

Fig. 29 Variation of Transverse Strain $\epsilon_x(1)$ Across Slab Thickness
Gages 27 and 24

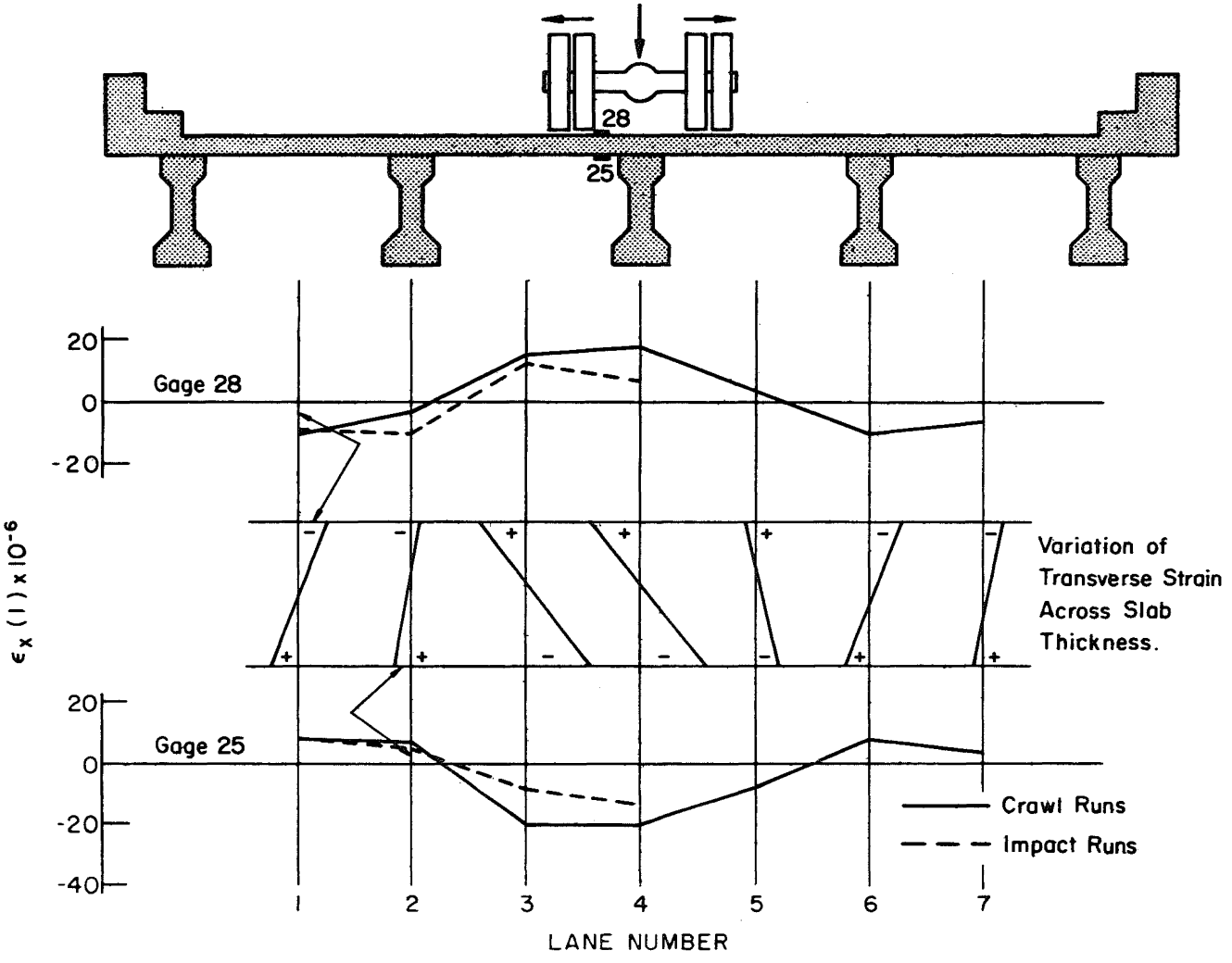

Fig. 30 Variation of Transverse Strain $\epsilon_x(1)$ Across Slab Thickness Gages 28 and 25

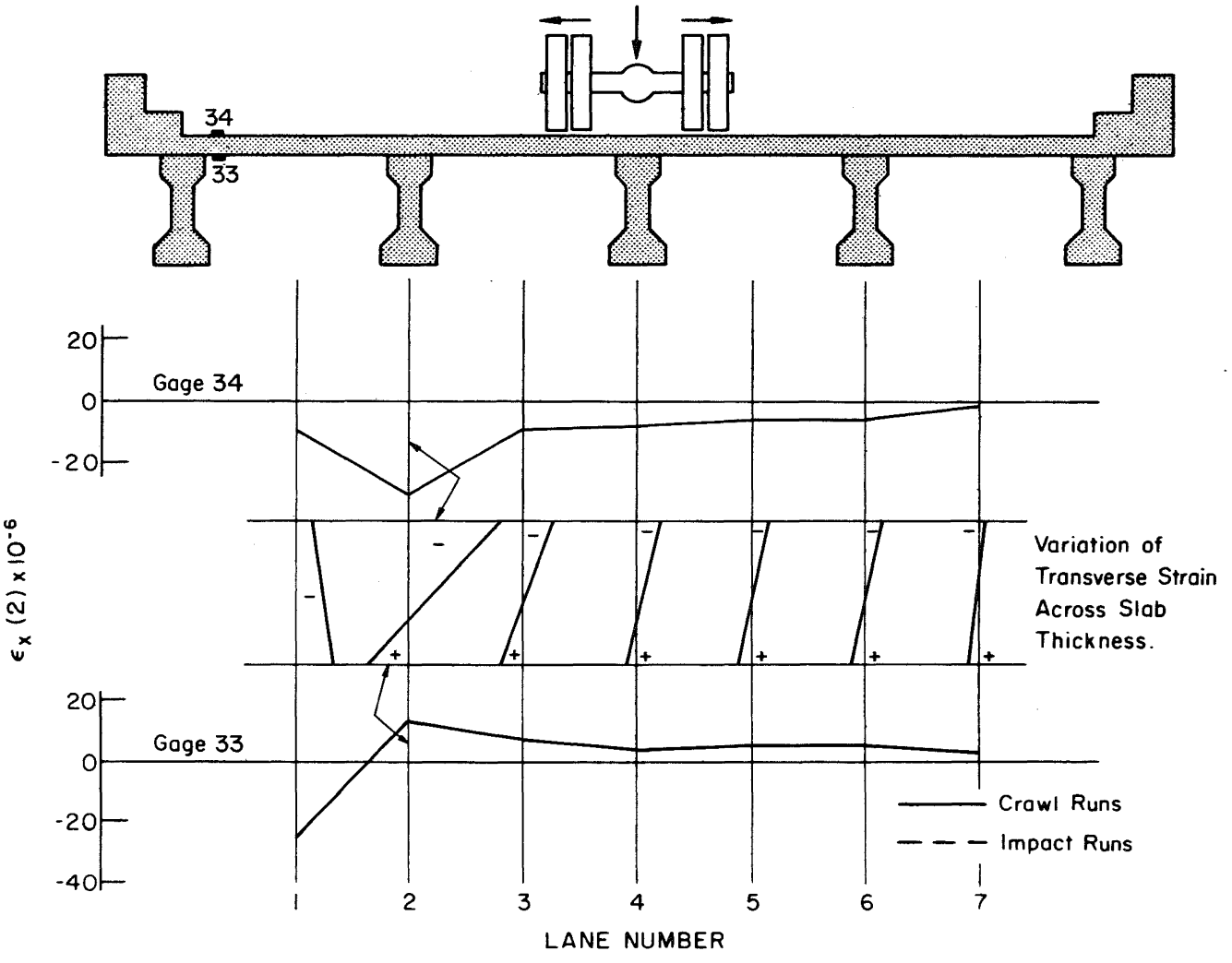

Fig. 31 Variation of Transverse Strains $\epsilon_x(2)$ Across Slab Thickness Gages 34 and 33

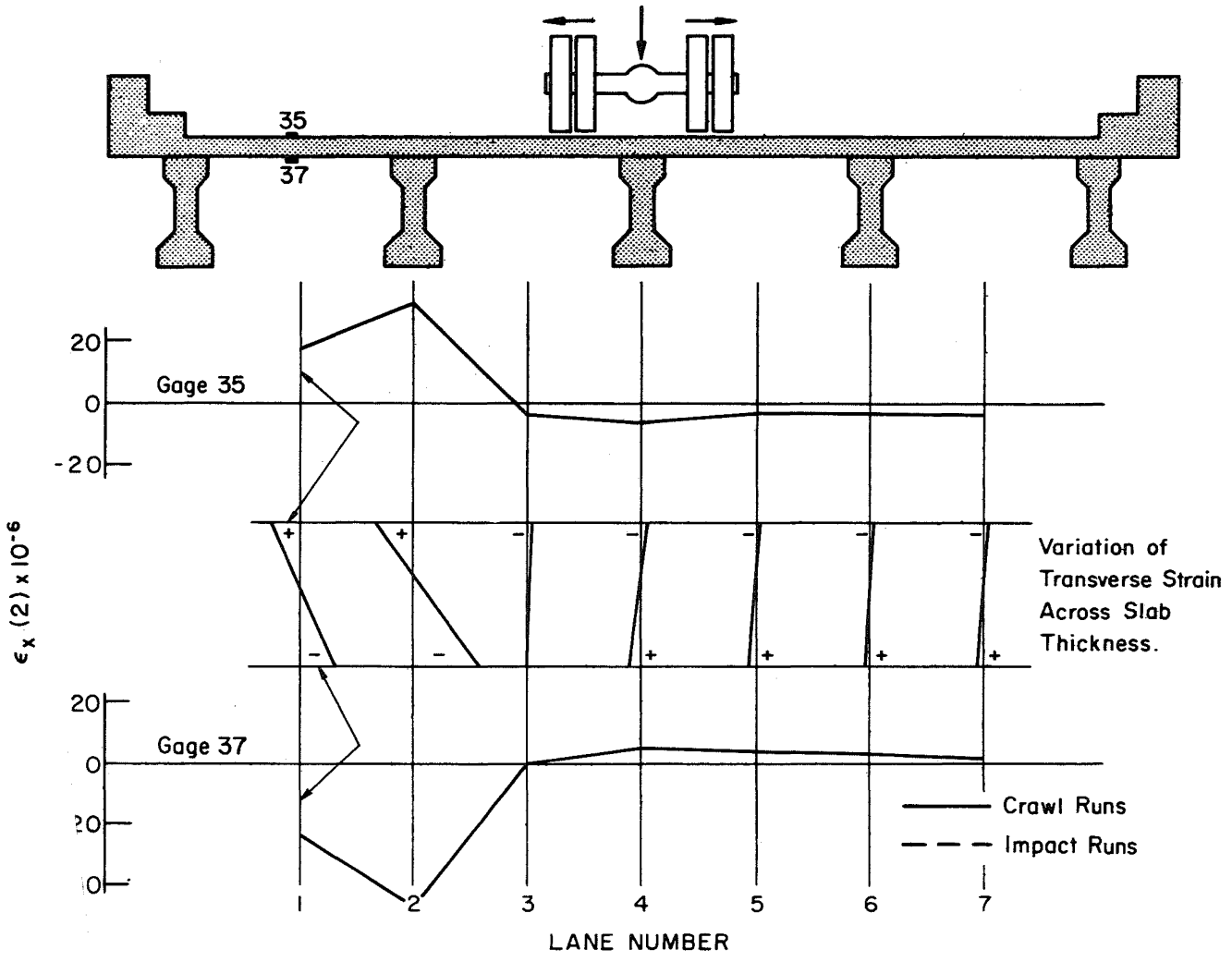

ig. 32 Variation of Transverse Strains ϵ_x(2) Across Slab Thickness
Gages 35 and 37

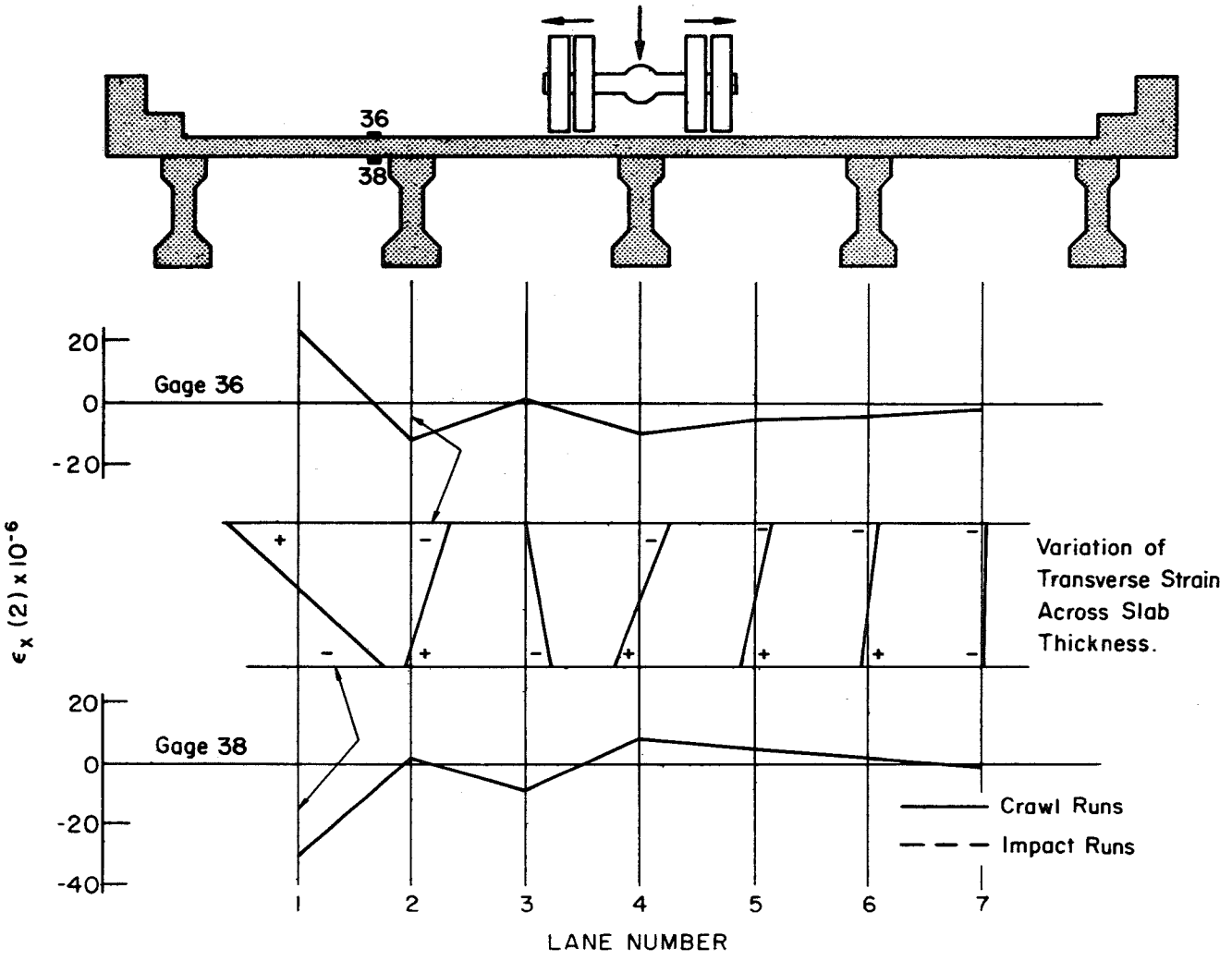

Fig. 33 Variation of Transverse Strains $\epsilon_x(2)$ Across Slab Thickness Gages 36 and 38

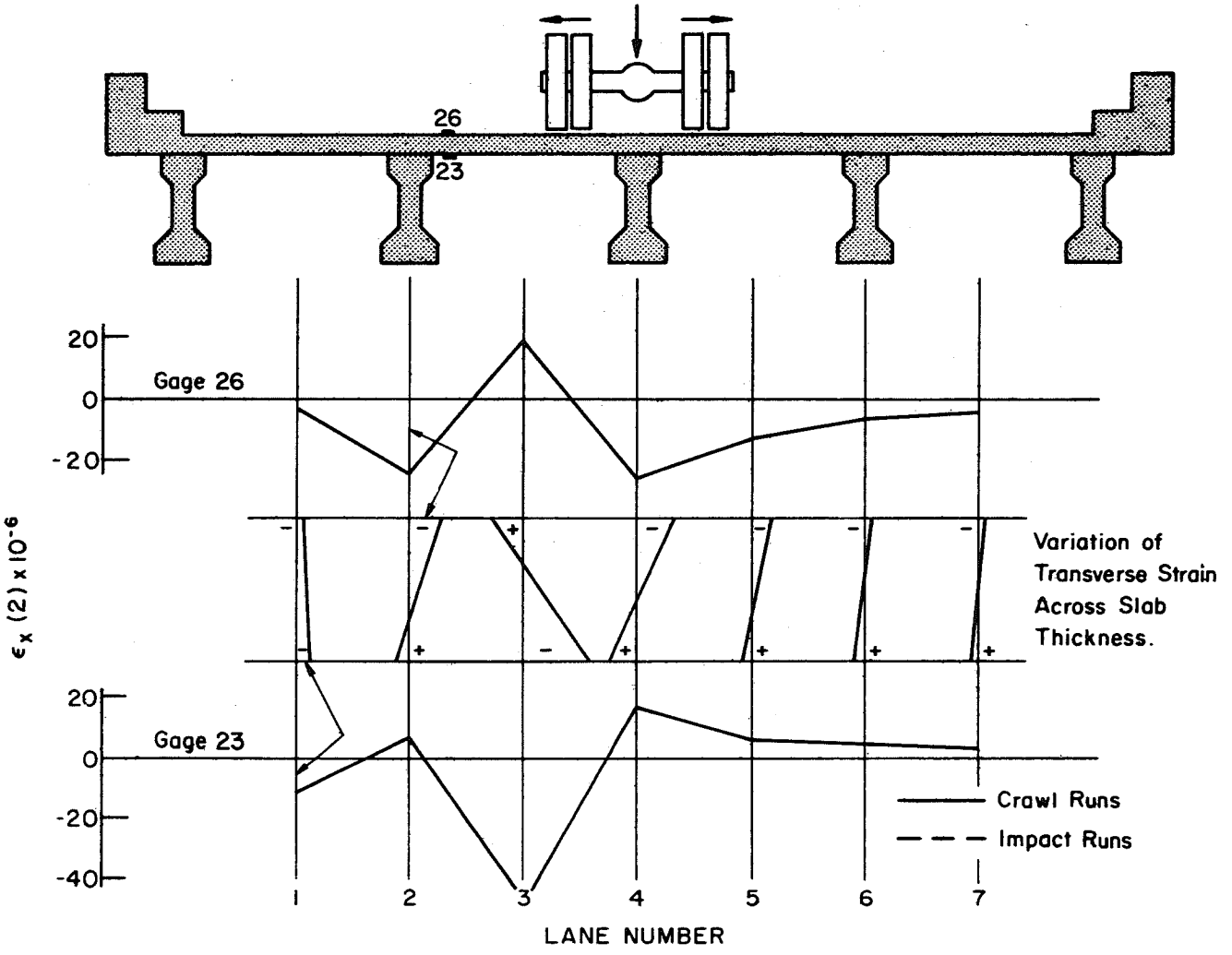

Fig. 34 Variation of Transverse Strains ϵ_x(2) Across Slab Thickness
Gages 26 and 23

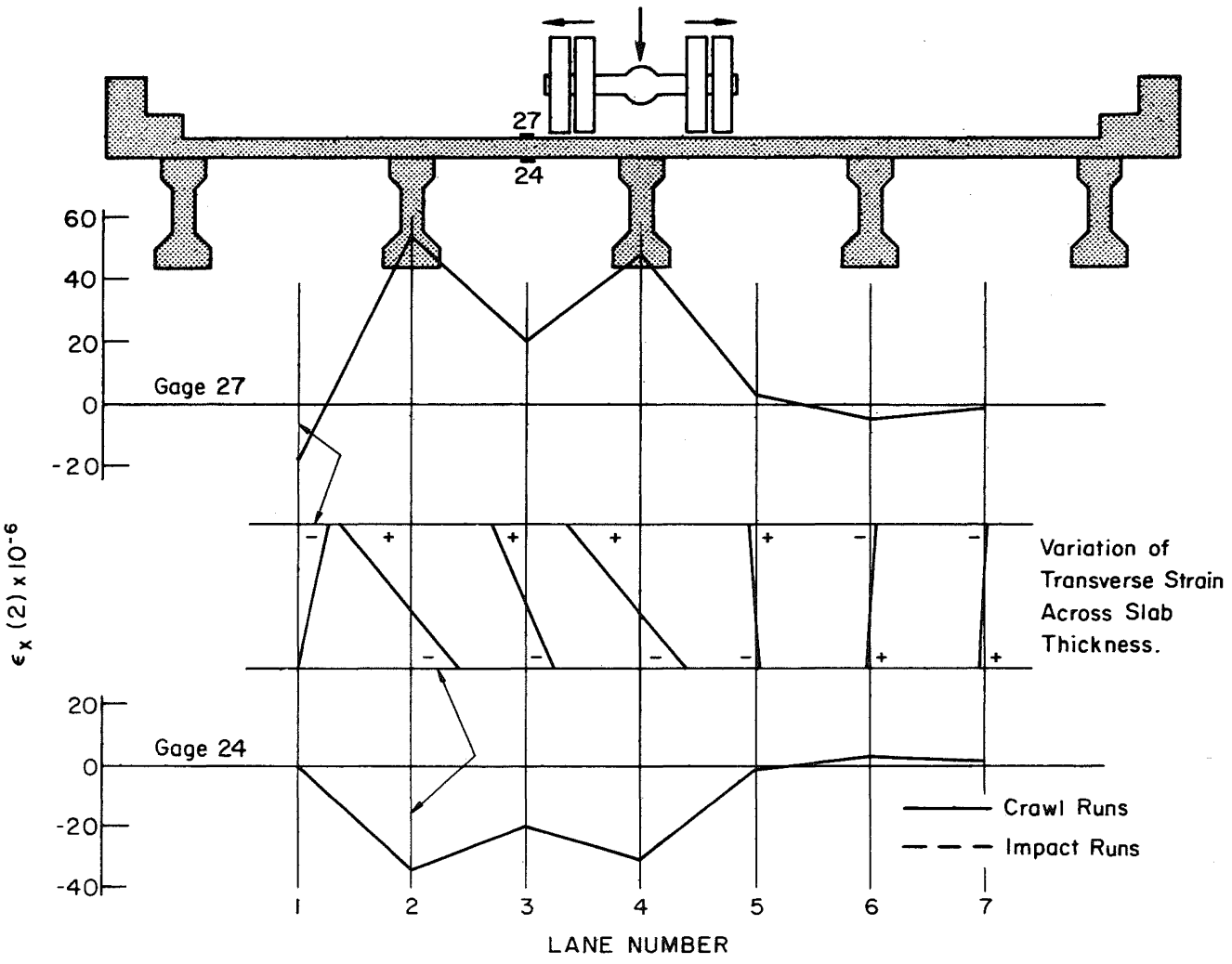

Fig. 35 Variation of Transverse Strains $\epsilon_x(2)$ Across Slab Thickness
Gages 27 and 24

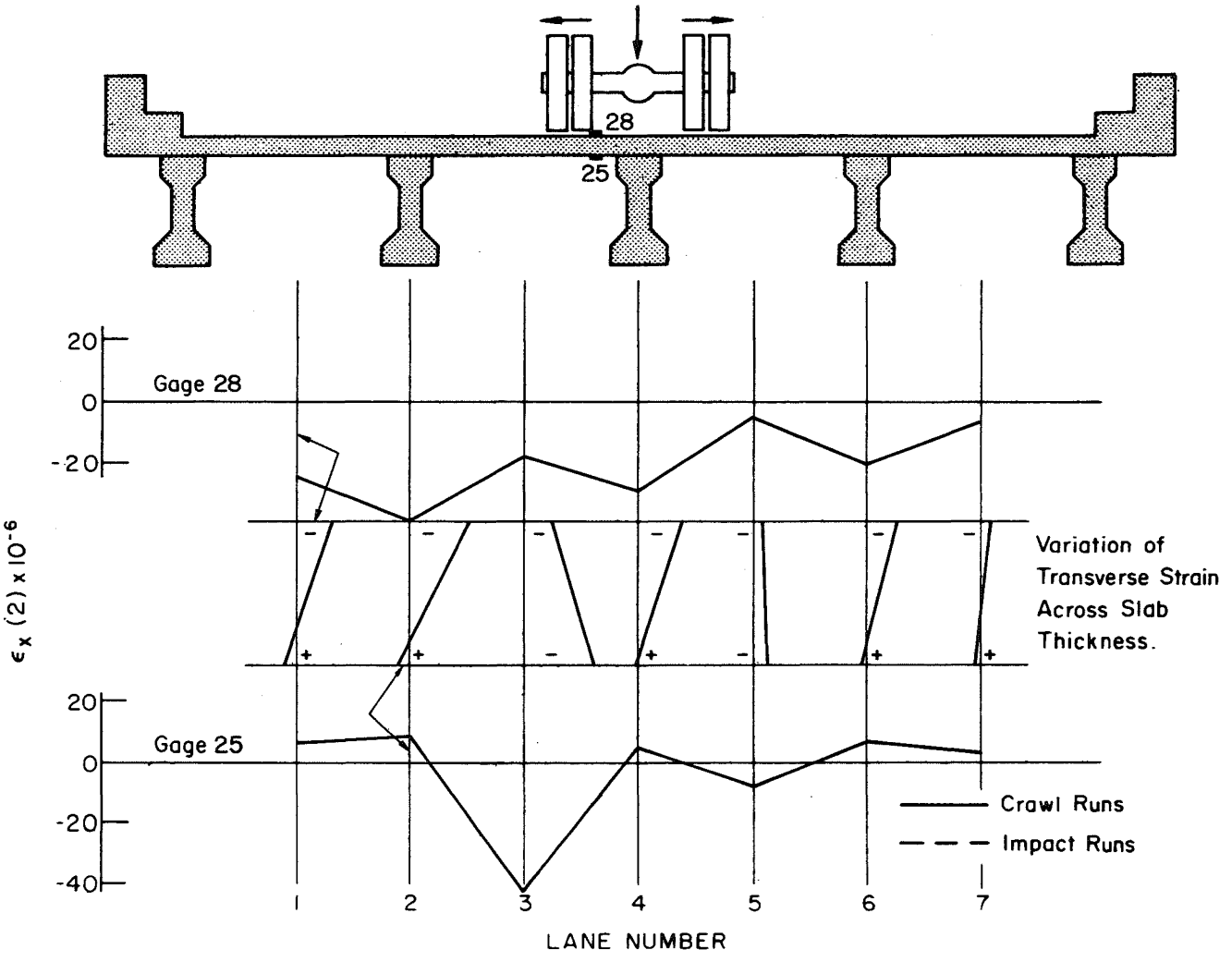

Fig. 36 Variation of Transverse Strains $\epsilon_x(2)$ Across Slab Thickness Gages 28 and 25

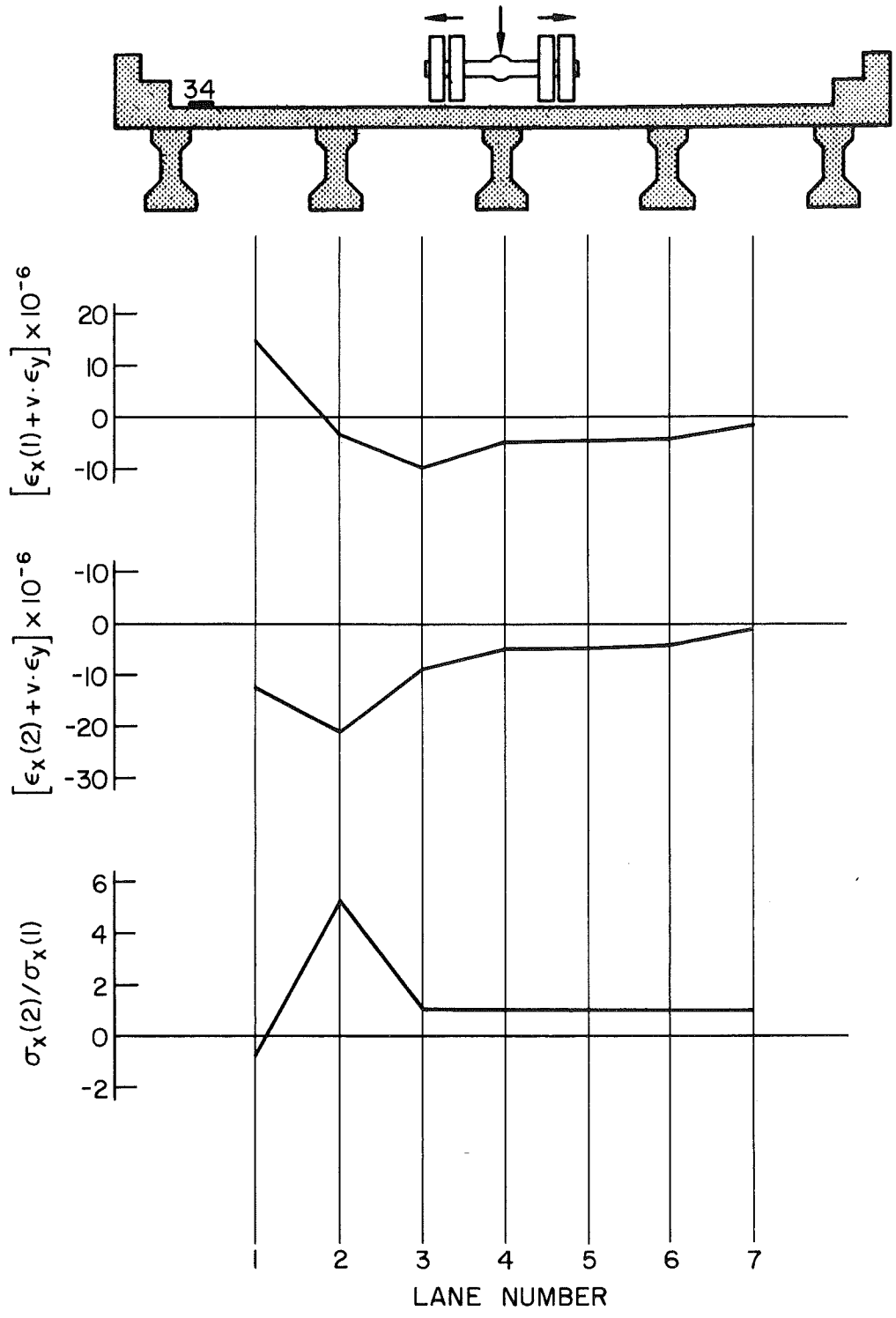

Fig. 37 Influence Lines for Transverse Strains - Crawl Runs
Gage 34

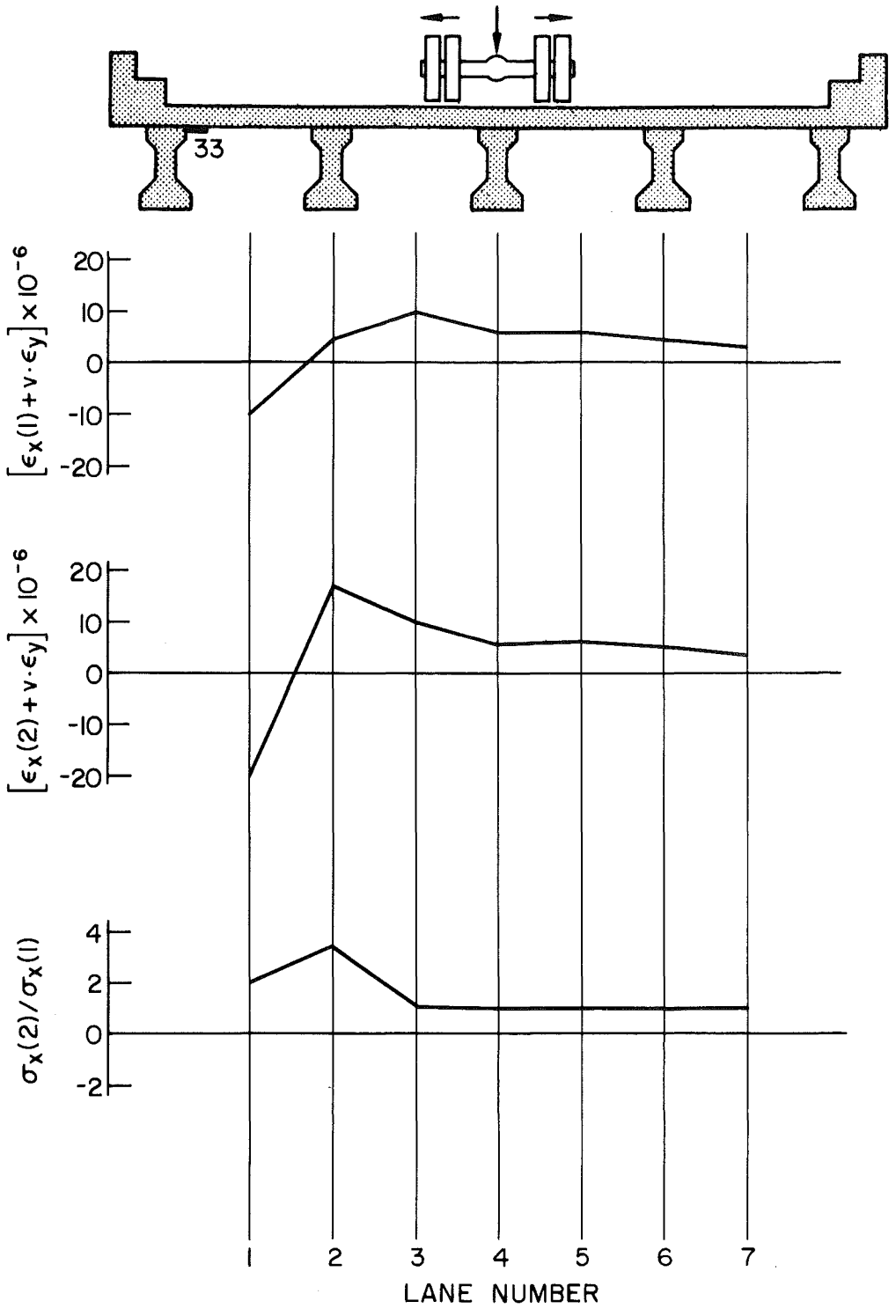

Fig. 38 Influence Lines for Transverse Strains - Crawl Runs
Gage 33

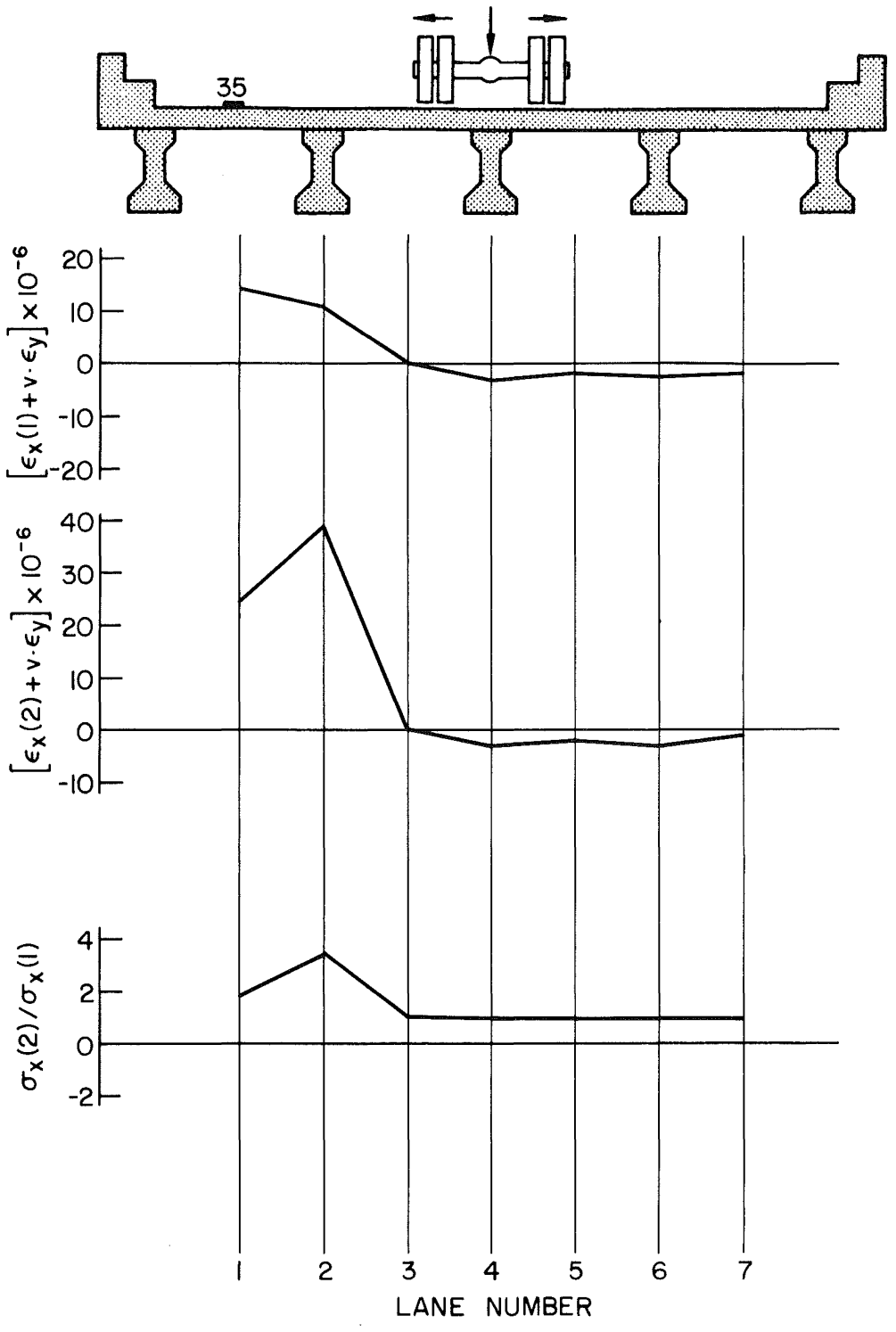

Fig. 39 Influence Lines for Transverse Strains - Crawl Runs
Gage 35

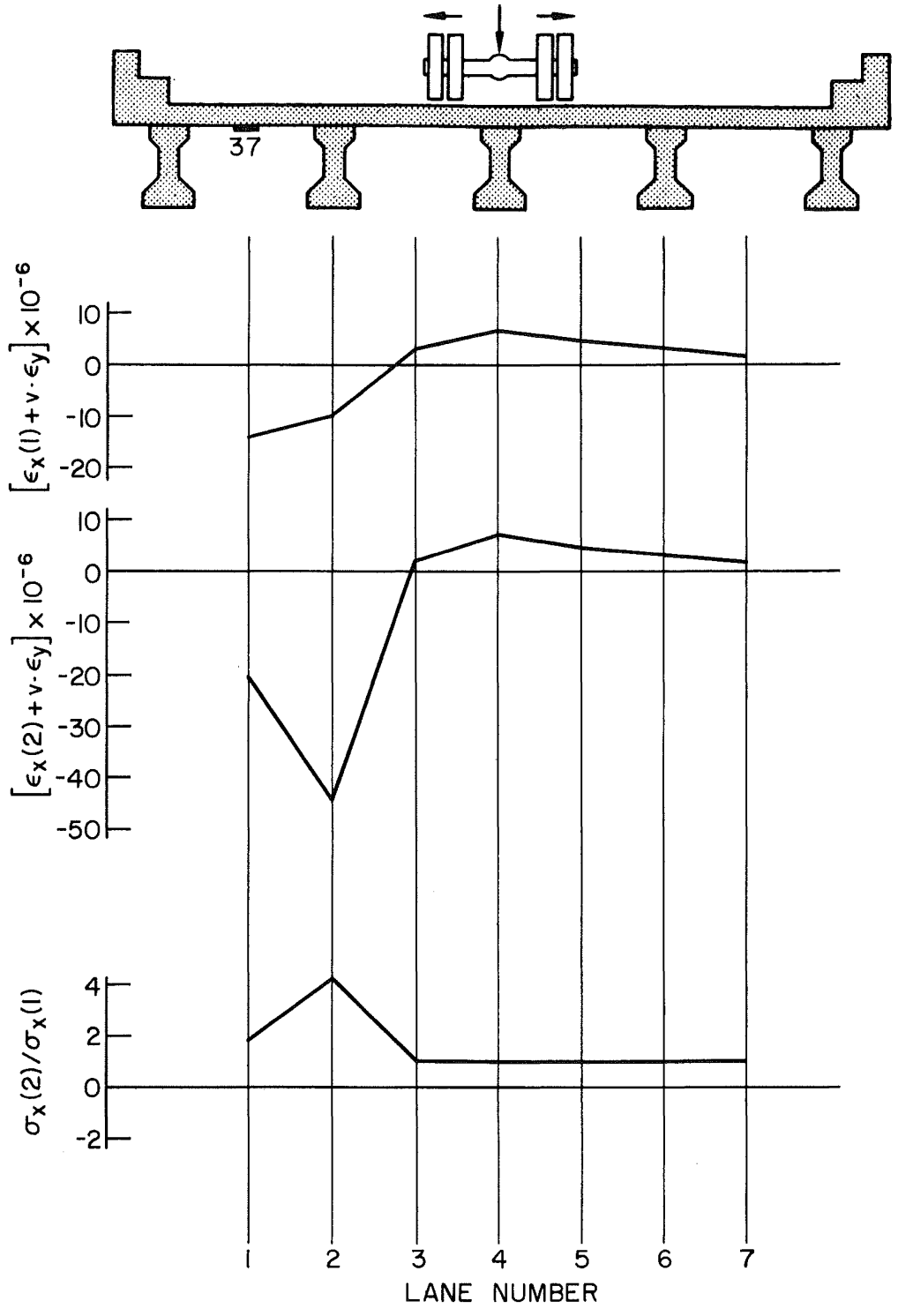

Fig. 40 Influence Lines for Transverse Strains - Crawl Runs
Gage 37

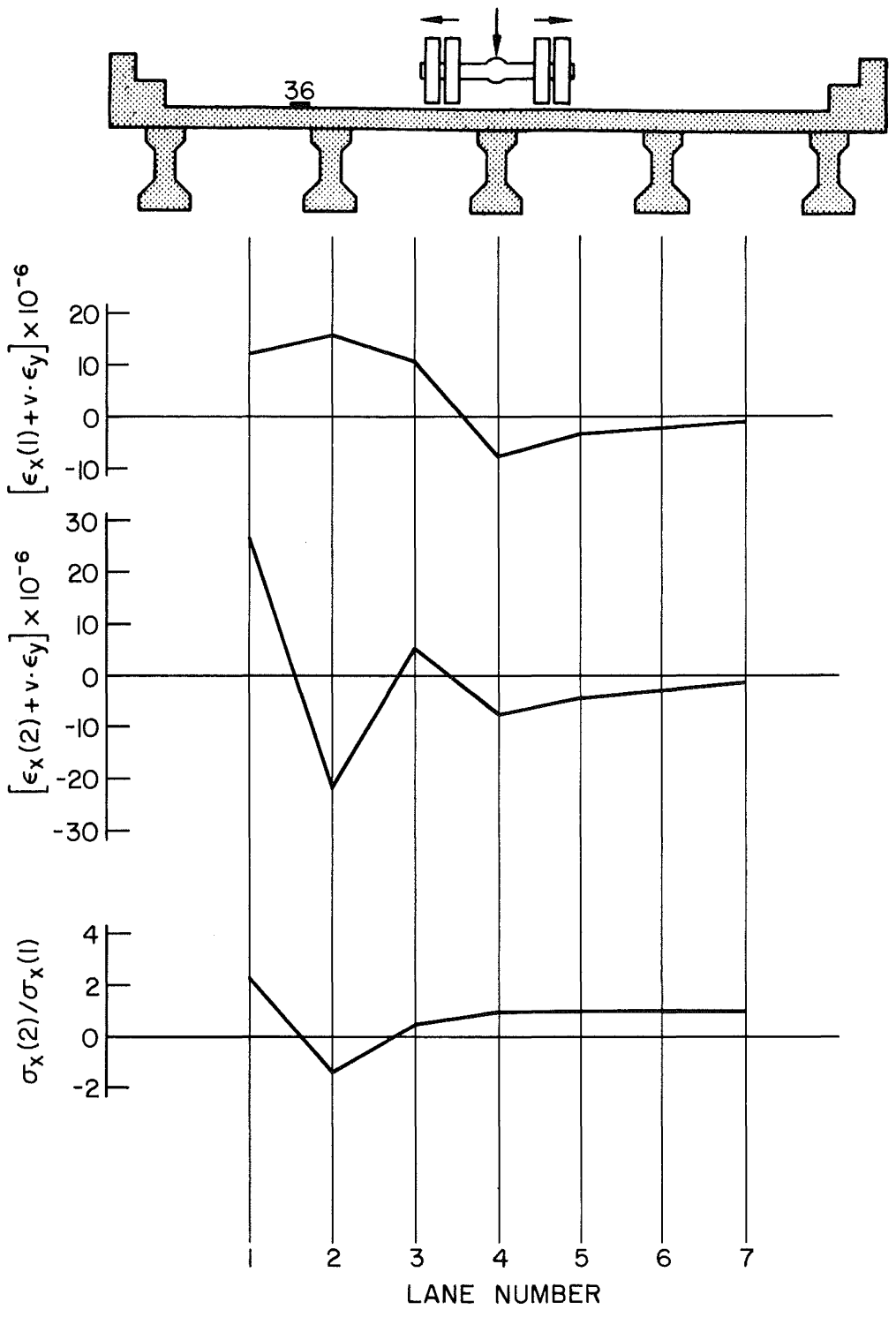

Fig. 41 Influence Lines for Transverse Strains - Crawl Runs
Gage 36

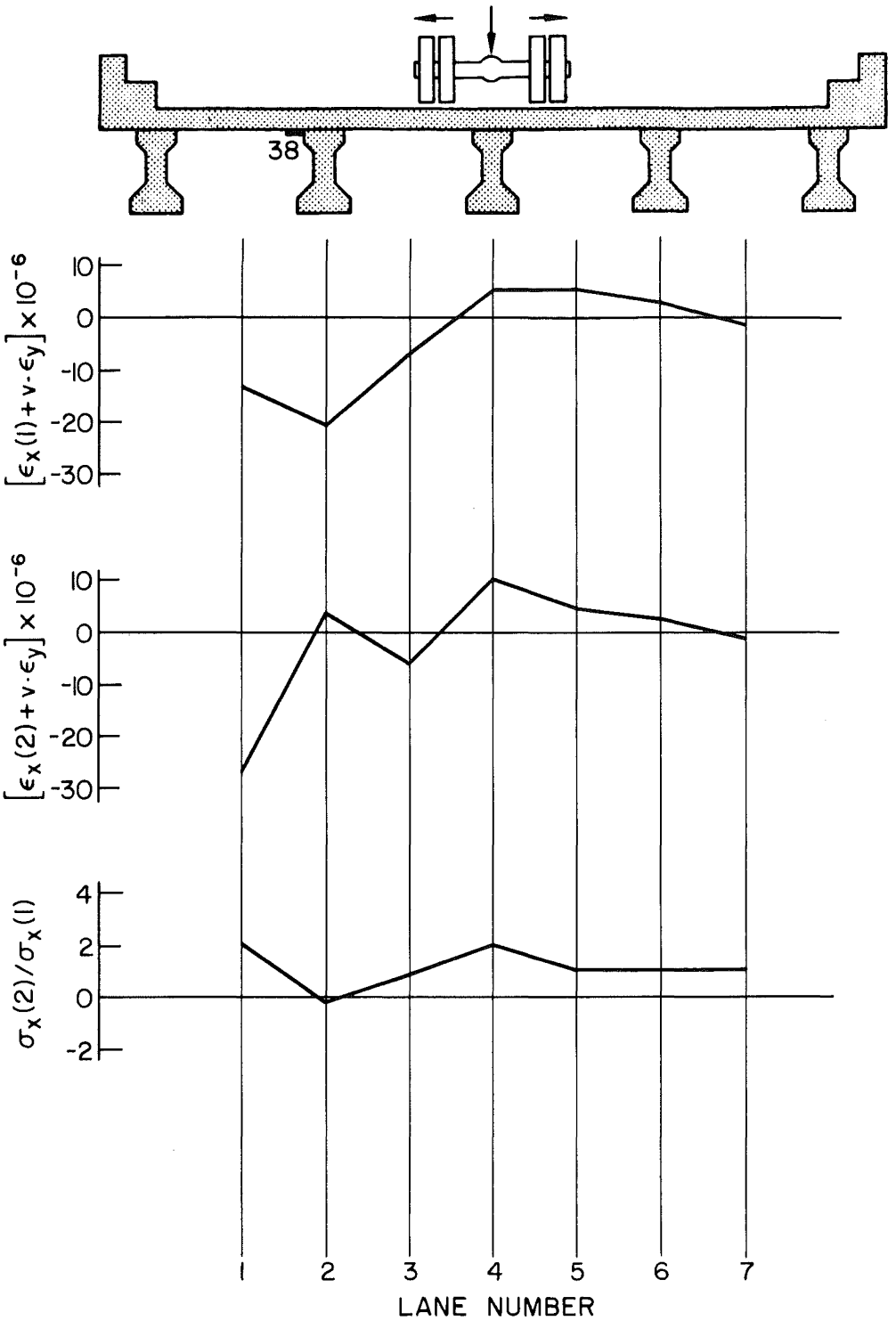

Fig. 42 Influence Lines for Transverse Strains - Crawl Runs
Gage 38

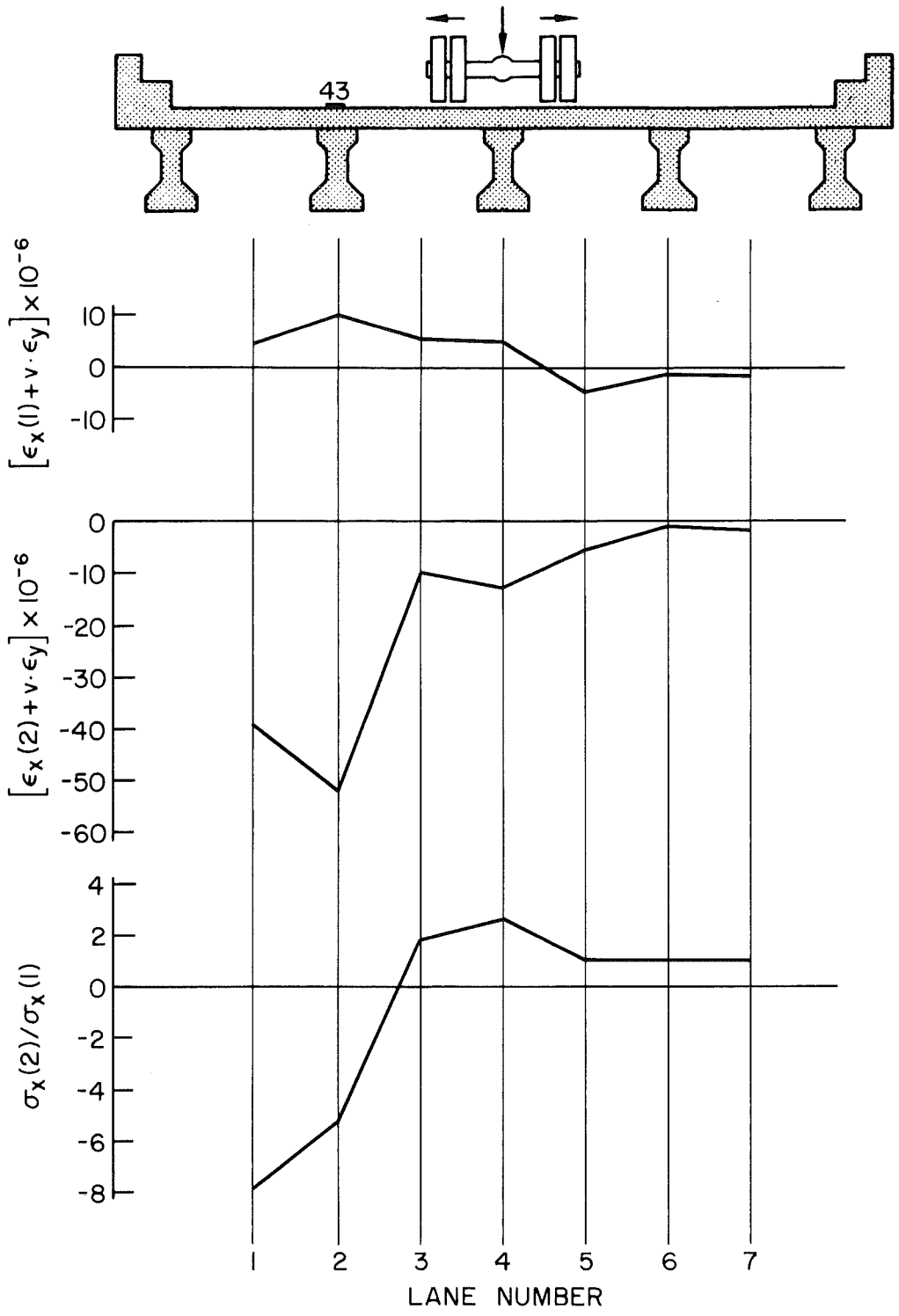

Fig. 43 Influence Lines for Transverse Strains - Crawl Runs
Gage 43

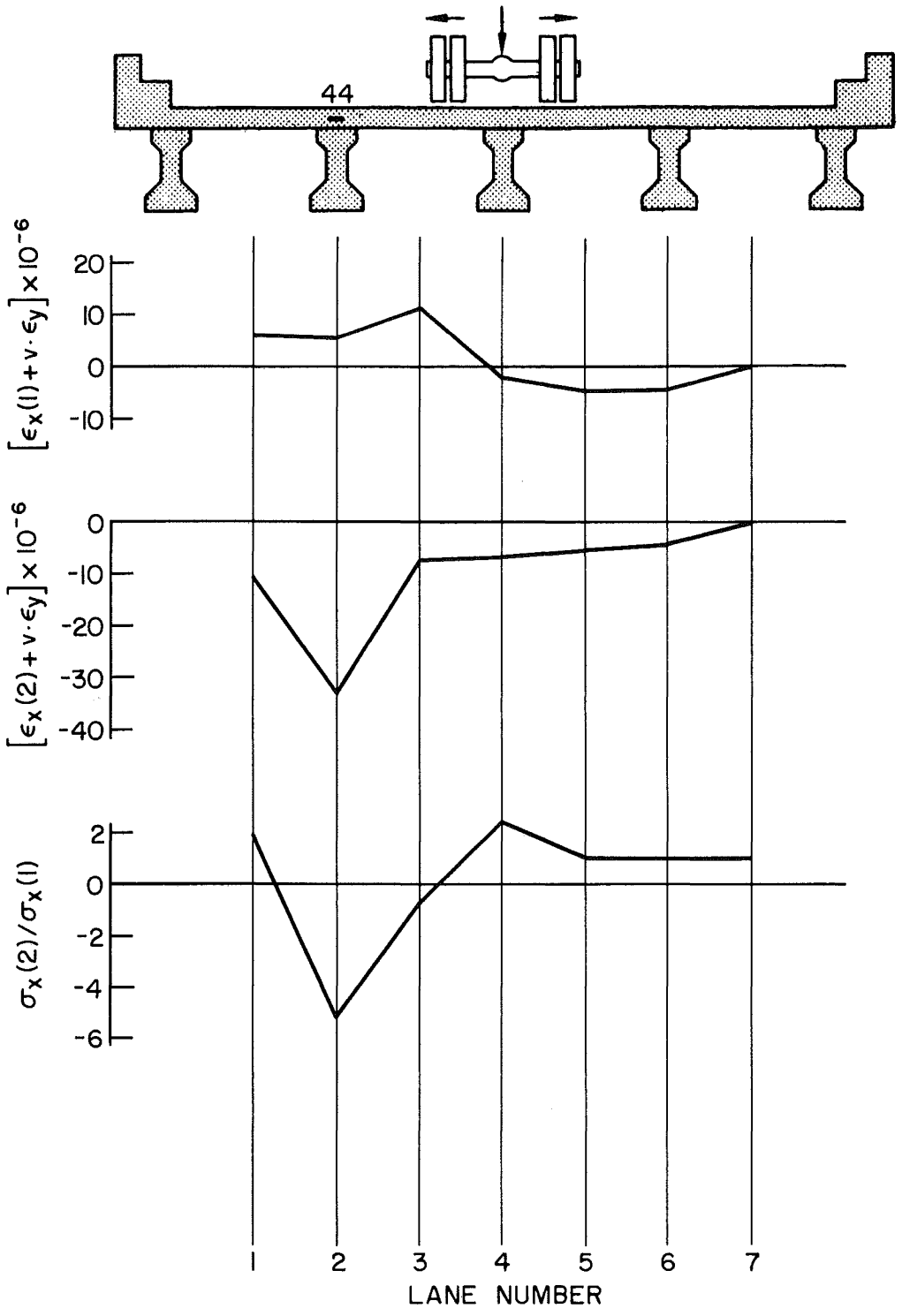

Fig. 44 Influence Lines for Transverse Strains - Crawl Runs
Gage 44

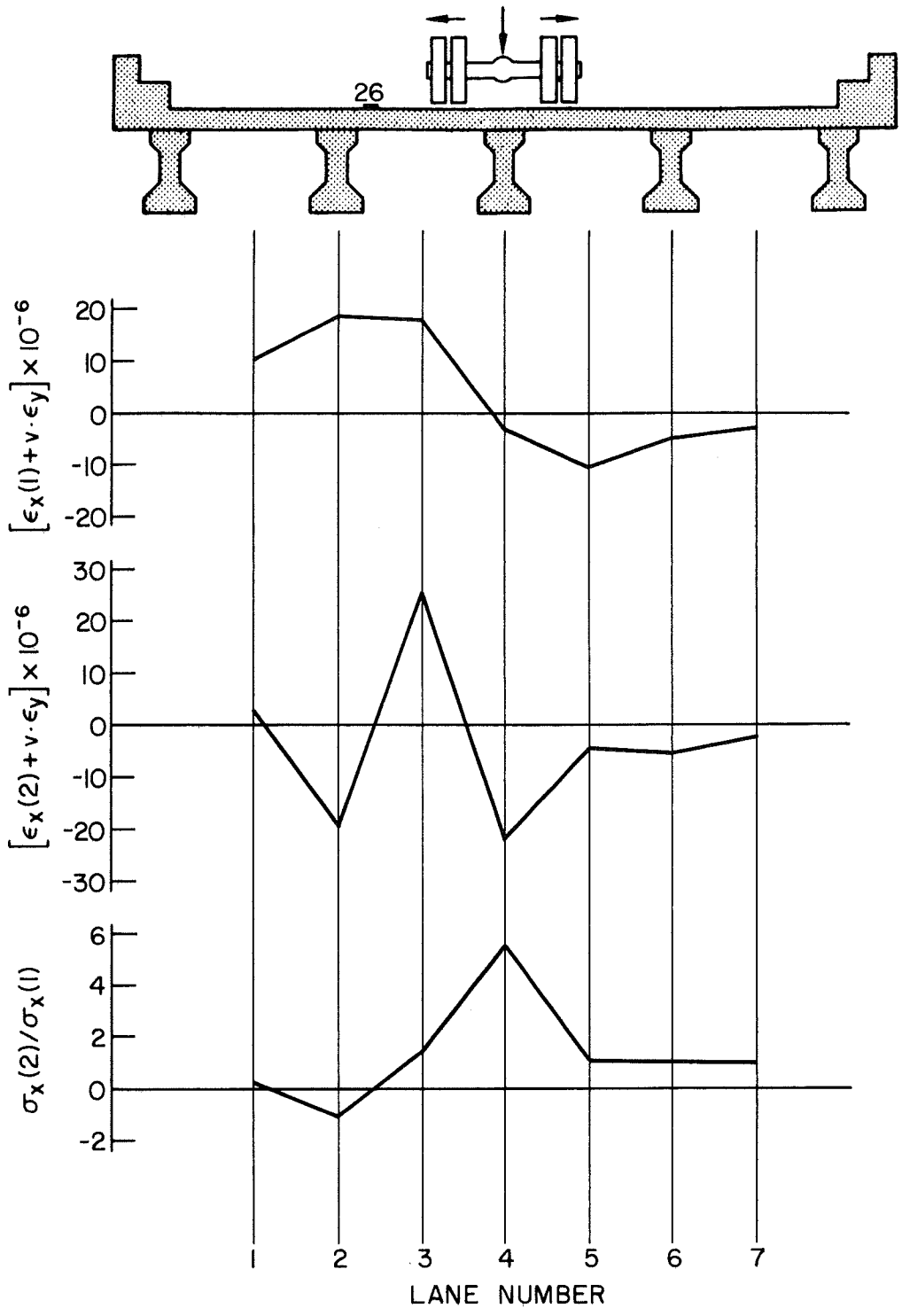

Fig. 45 Influence Lines for Transverse Strains - Crawl Runs
Gage 26

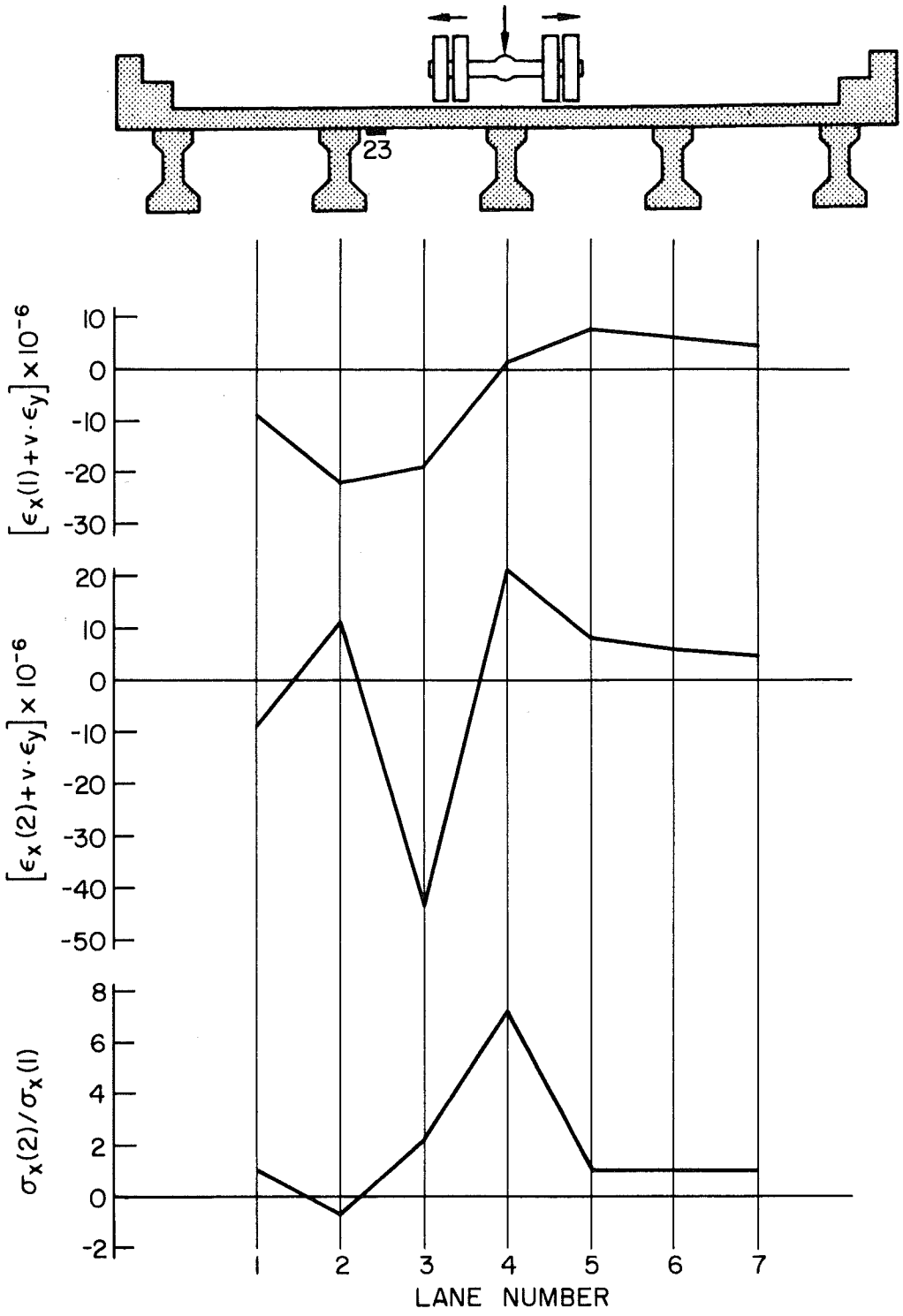

Fig. 46 Influence Lines for Transverse Strains - Crawl Runs
Gage 23

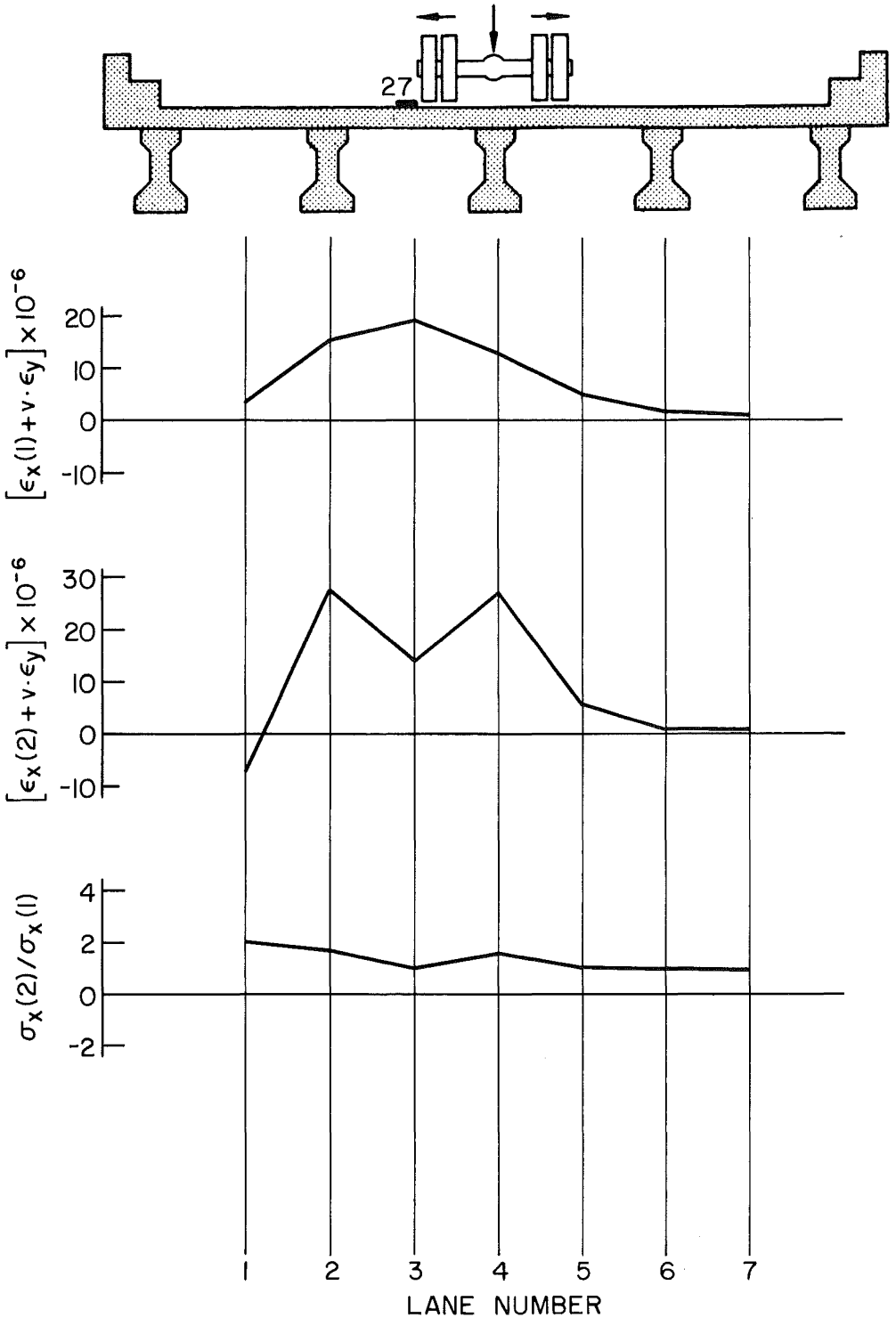

Fig. 47 Influence Lines for Transverse Strains - Crawl Runs
Gage 27

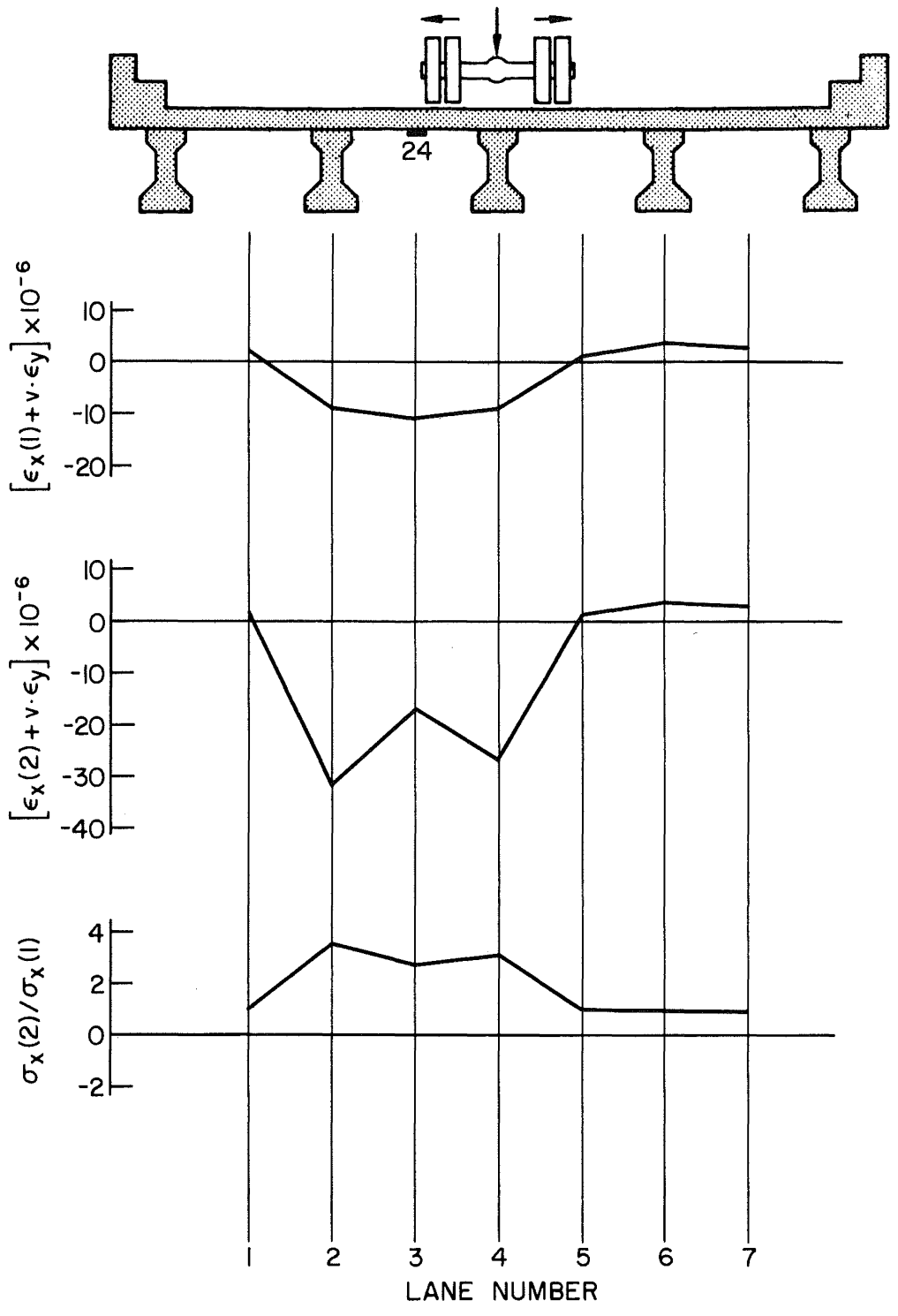

Fig. 48 Influence Lines for Transverse Strains - Crawl Runs
Gage 24

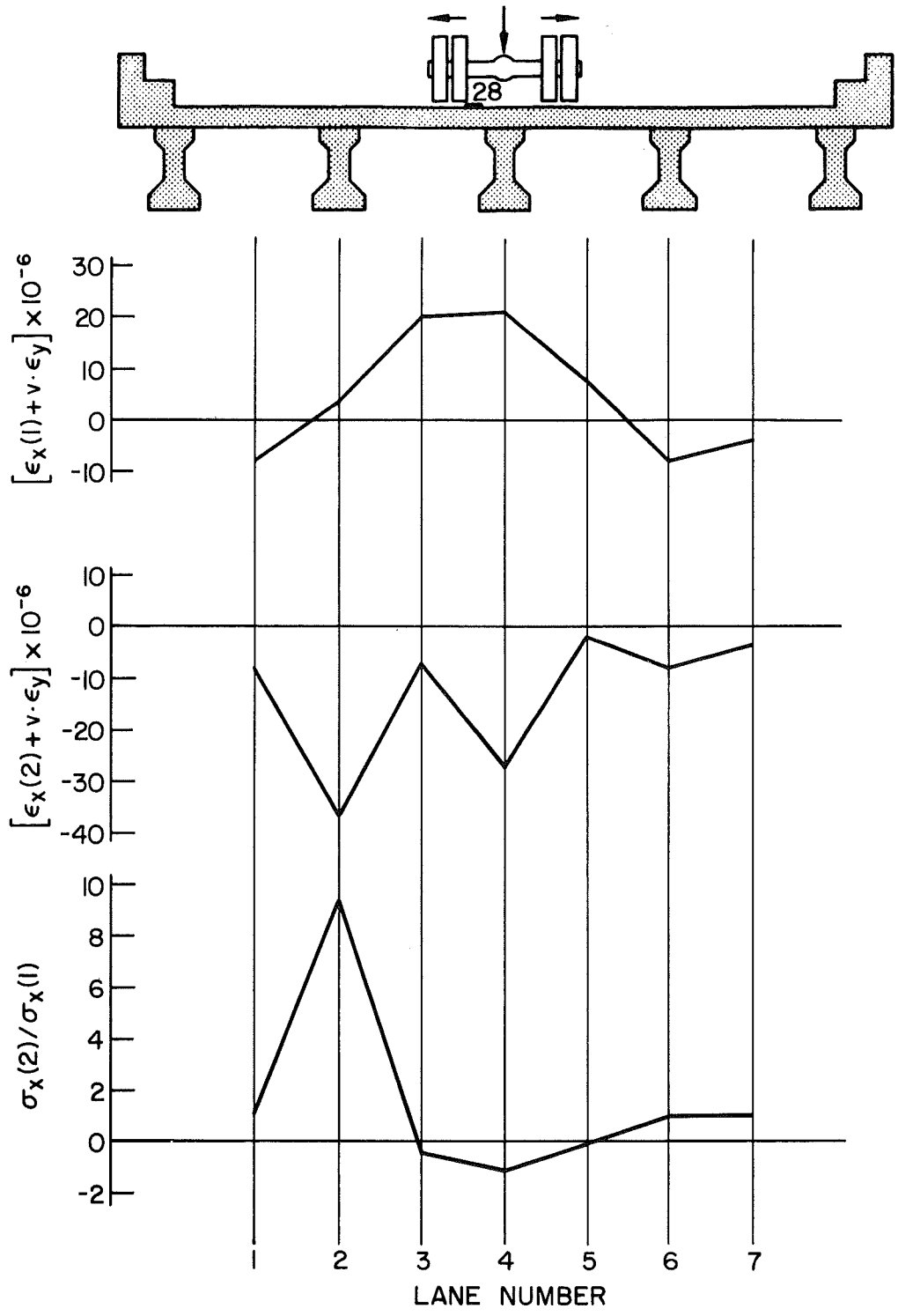

Fig. 49 Influence Lines for Transverse Strains - Crawl Runs
Gage 28

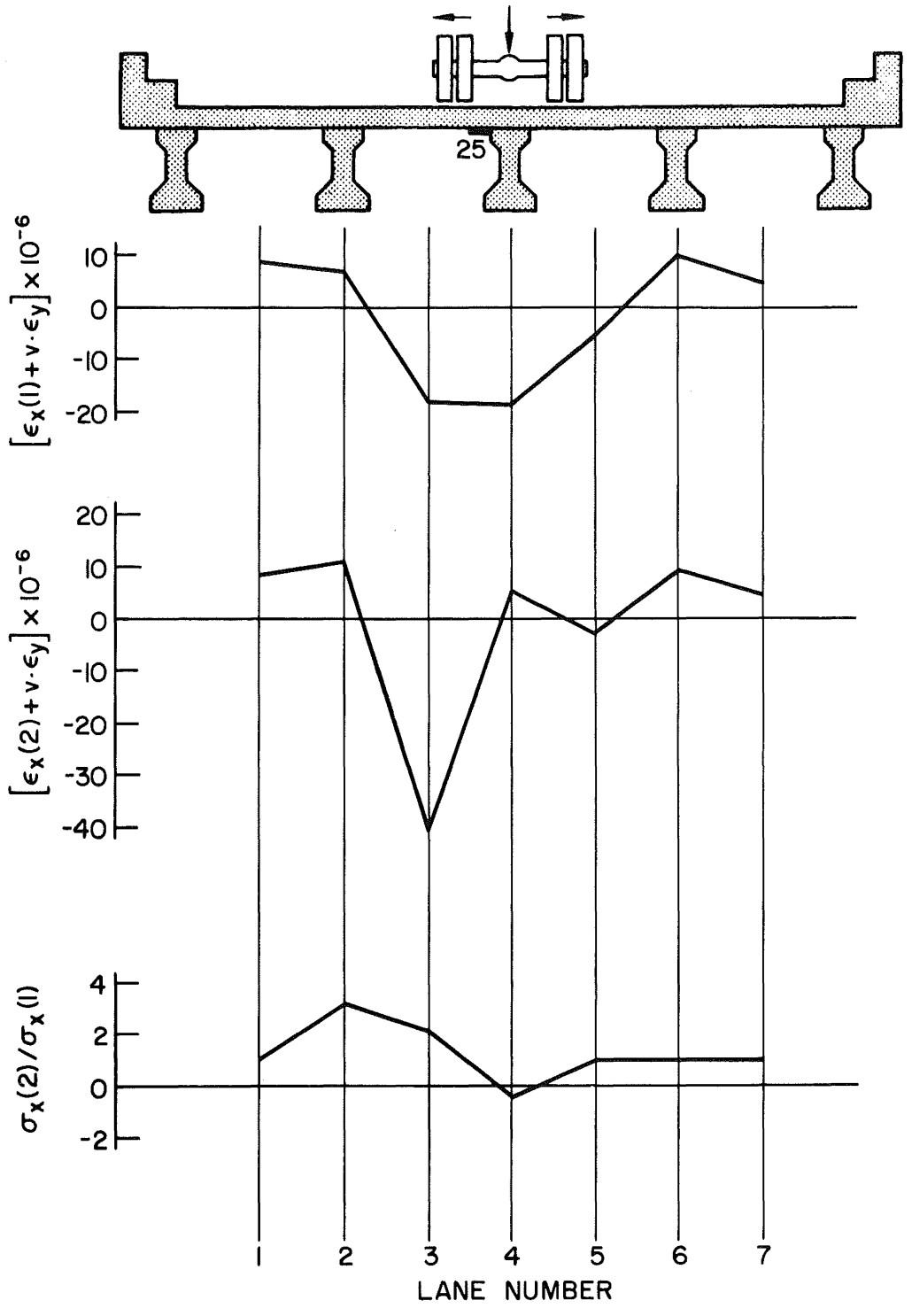

Fig. 50 Influence Lines for Transverse Strains - Crawl Runs
Gage 25

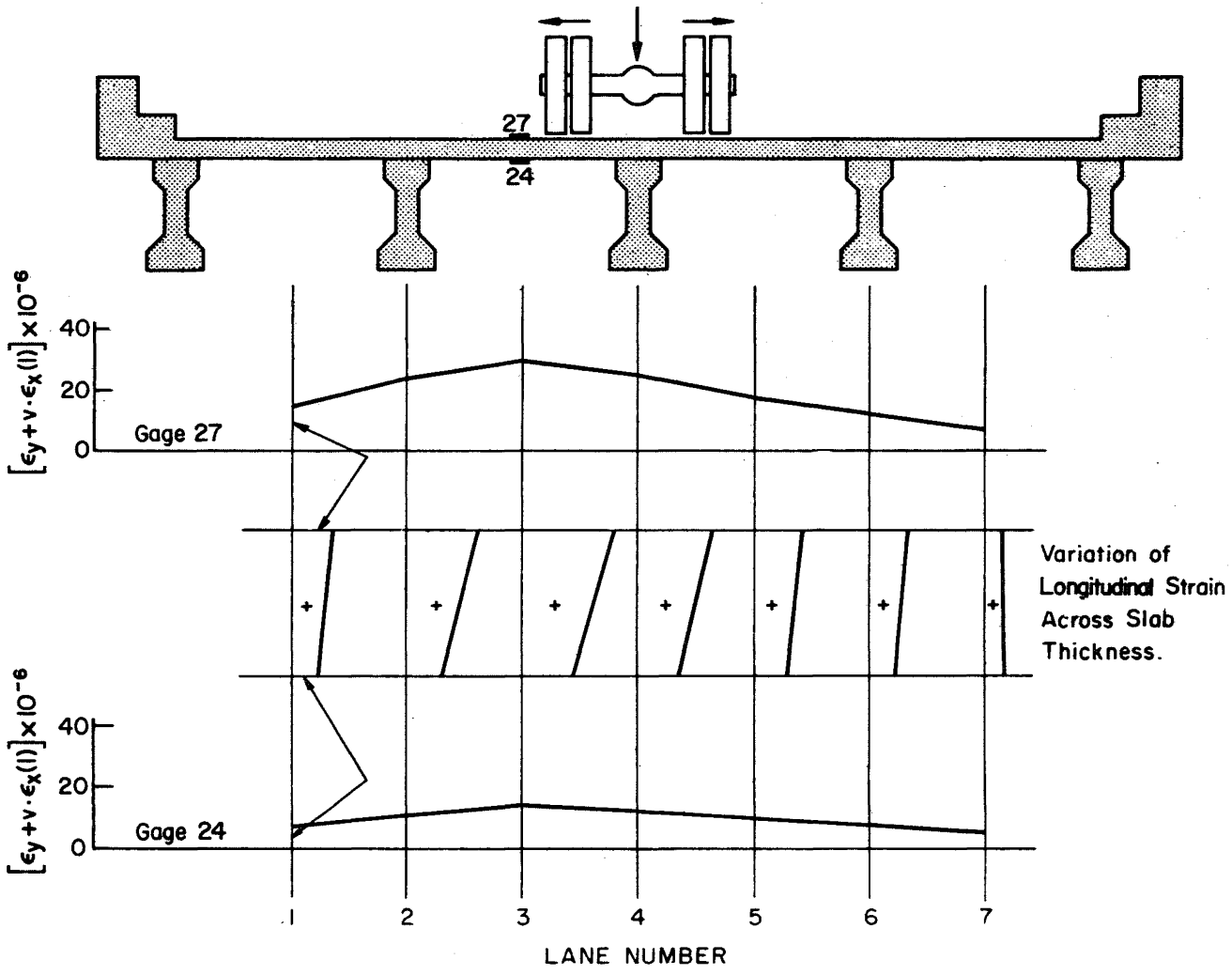

Fig. 51 Variation of Transverse Strains $\epsilon_x(1) + \nu\,\epsilon_y$ Across Slab Thickness Gages 34 and 33

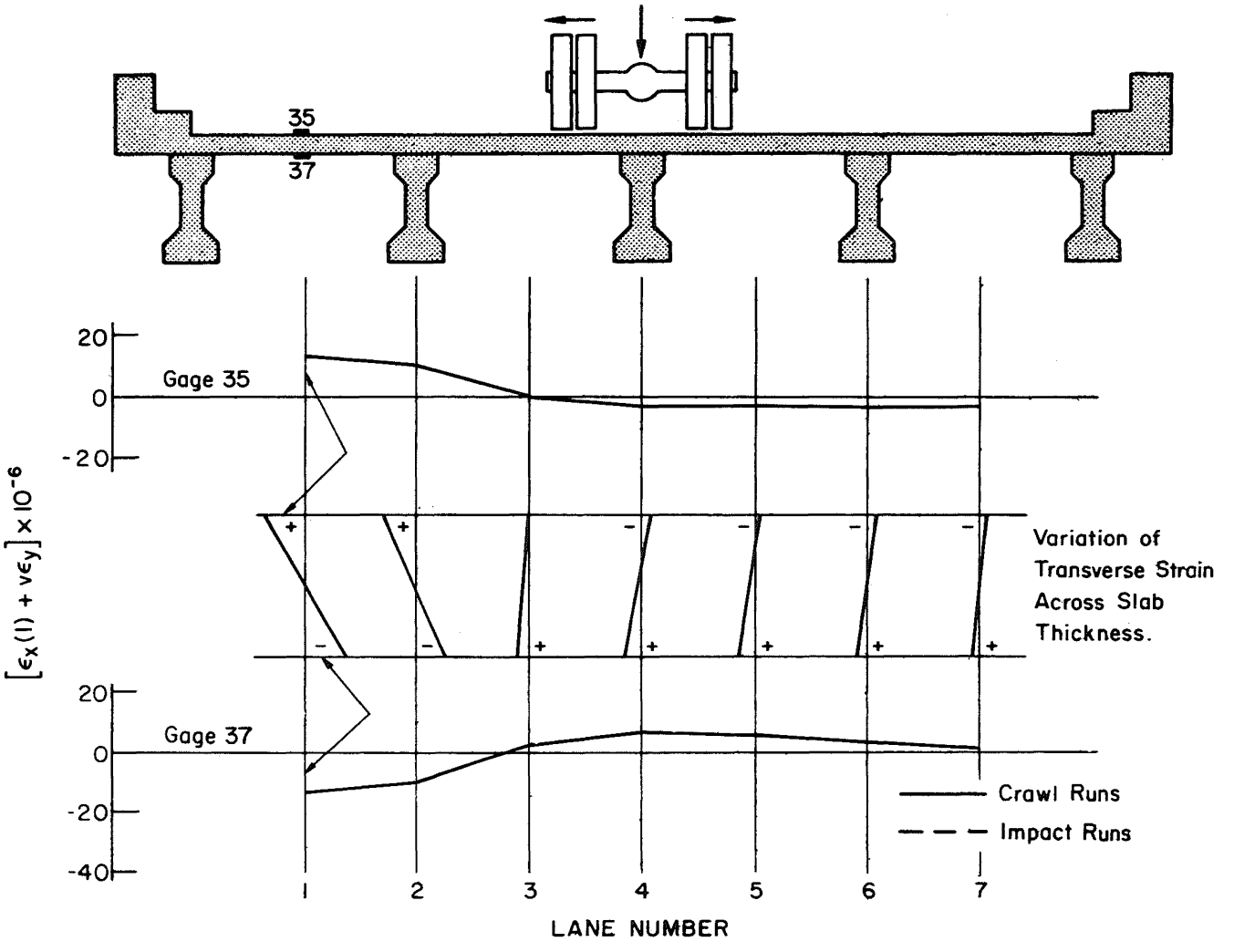

Fig. 52 Variation of Transverse Strains $\epsilon_x(1) + \nu\epsilon_y$ Across Slab Thickness Gages 35 and 37

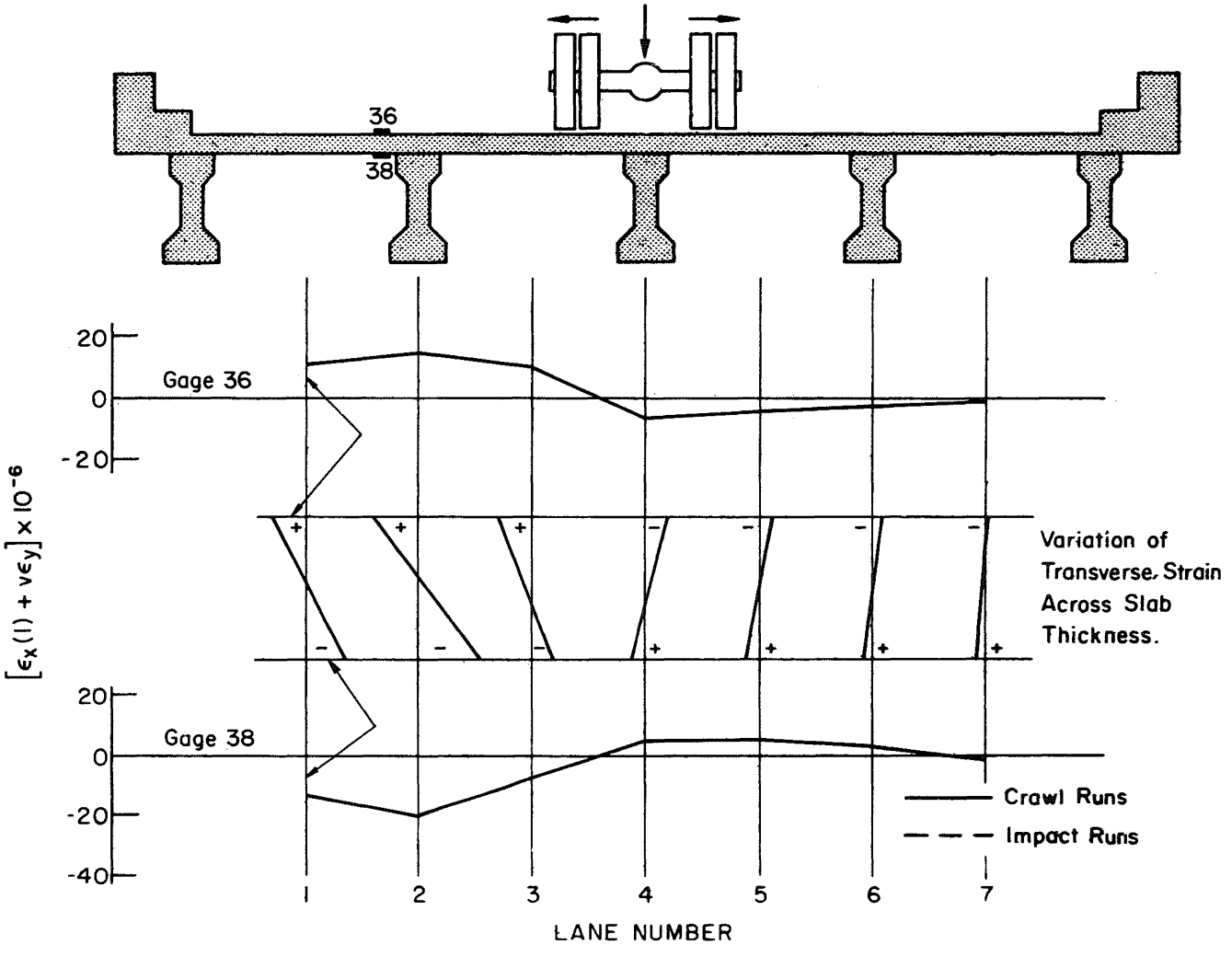

Fig. 53 Variation of Transverse Strains $\epsilon_x(1) + \nu\epsilon_y$ Across Slab Thickness
Gages 36 and 38

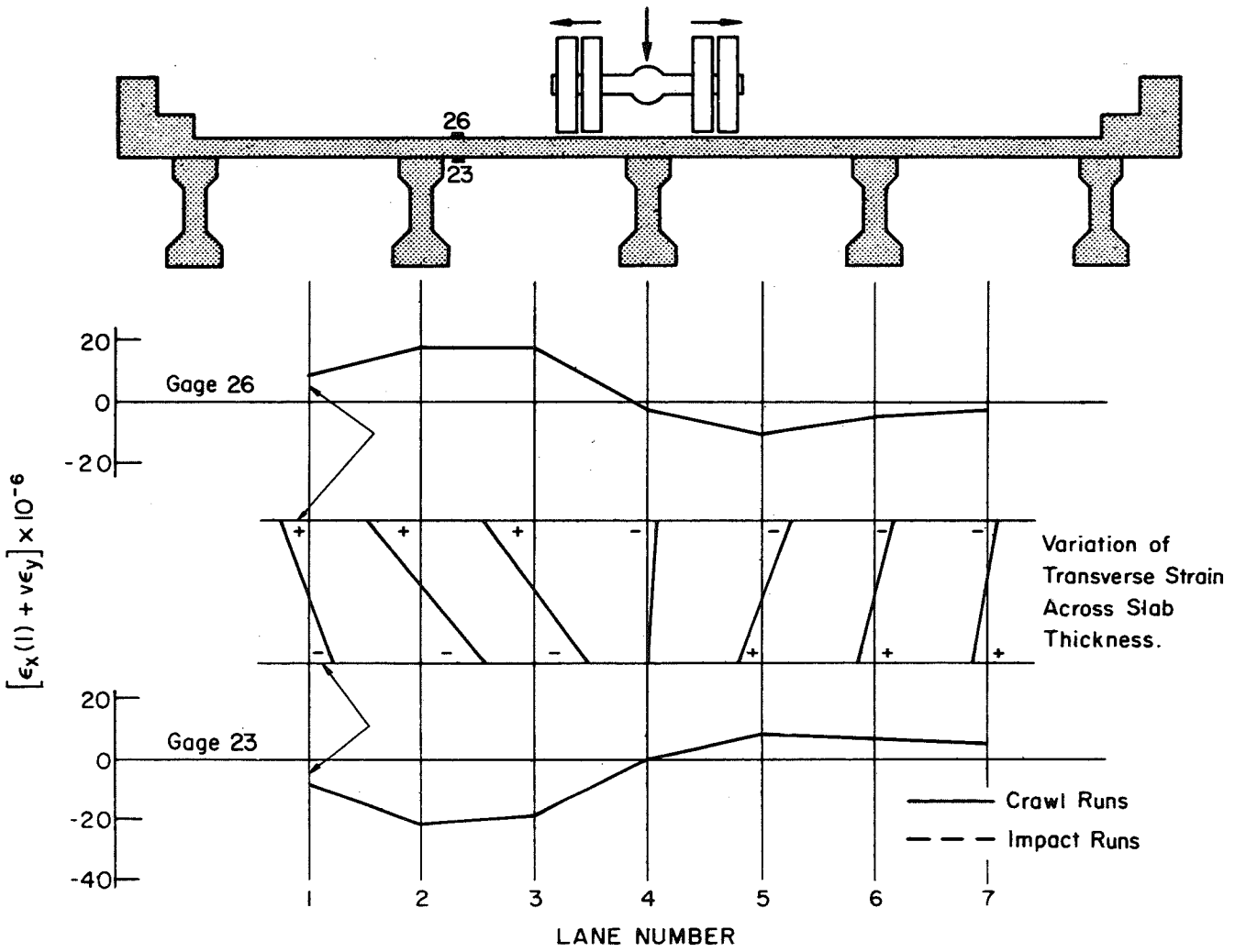

Fig. 54 Variation of Transverse Strains $\epsilon_x(1) + \nu\epsilon_y$ Across Slab Thickness Gages 26 and 23

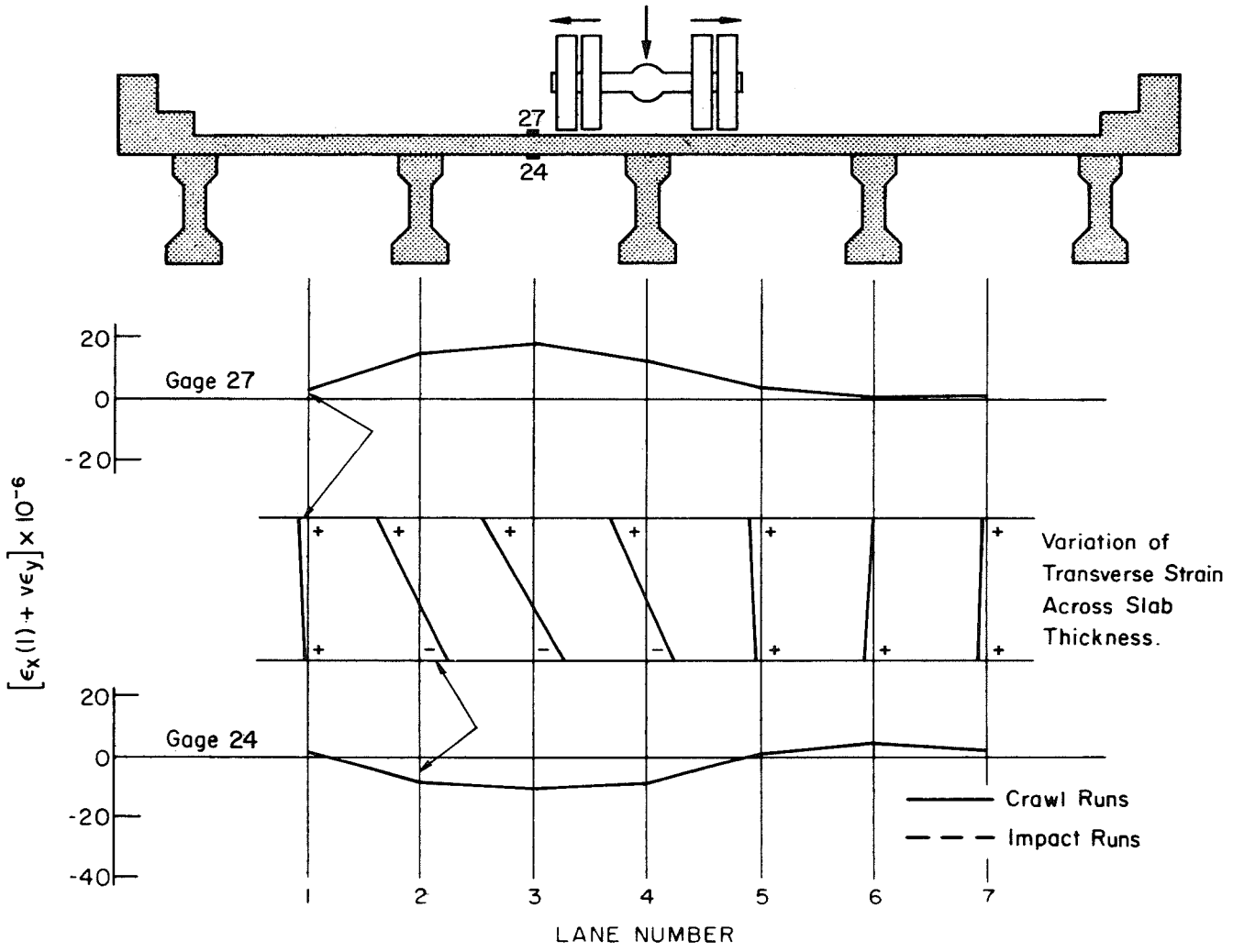

Fig. 55 Variation of Transverse Strains $\epsilon_x(1) + \nu\epsilon_y$ Across Slab Thickness Gages 27 and 24

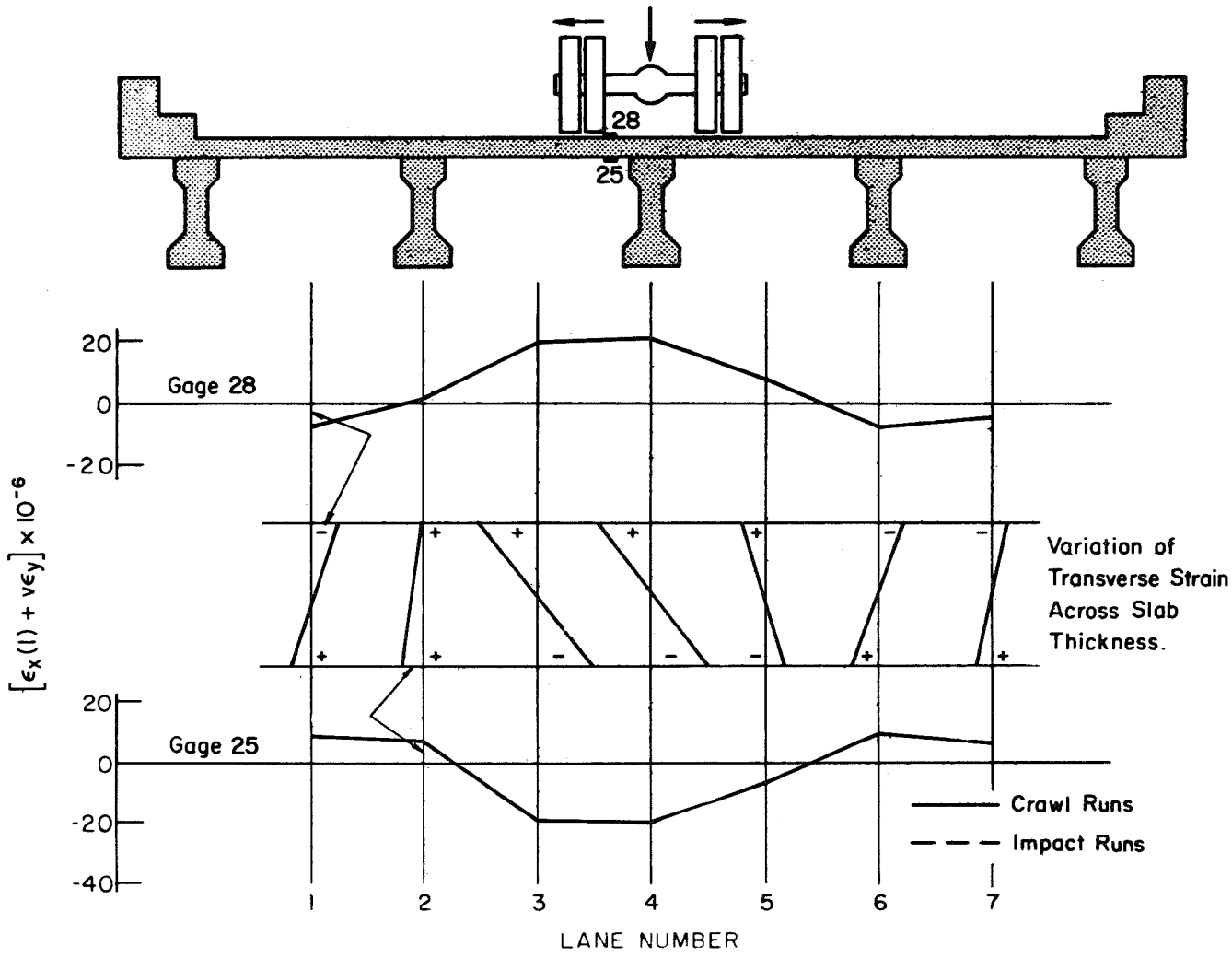

Fig. 56 Variation of Transverse Strains $\epsilon_x(1) + \nu\epsilon_y$ Across Slab Thickness Gages 28 and 25

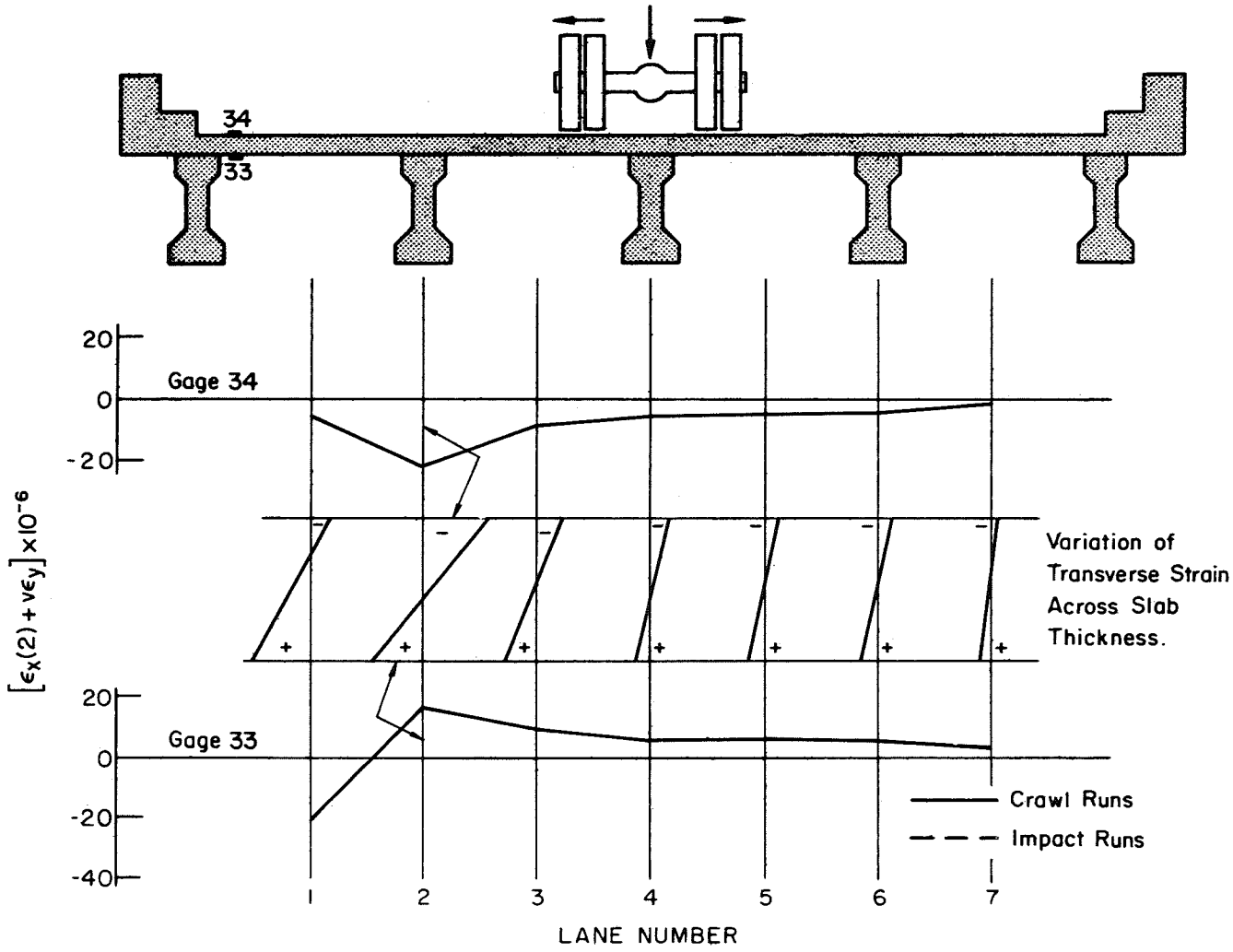

Fig. 57 Variation of Transverse Strains $\epsilon_x(2) + \nu\epsilon_y$ Across Slab Thickness Gages 34 and 33

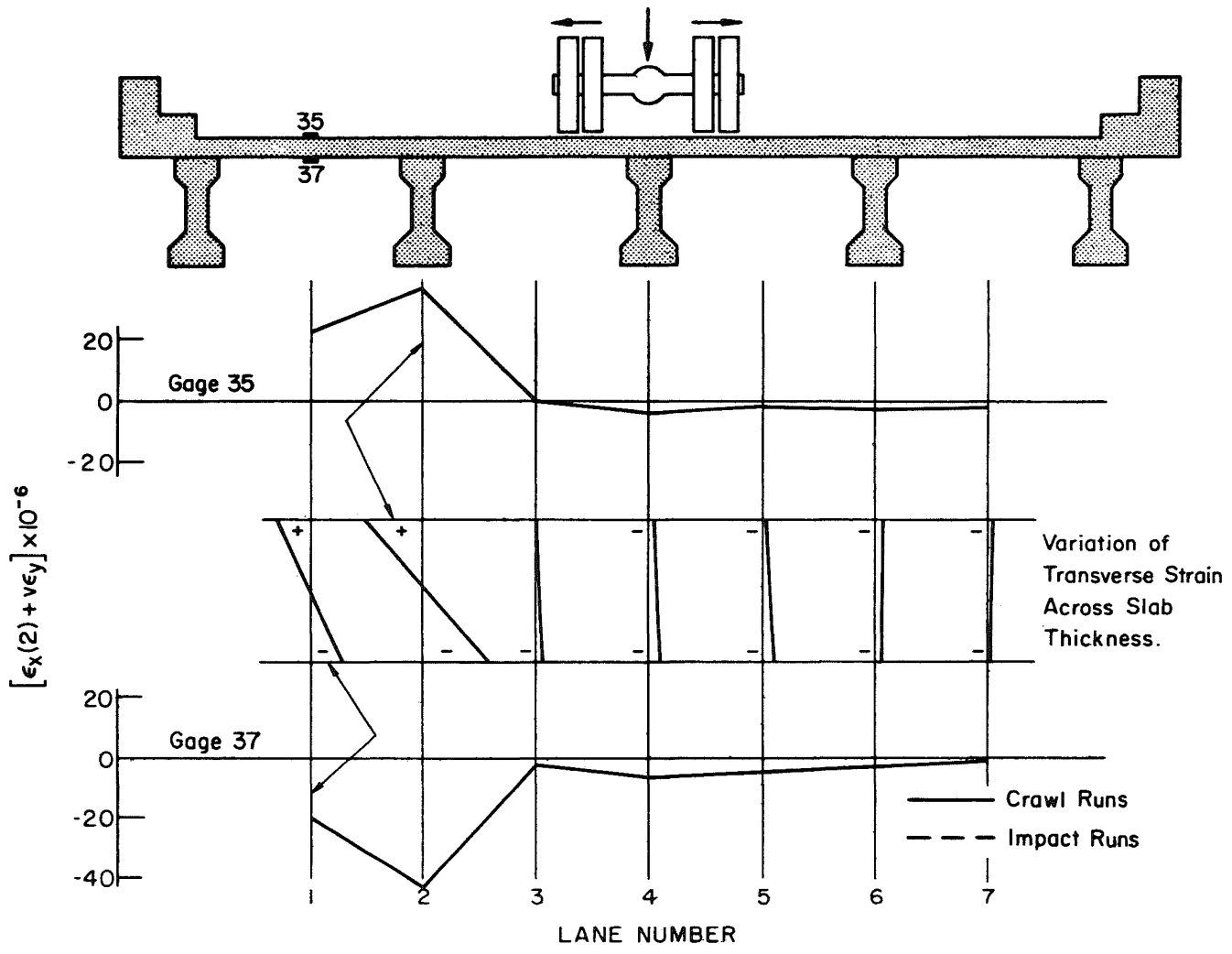

Fig. 58 Variation of Transverse Strains $\epsilon_x(2) + \nu\epsilon_y$ Across Slab Thickness Gages 35 and 37

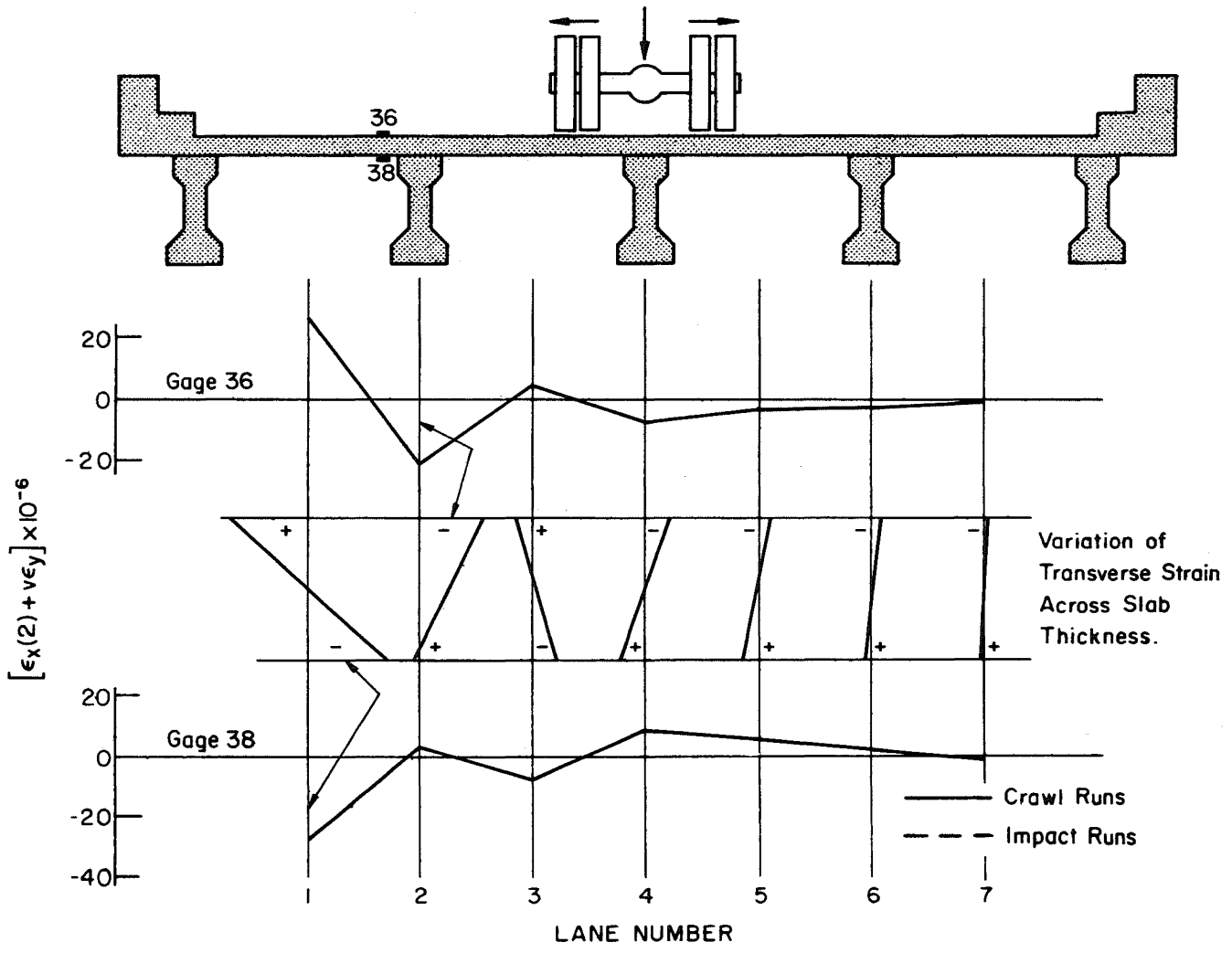

Fig. 59 Variation of Transverse Strains $\epsilon_x(2) + \nu\,\epsilon_y$ Across Slab Thickness Gages 36 and 38

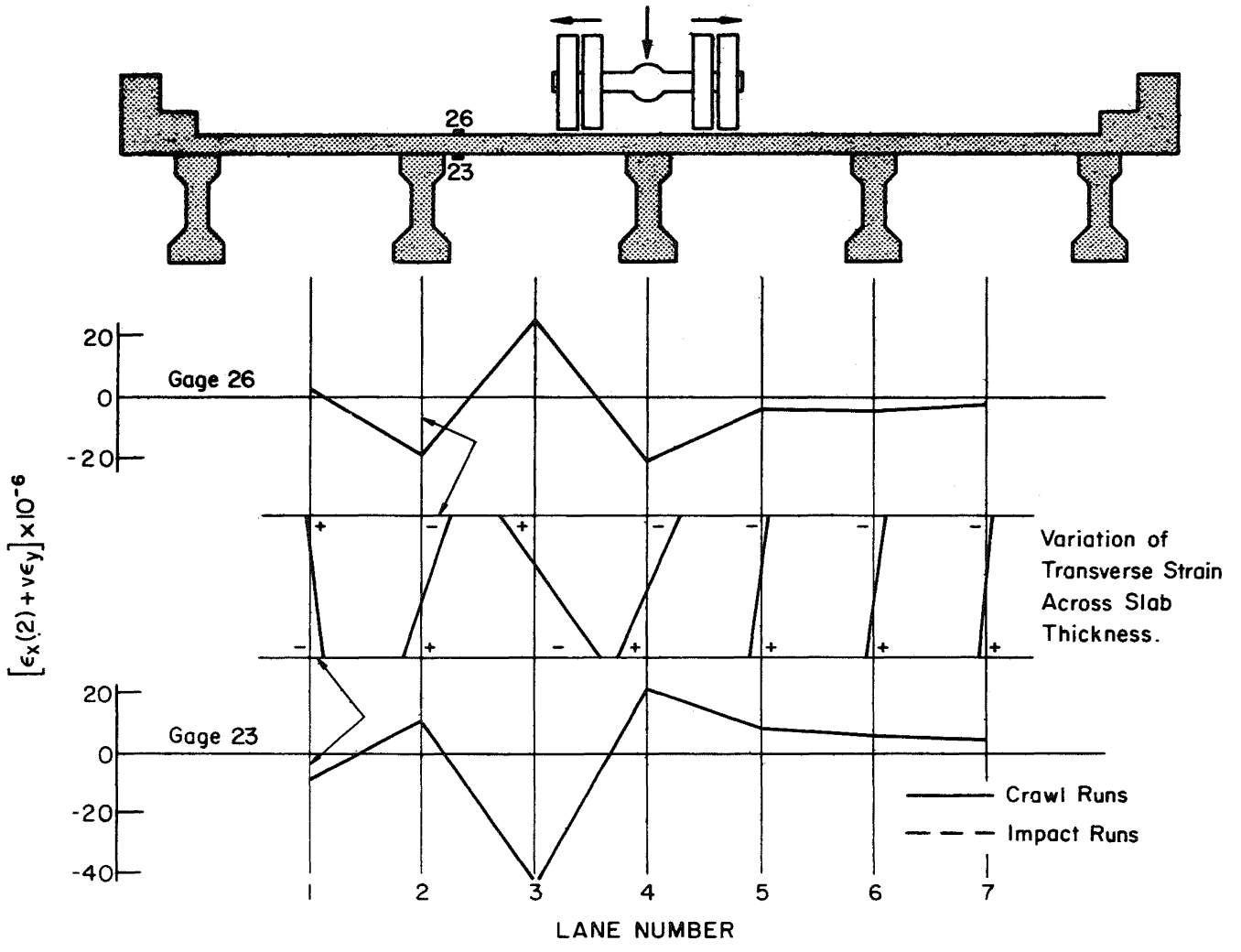

Fig. 60 Variation of Transverse Strains $\epsilon_x(2) + \nu\,\epsilon_y$ Across Slab Thickness
Gages 26 and 23

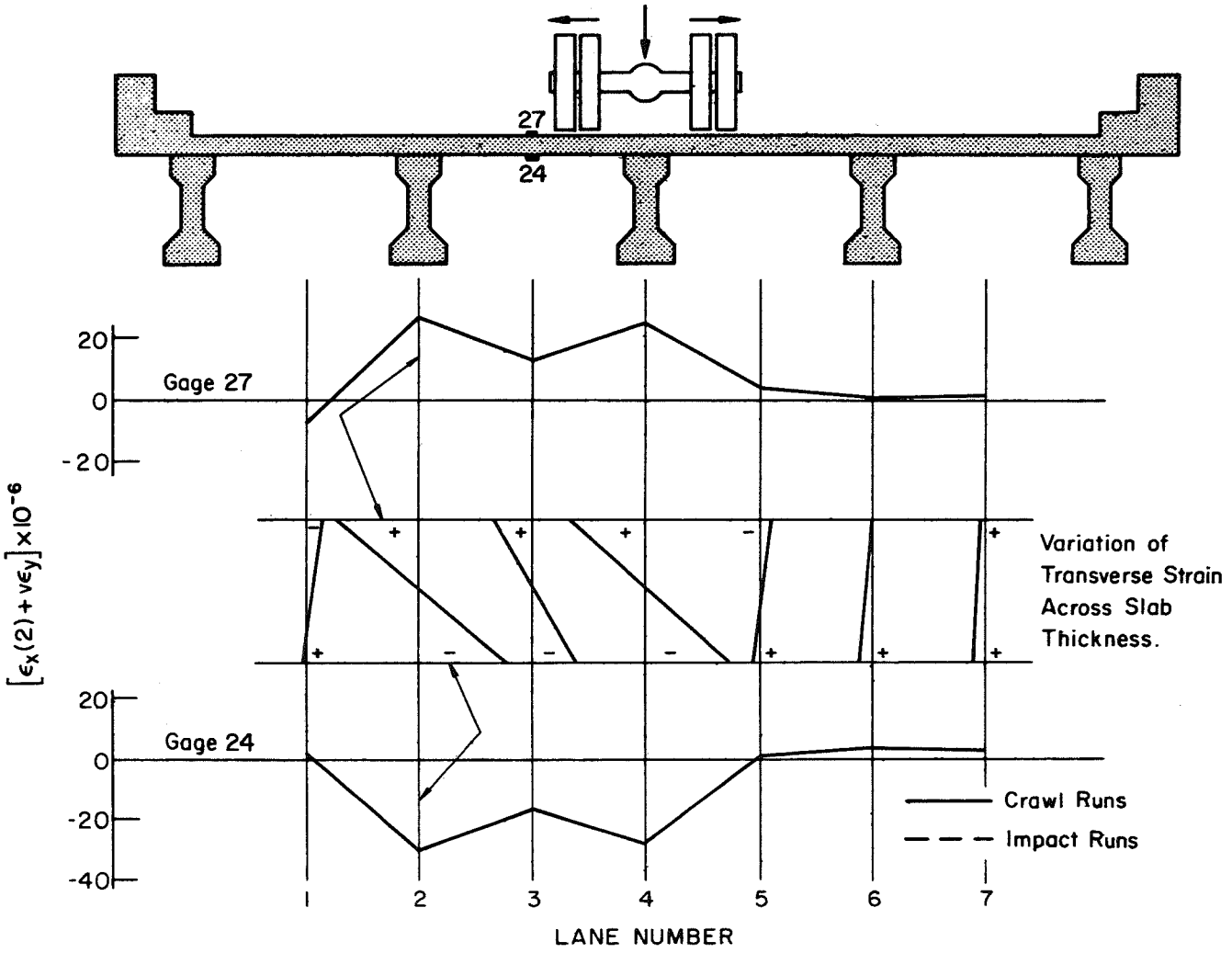

Fig. 61 Variation of Transverse Strains $\epsilon_x(2) + \nu\epsilon_y$ Across Slab Thickness
Gages 27 and 24

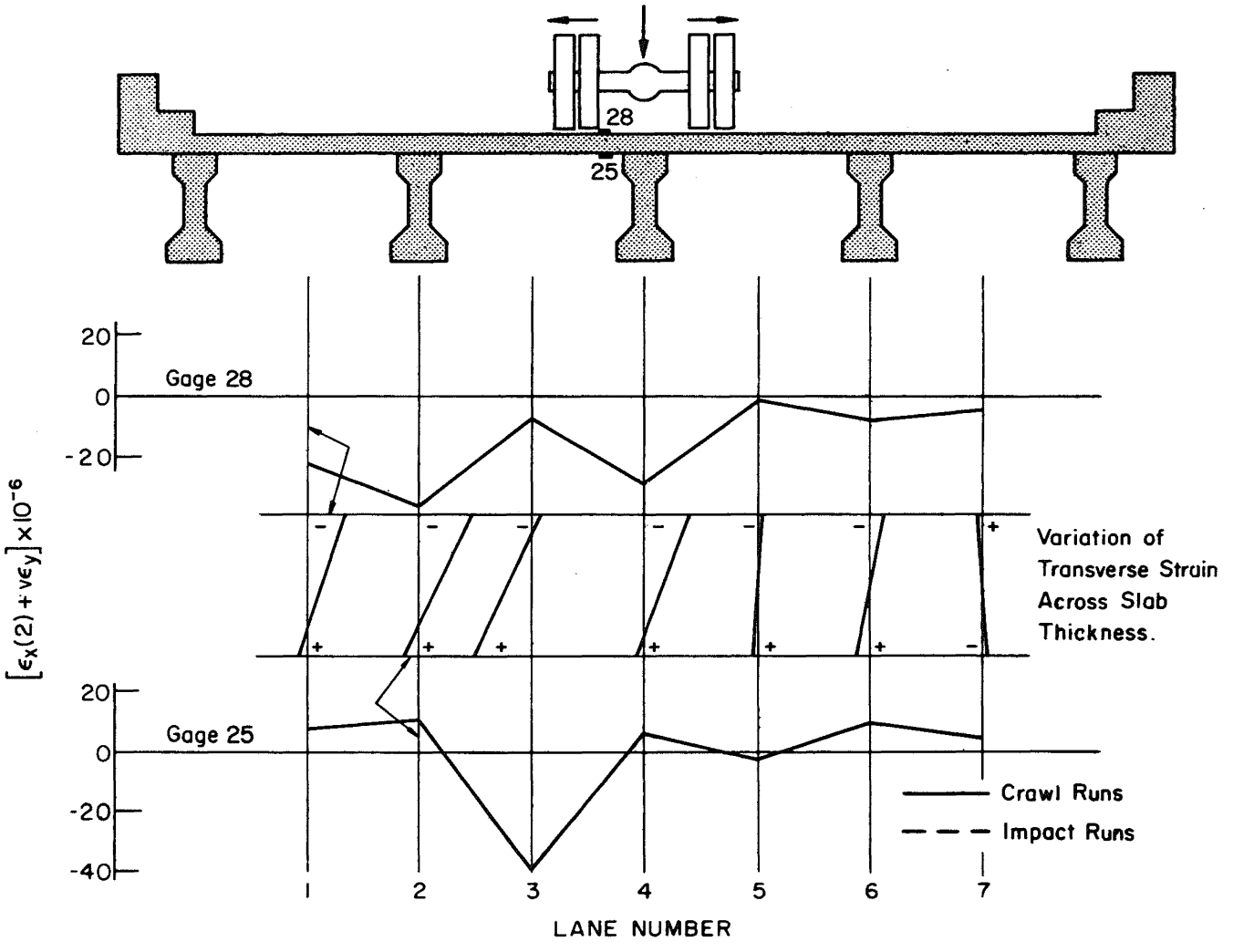

Fig. 62 Variation of Transverse Strains $\epsilon_x(2) + \nu\epsilon_y$ Across Slab Thickness
Gages 28 and 25

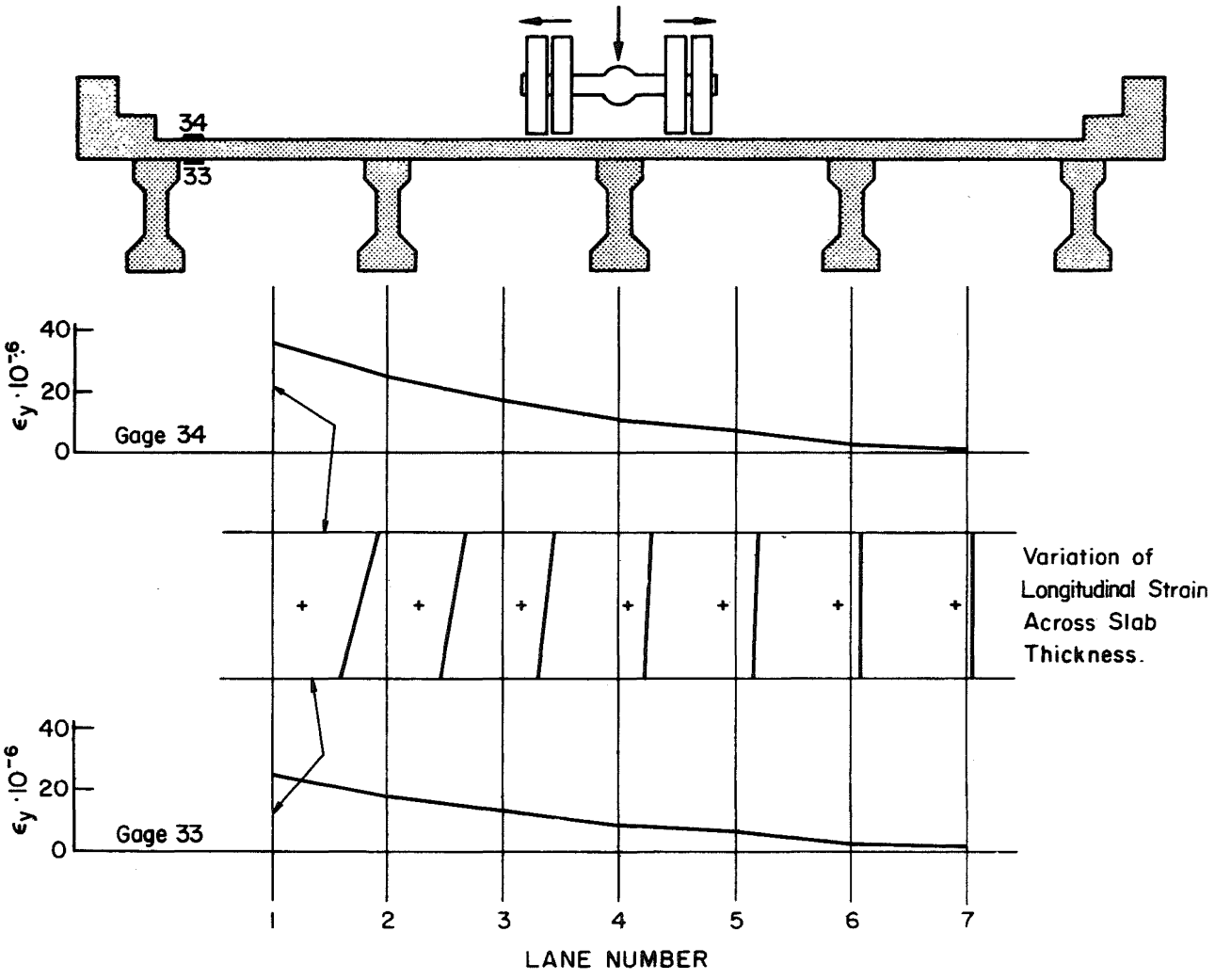

Fig. 63 Variation of Longitudinal Strains ϵ_y Across Slab Thickness
Gages 34 and 33

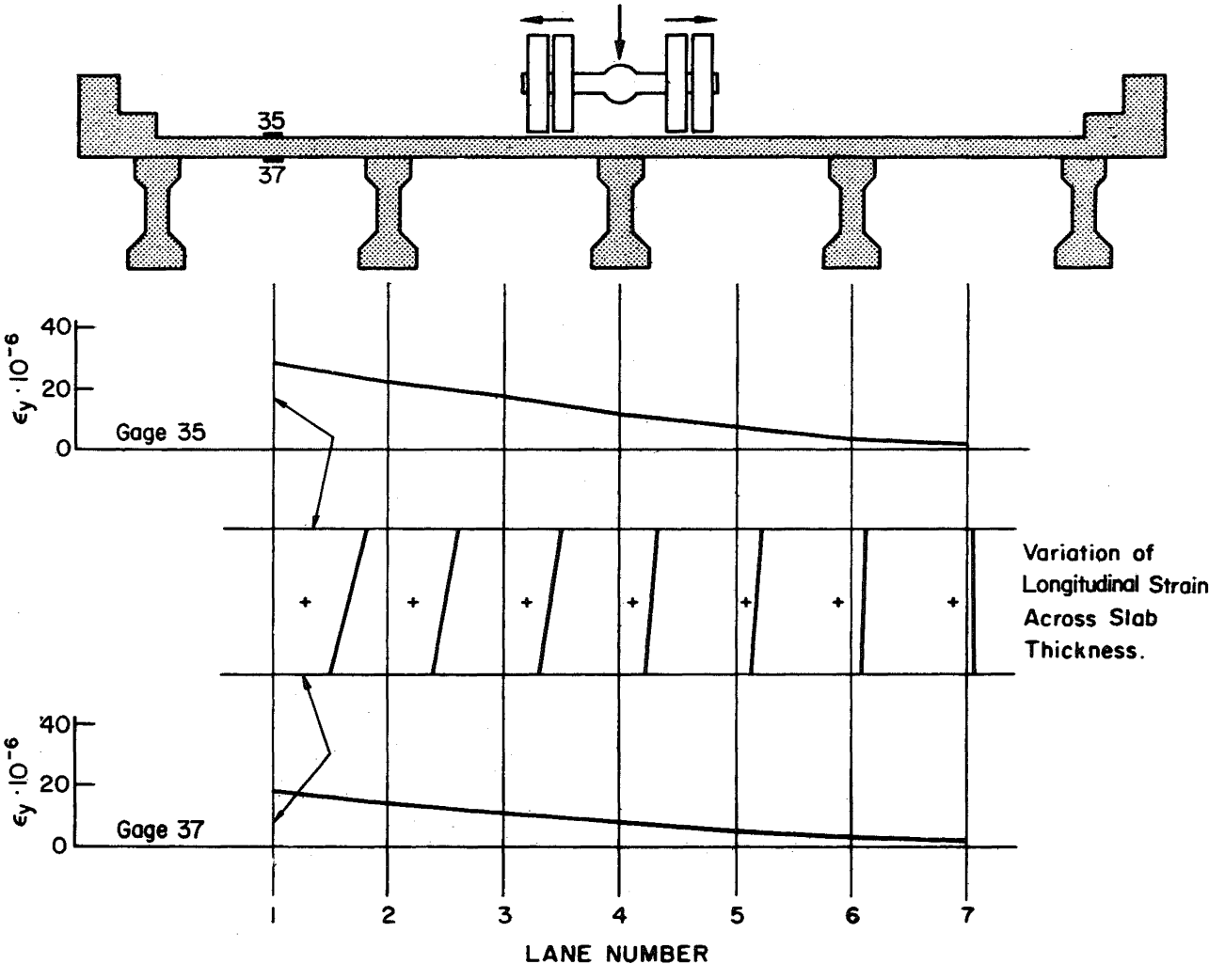

Fig. 64 Variation of Longitudinal Strains ϵ_y Across Slab Thickness
Gages 35 and 37

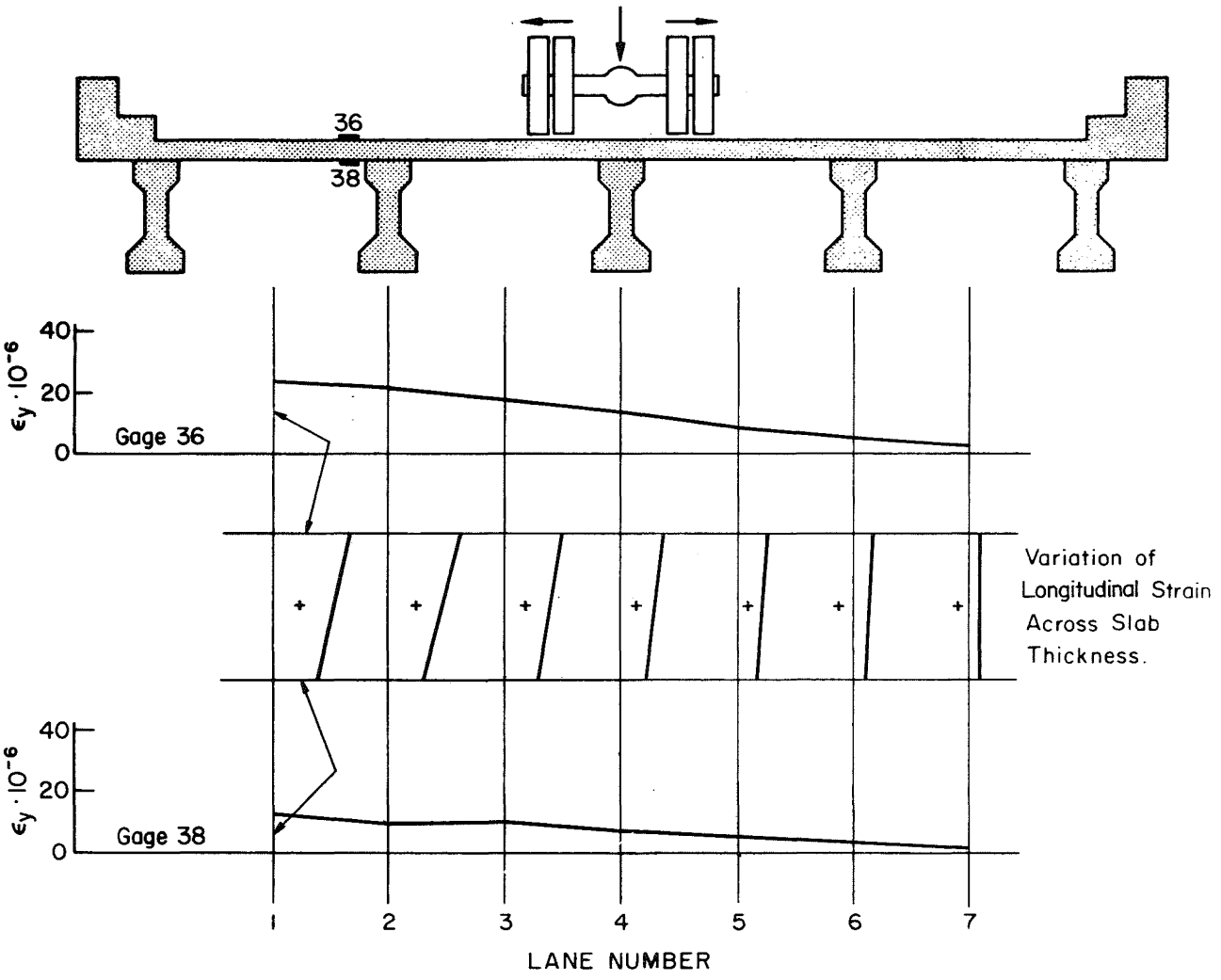

Fig. 65 Variation of Longitudinal Strains ϵ_y Across Slab Thickness
Gages 36 and 38

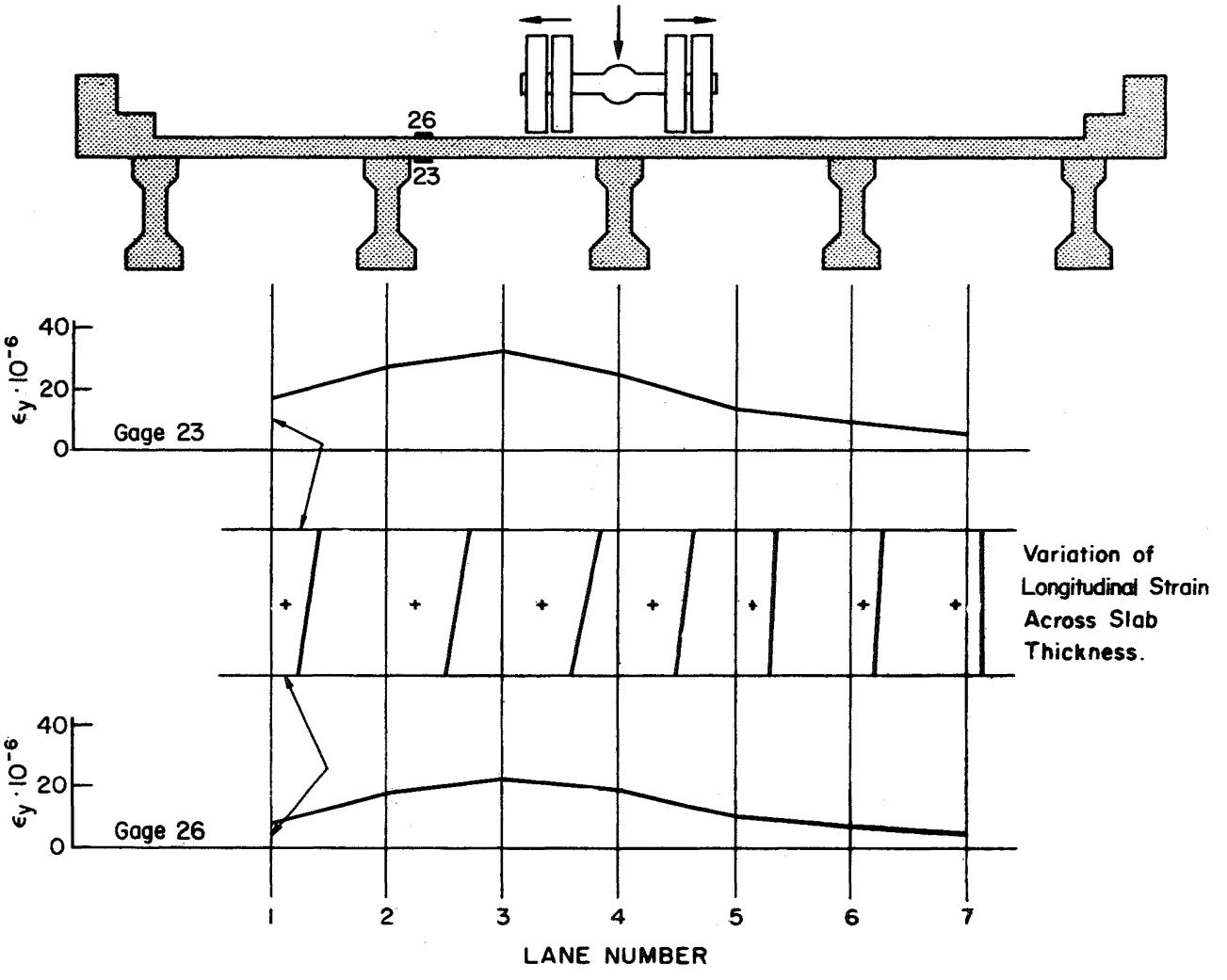

Fig. 66 Variation of Longitudinal Strains ϵ_y Across Slab Thickness
Gages 26 and 23

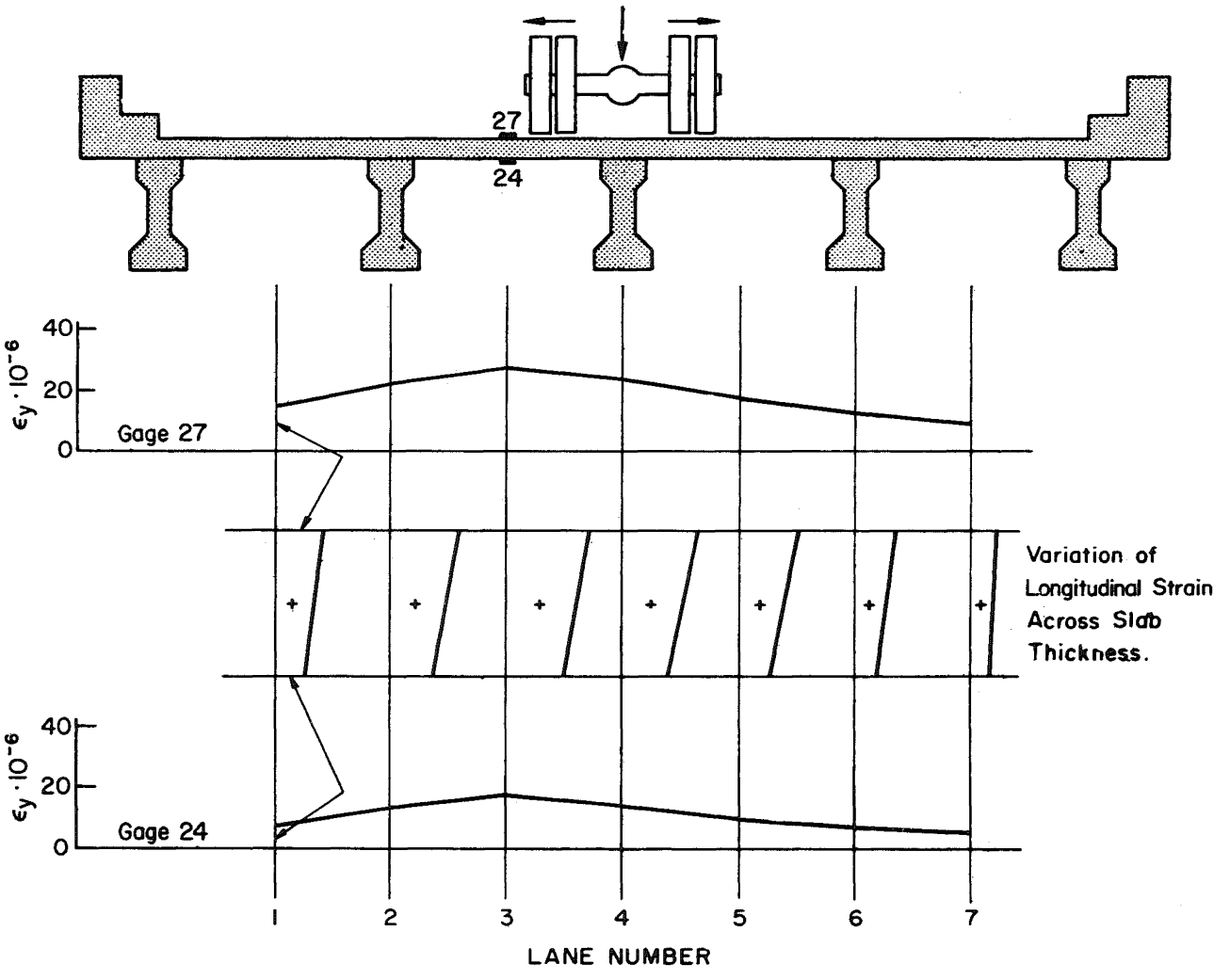

Fig. 67 Variation of Longitudinal Strains ϵ_y Across Slab Thickness
Gages 27 and 24

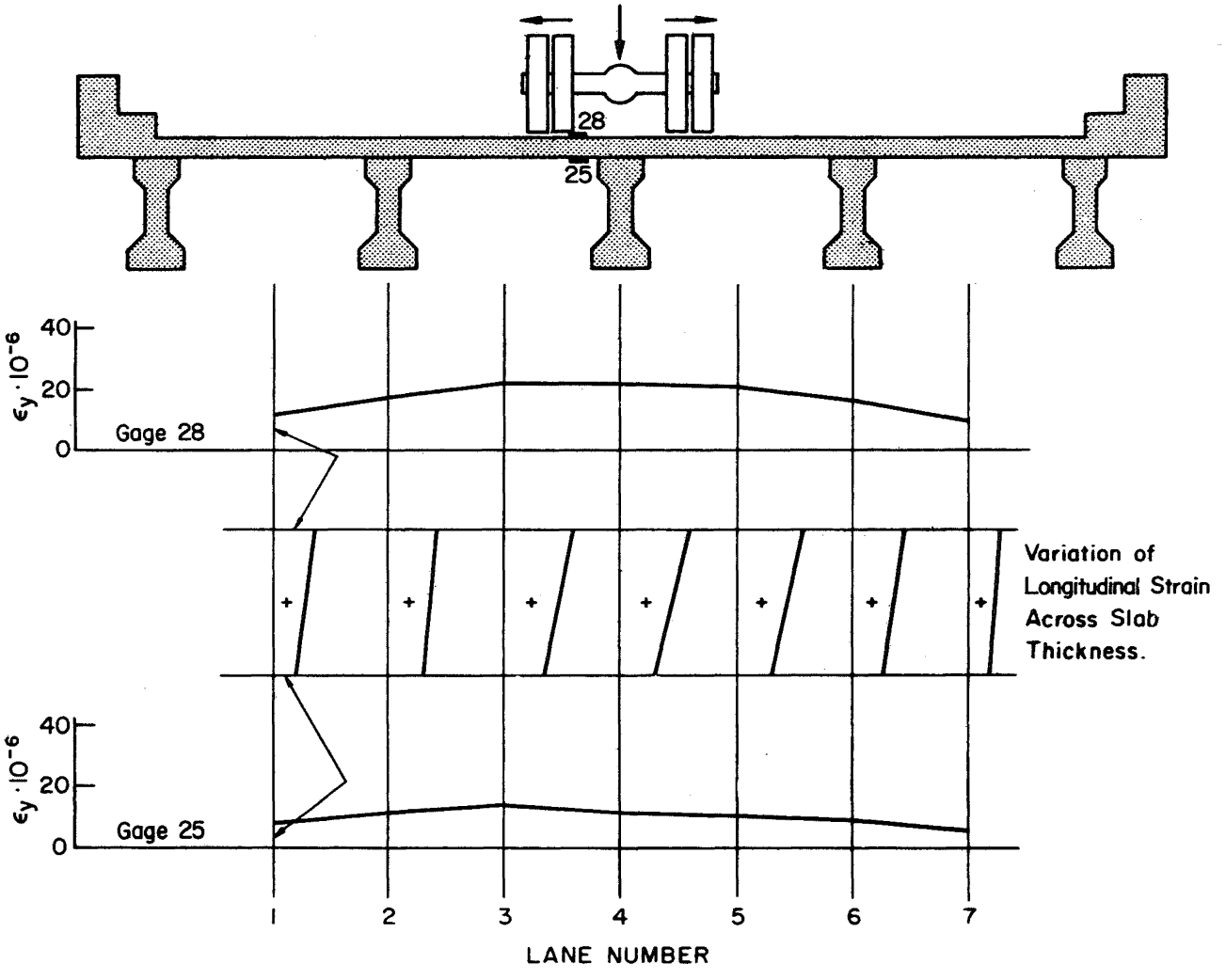

Fig. 68 Variation of Longitudinal Strains ϵ_y Across Slab Thickness
Gages 28 and 25

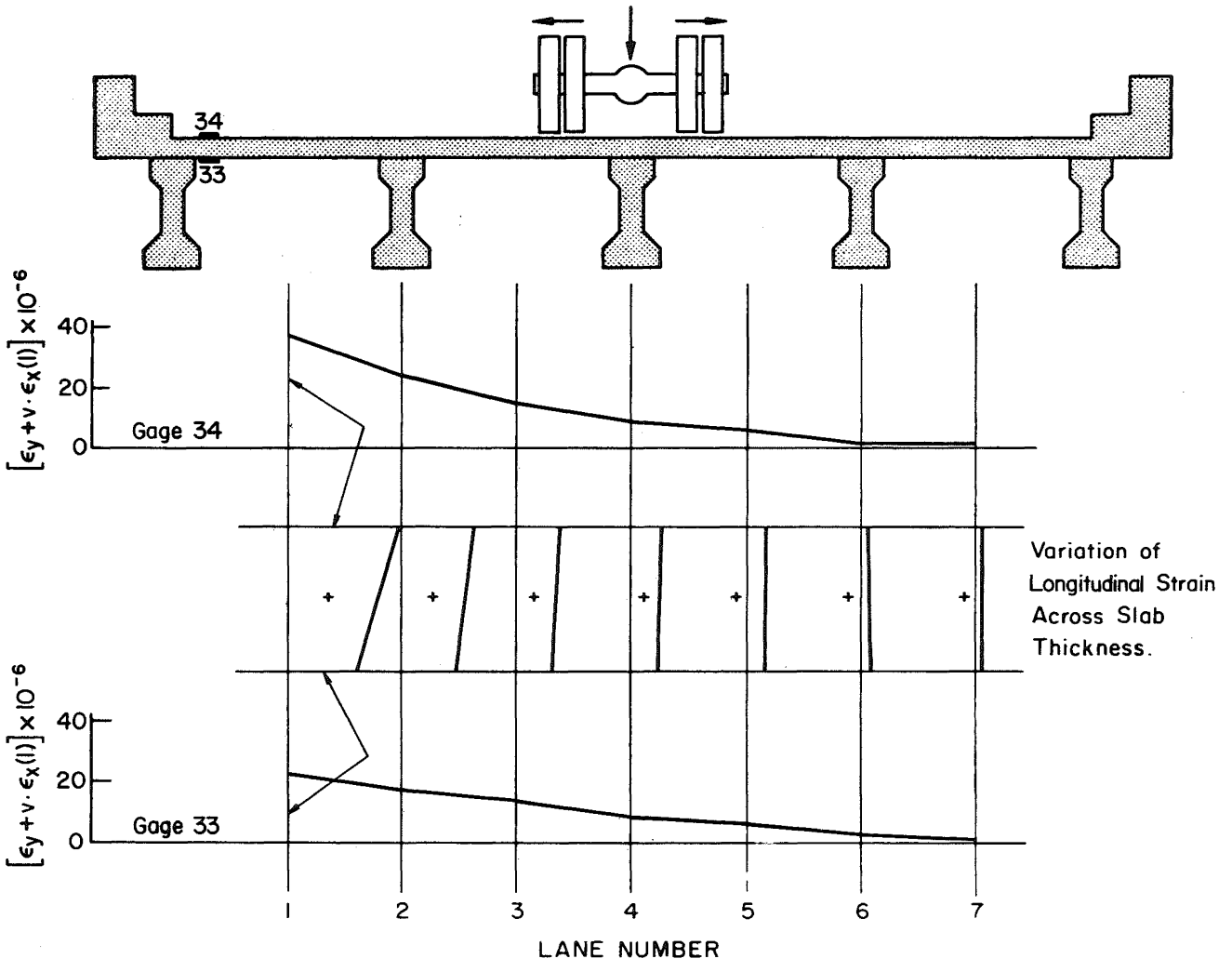

Fig. 69 Variation of Longitudinal Strains $\epsilon_y + \nu \epsilon_x(1)$ Across Slab Thickness Gages 34 and 33

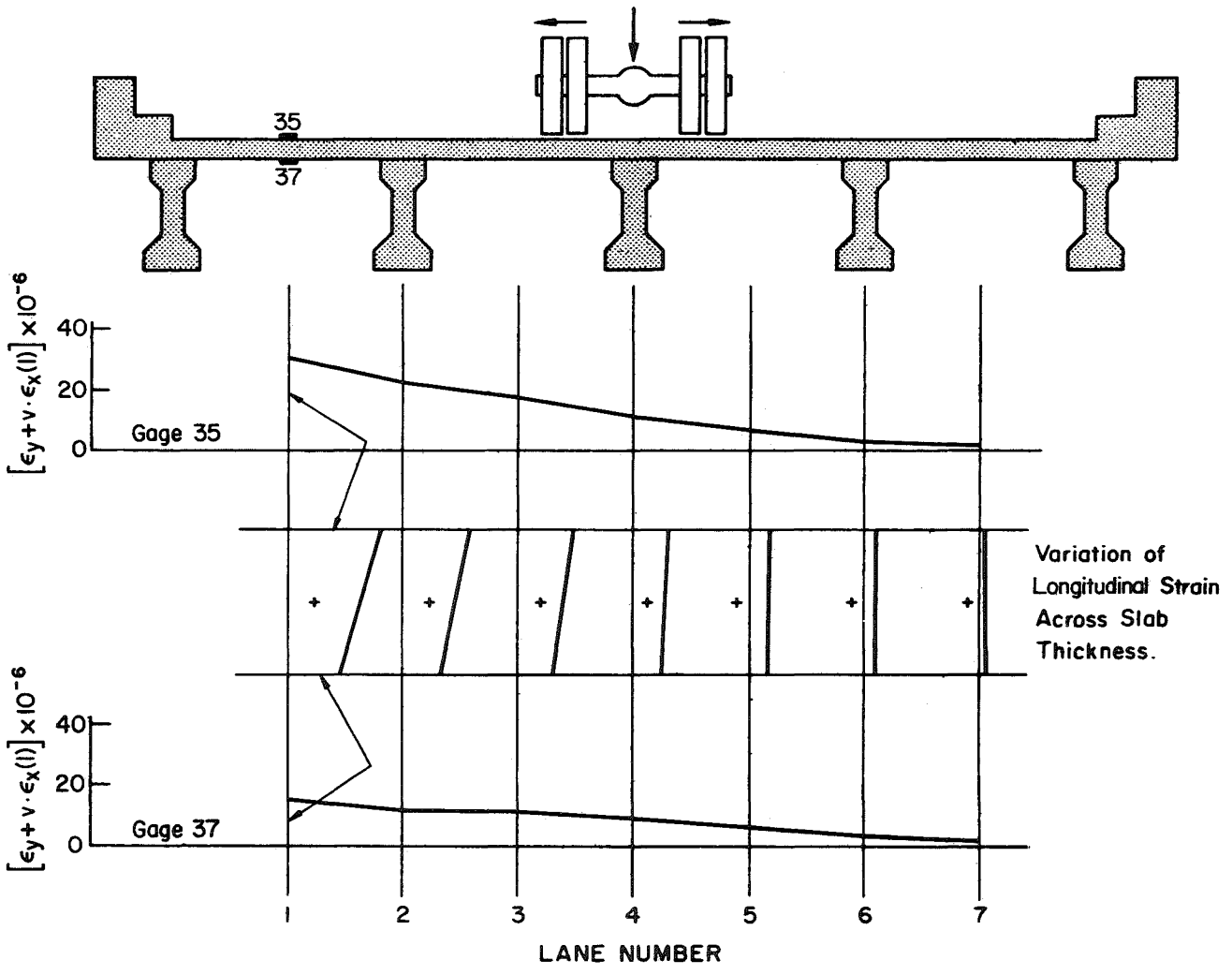

Fig. 70 Variation of Longitudinal Strains $\epsilon_y + \nu\,\epsilon_x(l)$ Across Slab Thickness Gages 35 and 37

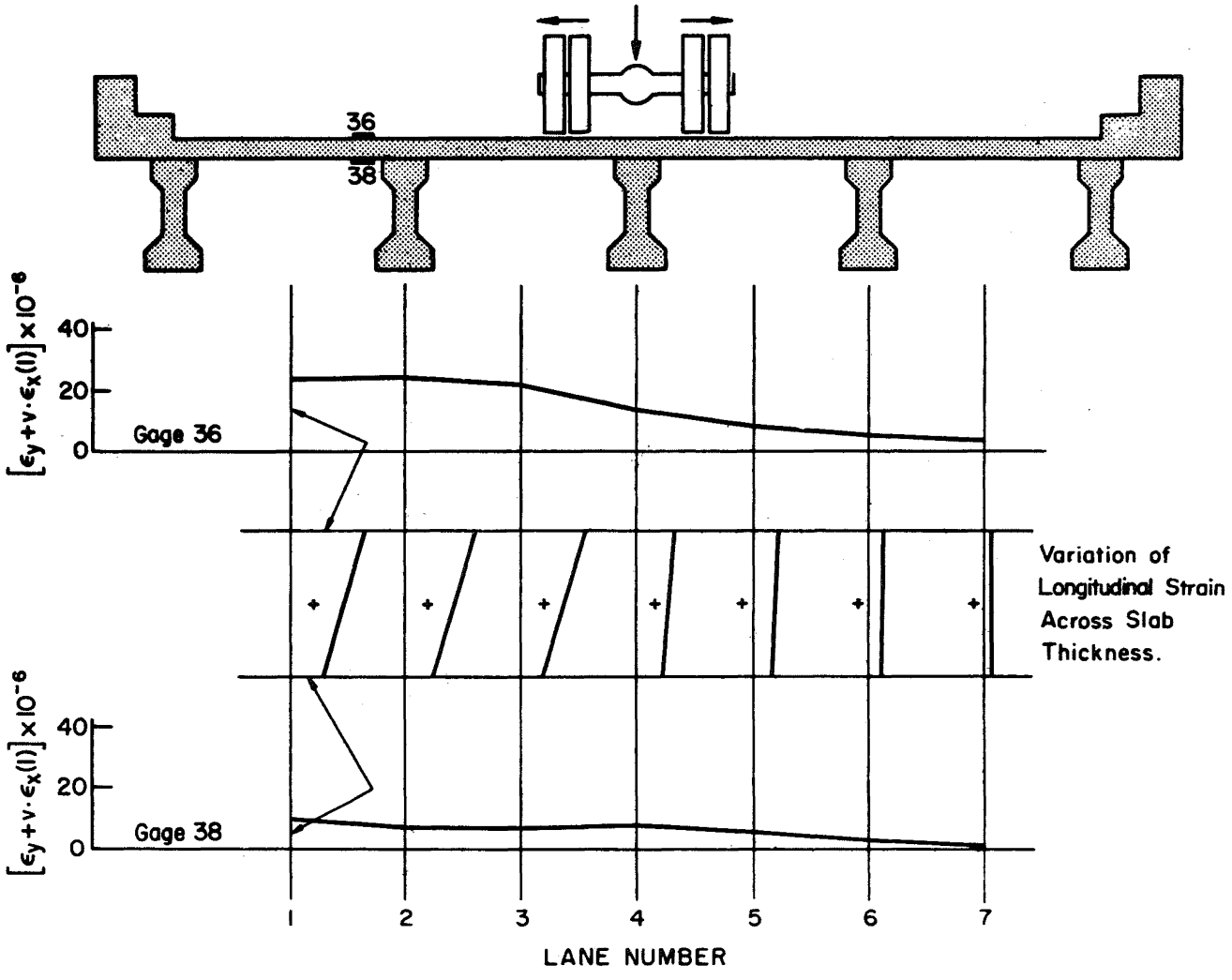

Fig. 71 Variation of Longitudinal Strains $\epsilon_y + \nu \epsilon_x(1)$ Across Slab Thickness Gages 36 and 38

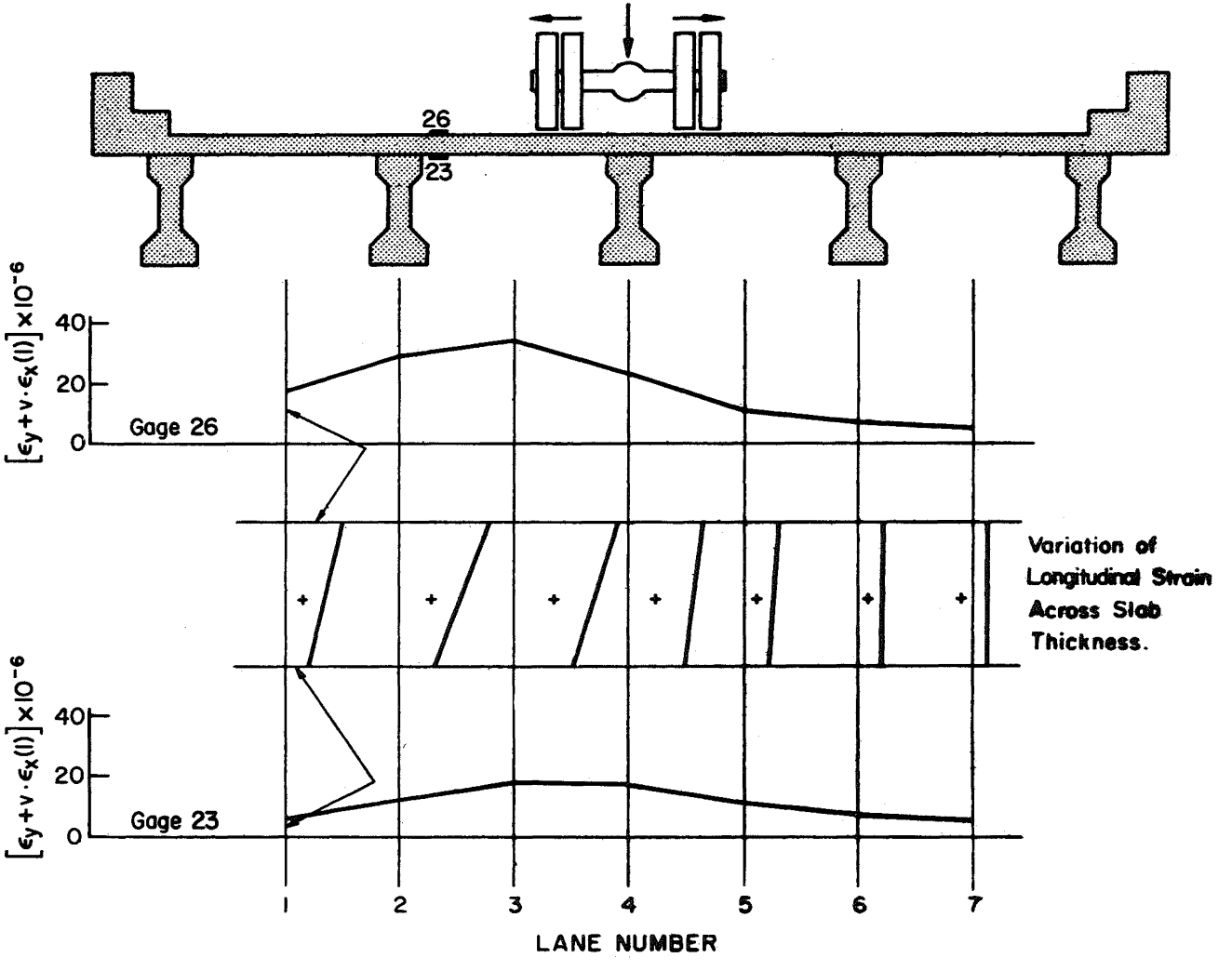

Fig. 72 Variation of Longitudinal Strains $\epsilon_y + \nu \epsilon_x(1)$ Across Slab Thickness Gages 26 and 23

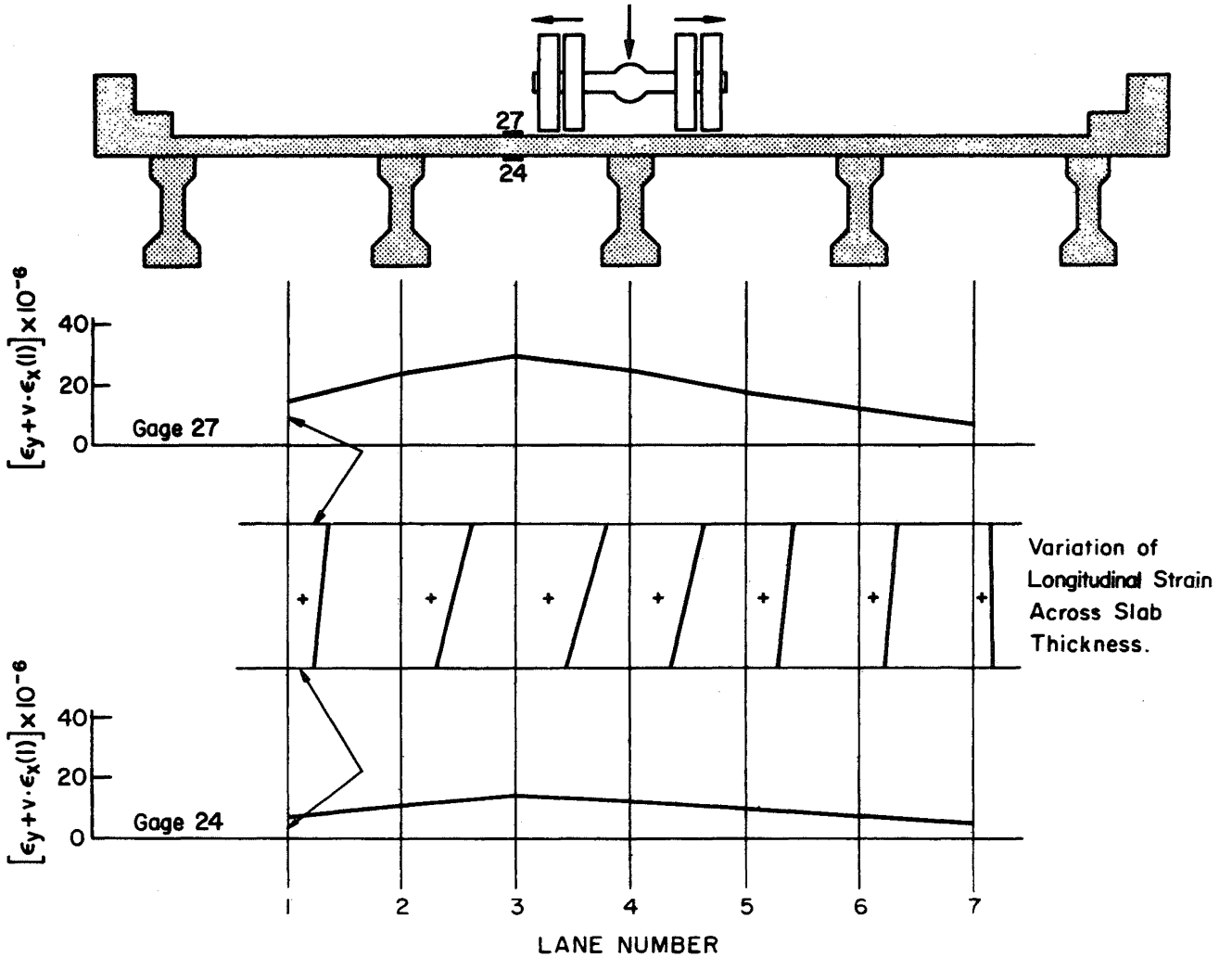

Fig. 73 Variation of Longitudinal Strains $\epsilon_y + \nu\,\epsilon_x(l)$ Across Slab Thickness Gages 27 and 24

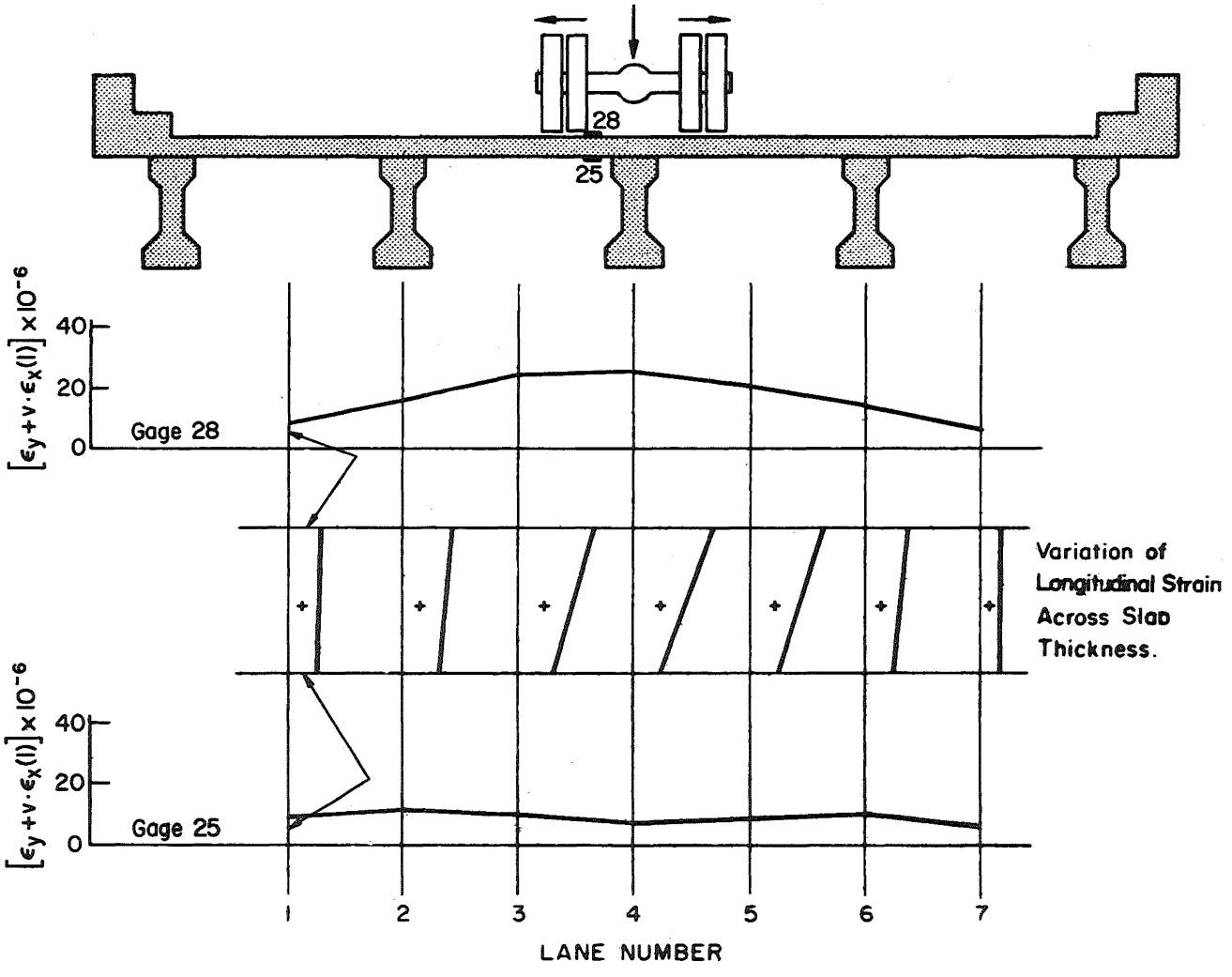

Fig. 74 Variation of Longitudinal Strains $\epsilon_y + \nu\,\epsilon_x(1)$ Across Slab Thickness Gages 28 and 25

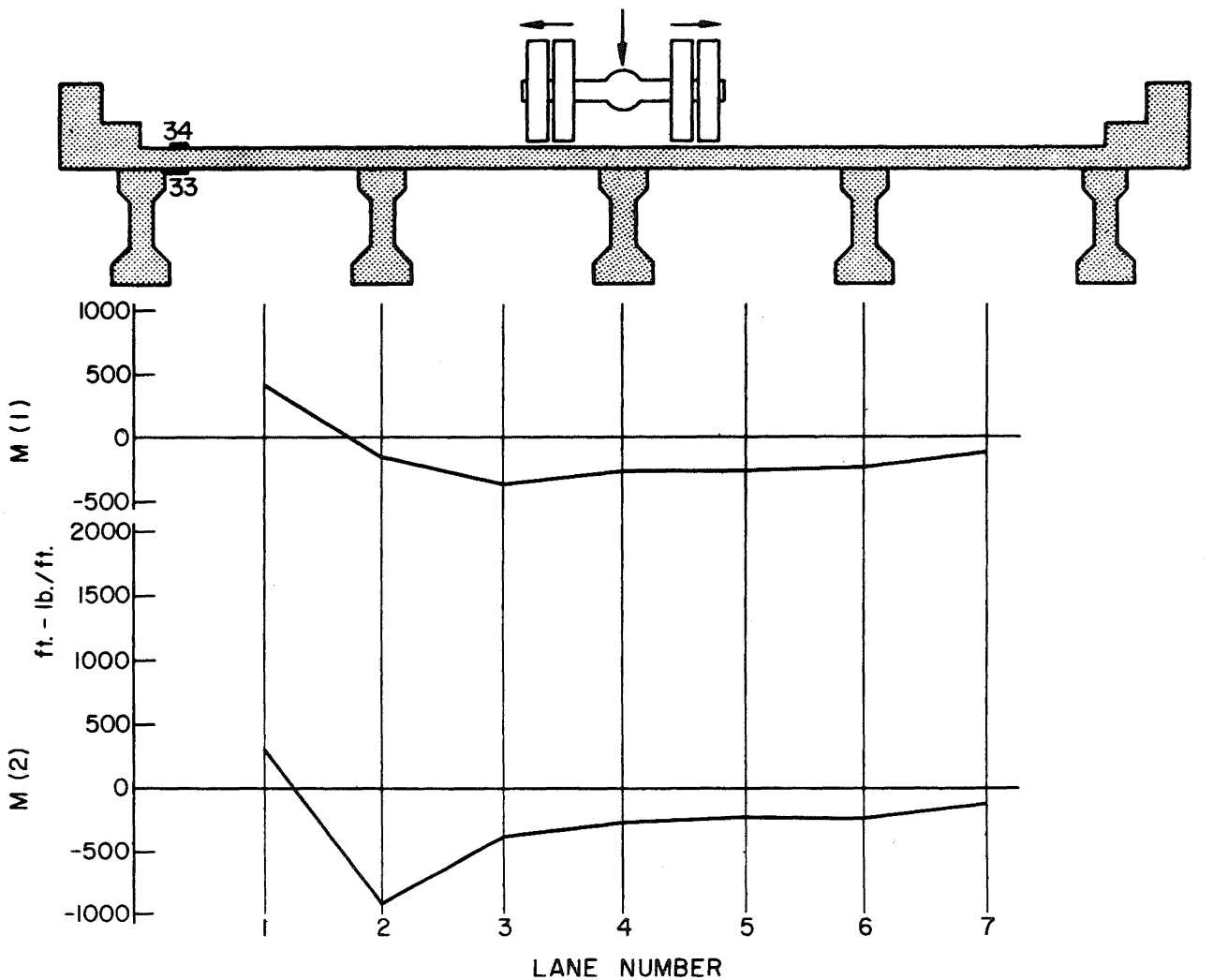

Fig. 75 Influence Lines for Transverse Slab Bending Moments At Gages 34 and 33

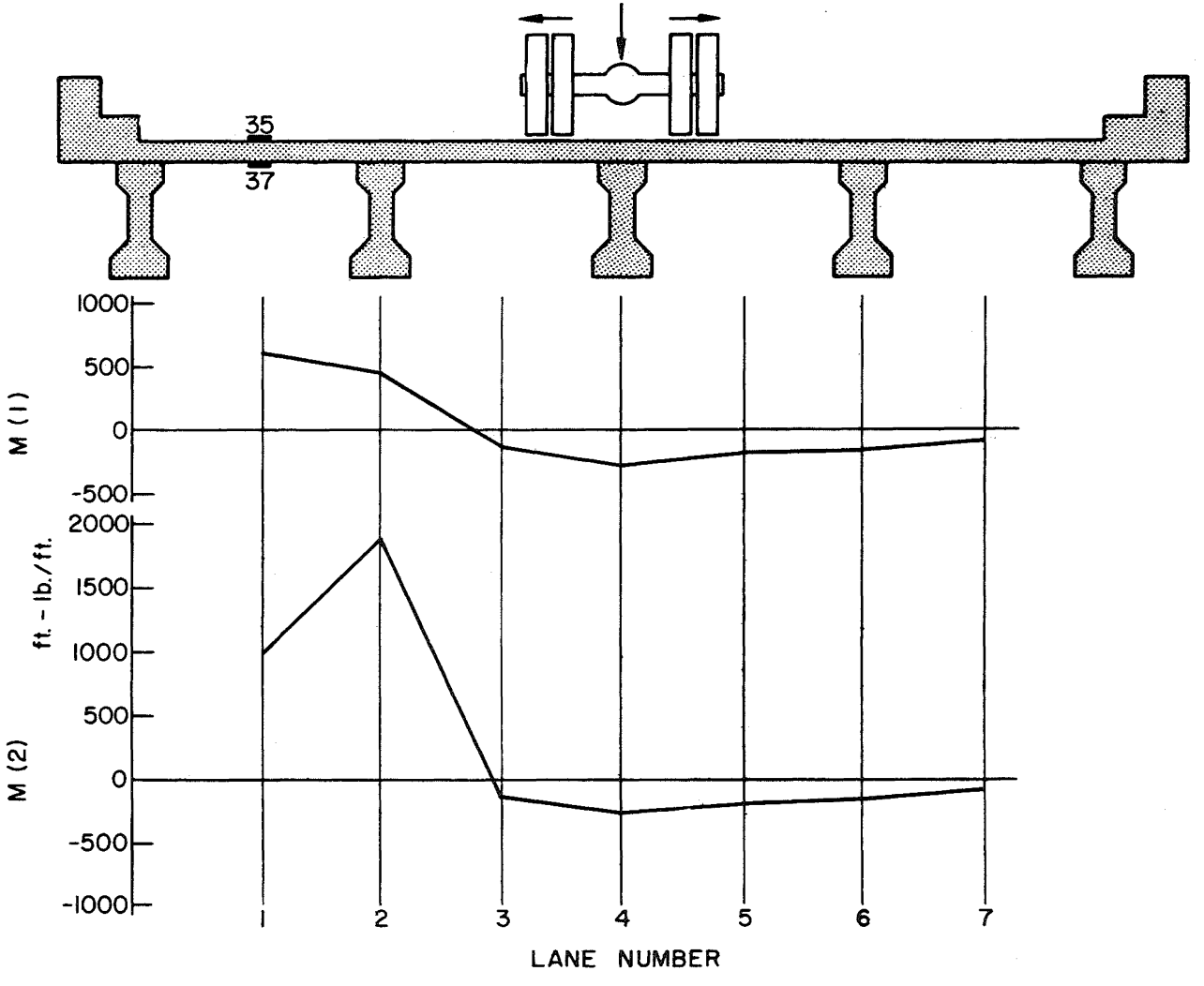

Fig. 76 Influence Lines for Transverse Slab Bending Moments At Gages 35 and 37

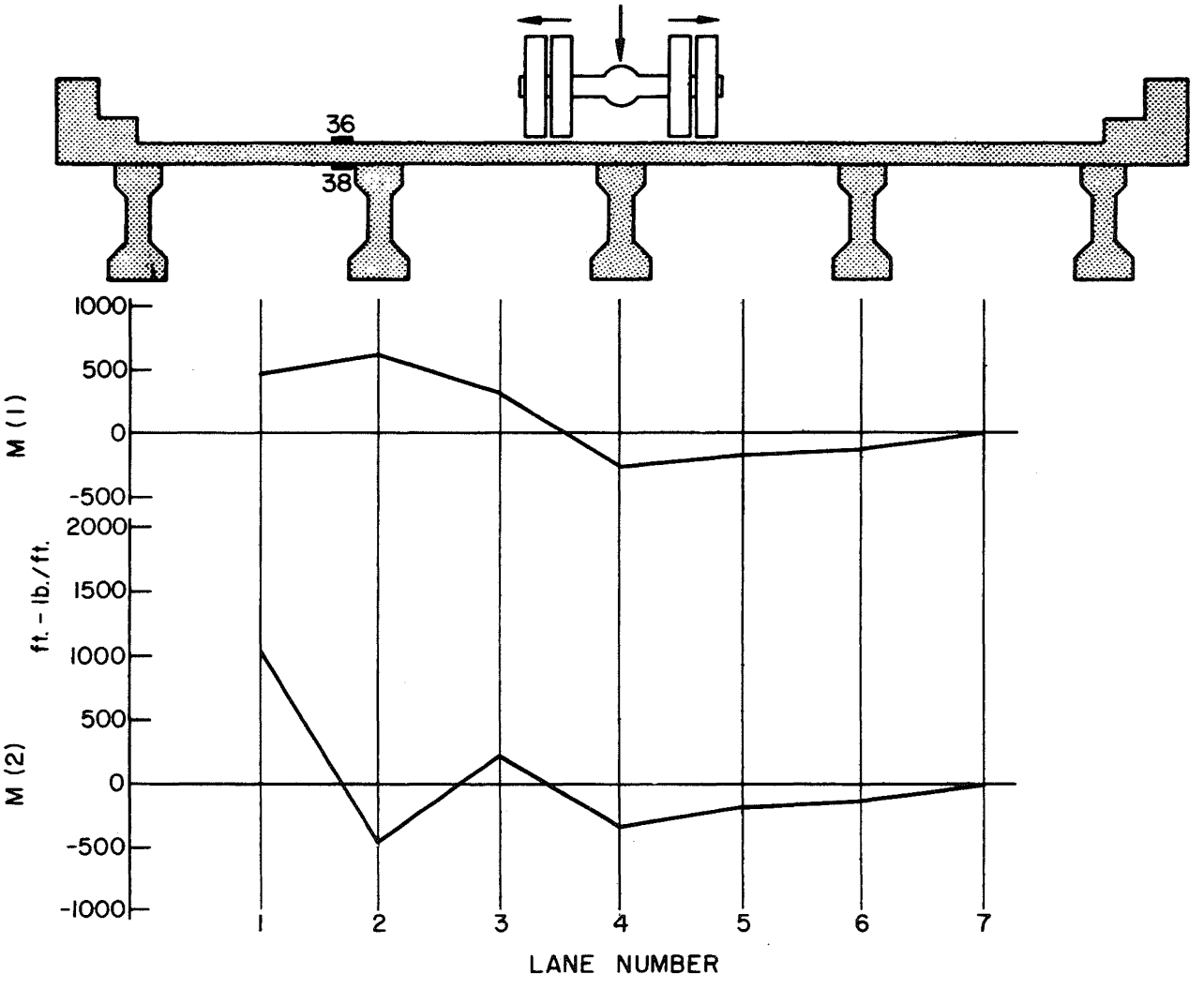

Fig. 77 Influence Lines for Transverse Slab Bending Moments At Gages 36 and 38

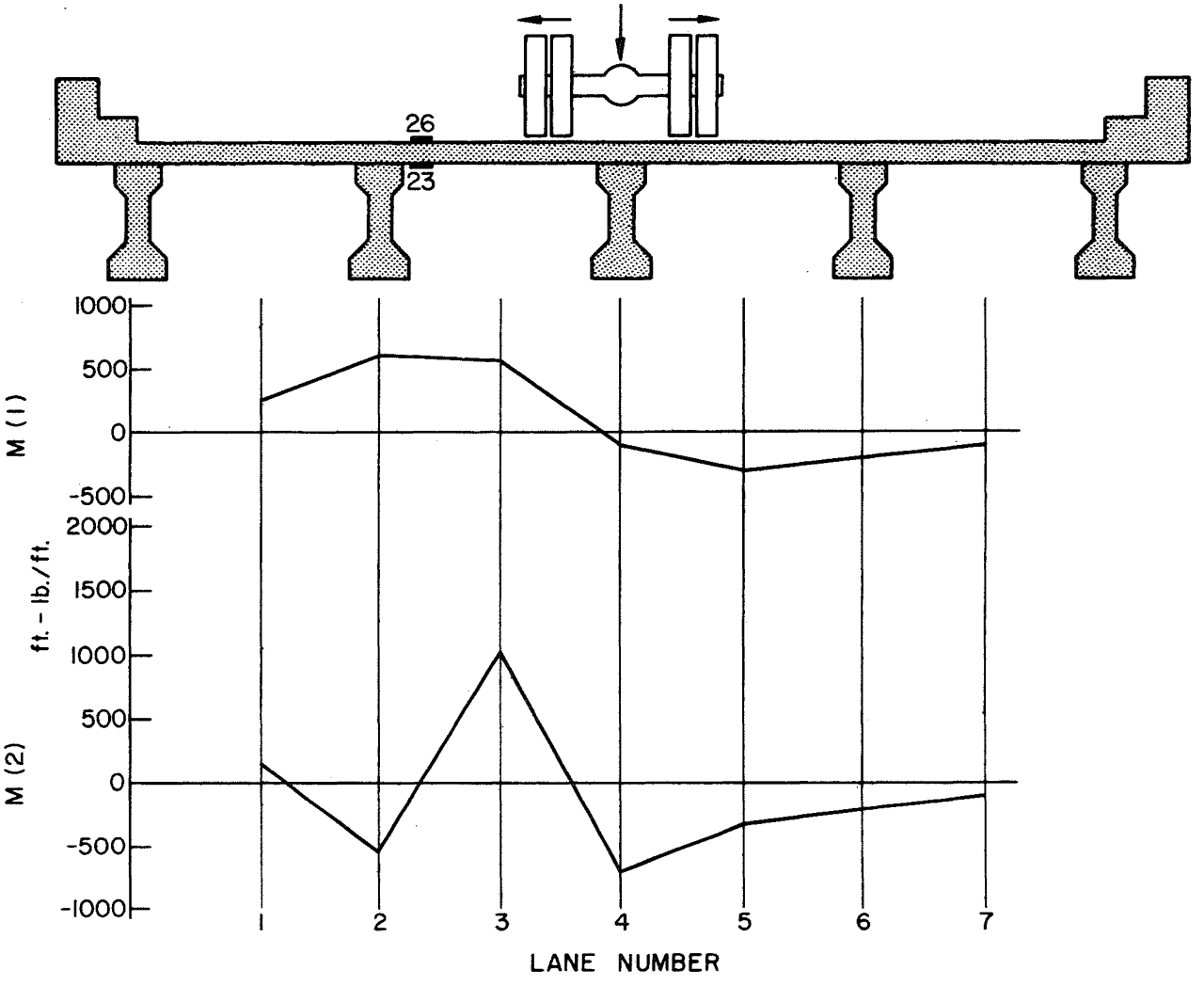

Fig. 78 Influence Lines for Transverse Slab Bending Moments At Gages 26 and 23

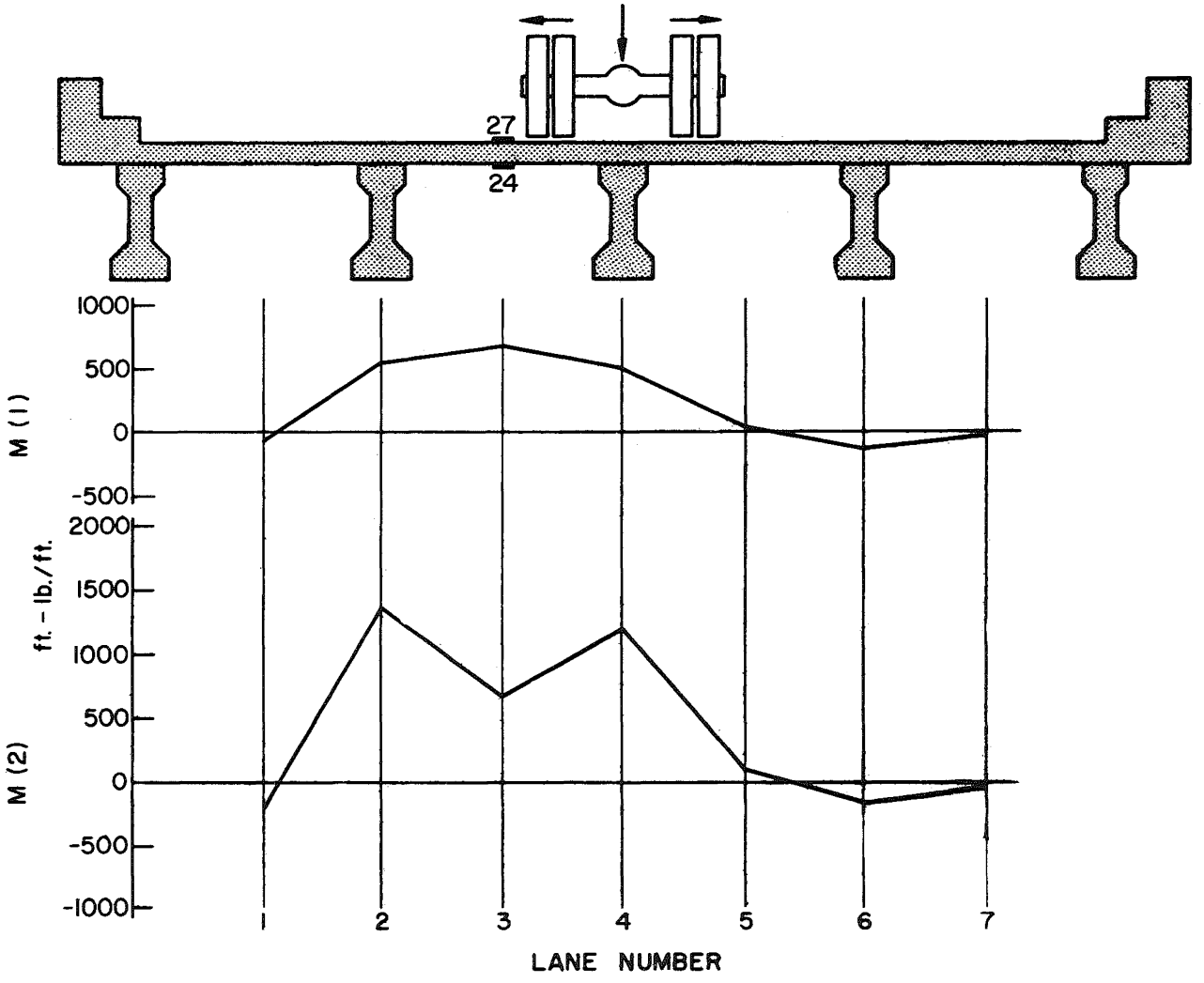

Fig. 79 Influence Lines for Transverse Slab Bending Moments At Gages 27 and 24

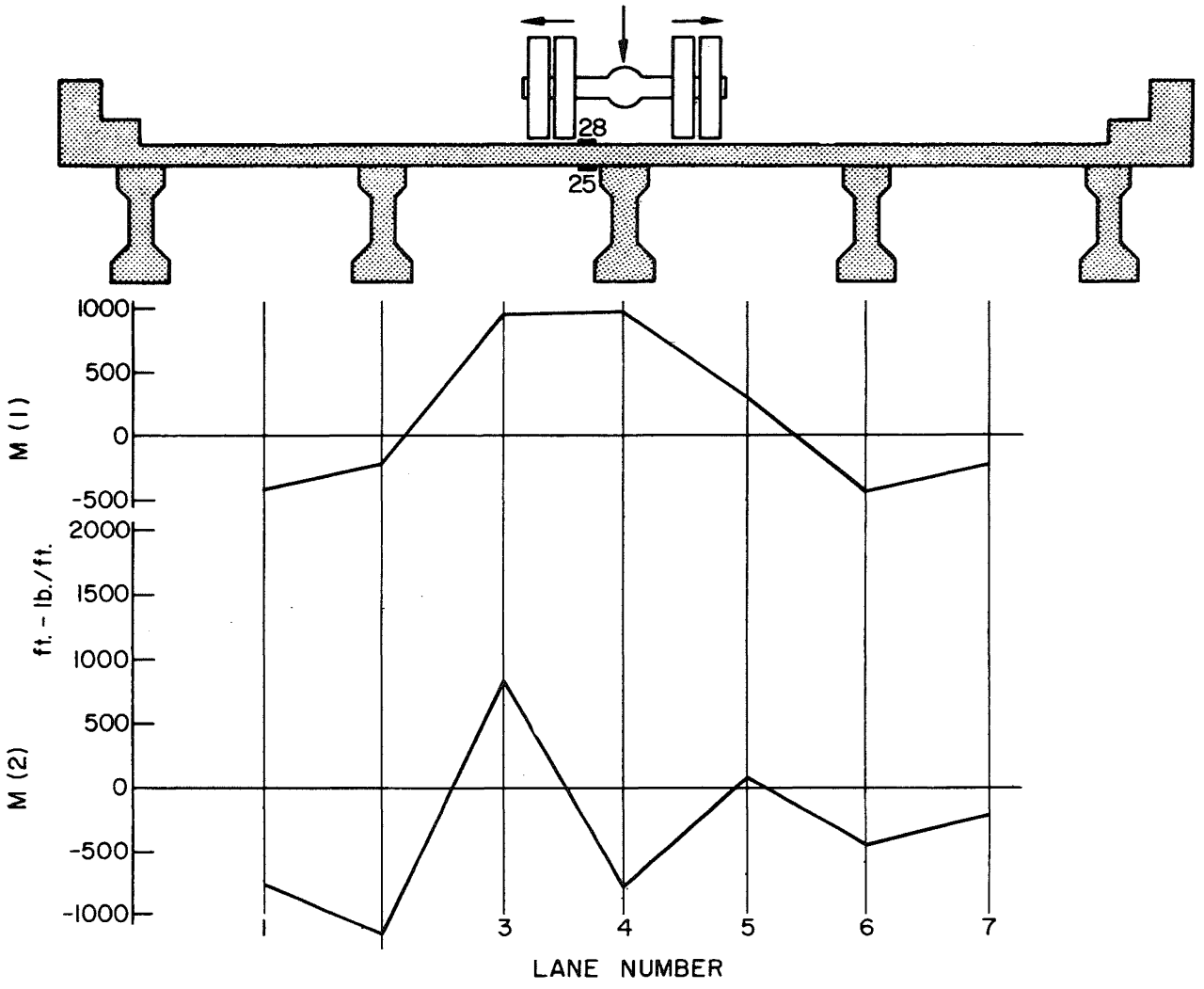

Fig. 80 Influence Lines for Transverse Slab Bending Moments At Gages 28 and 25

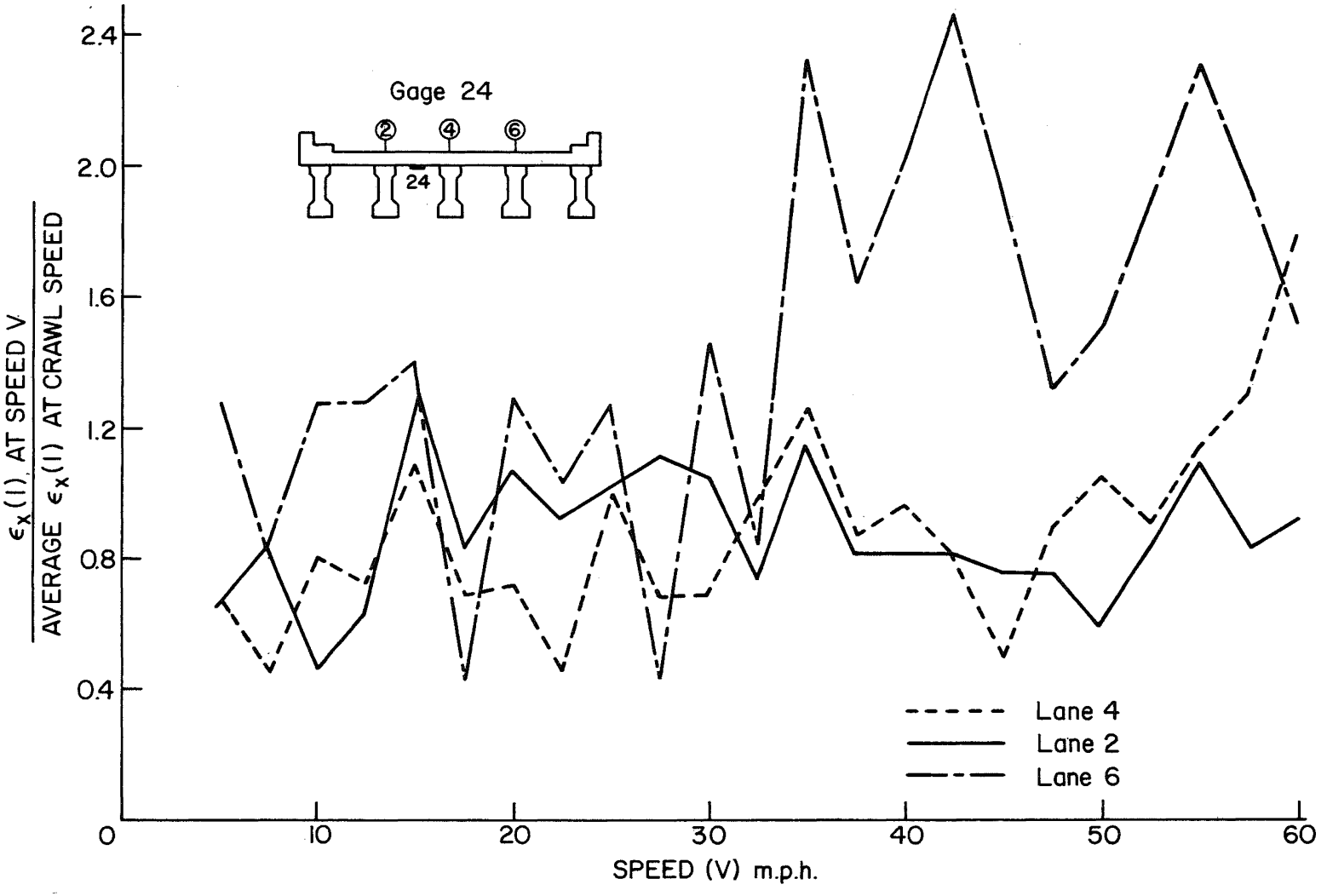

Fig. 81 Variation of Transverse Strains $\epsilon_x(1)$ with Vehicle Speed
Gage 24

10. REFERENCES

1. American Association of State Highway Officials, STANDARD SPECIFICATIONS FOR HIGHWAY BRIDGES, Washington, D.C., 1969.

2. American Concrete Institute
   ACI STANDARD BUILDING CODE REQUIREMENTS FOR REINFORCED CONCRETE, June, 1963.

3. Reese, R. T.
   A SUMMARY AND EXAMINATION OF EXISTING METHODS OF ANALYSIS AND DESIGN OF LOAD DISTRIBUTION IN HIGHWAY BRIDGE FLOORS, M.S. Thesis, Brigham Young University, 1966.

4. Westergaard, H. M.
   COMPUTATION OF STRESSES IN BRIDGE SLABS DUE TO WHEEL LOADS, Public Roads, 11, 1, March, 1930.

5. Newmark, N. M. and Seiss, C. P.
   MOMENTS IN TWO-WAY CONCRETE FLOOR SLABS, University of Illinois Engineering Experiment Station Bulletin No. 385, February, 1950.

6. Kelley, E. F.
   EFFECTIVE WIDTH OF CONCRETE BRIDGE SLABS SUPPORTING CONCENTRATED LOADS, Public Roads, 7, 1, March, 1926.

7. Richart, F. E. and Kluge, R. W.
   TESTS OF REINFORCED CONCRETE SLABS SUBJECTED TO CONCENTRATED LOADS, University of Illinois Engineering Experiment Station Bulletin No. 314, 1939.

8. Newmark, N. M. and Lepper, H. A.
   TESTS OF PLASTER MODEL SLABS SUBJECTED TO CONCENTRATED LOADS, University of Illinois Engineering Experiment Station Bulletin No. 313, 1939.

9. Richart, F. E.
LABORATORY RESEARCH ON CONCRETE BRIDGE FLOORS, ASCE Proceedings, pp. 288 - 304, March, 1948.

10. Douglas, W. J. and VanHorn, D. A.
LATERAL DISTRIBUTION OF STATIC LOADS IN A PRESTRESSED CONCRETE BOX-BEAM BRIDGE - DREHERSVILLE BRIDGE, Fritz Engineering Laboratory Report 315.1, August, 1966.

11. Guilford, A. A. and VanHorn, D. A.
LATERAL DISTRIBUTION OF DYNAMIC LOADS IN A PRESTRESSED CONCRETE BOX-BEAM BRIDGE - DREHERSVILLE BRIDGE, Fritz Engineering Laboratory Report 315.2, February, 1967.

12. Guilford, A. A. and VanHorn, D. A.
LATERAL DISTRIBUTION OF VEHICULAR LOADS IN A PRESTRESSED CONCRETE BOX-BEAM BRIDGE - BERWICK BRIDGE, Fritz Engineering Laboratory Report 315.4, October, 1967.

13. Schaffer, T. and VanHorn, D. A.
STRUCTURAL RESPONSE OF A 45° SKEW PRESTRESSED CONCRETE BOX-GIRDER HIGHWAY BRIDGE SUBJECTED TO VEHICULAR LOADING - BROOKVILLE BRIDGE, Fritz Engineering Laboratory Report 315.5, October, 1967.

14. Guilford, A. A. and VanHorn, D. A.
LATERAL DISTRIBUTION OF VEHICULAR LOADS IN A PRESTRESSED CONCRETE BOX-BEAM BRIDGE - WHITE HAVEN BRIDGE, Fritz Engineering Laboratory Report 315.7, August, 1968.

15. Lin, C. S. and VanHorn, D. A.
THE EFFECT OF MIDSPAN DIAPHRAGMS ON LOAD DISTRIBUTION IN A PRESTRESSED CONCRETE BOX-BEAM BRIDGE - PHILADELPHIA BRIDGE, Fritz Engineering Laboratory Report 315.6, June, 1968.

16. Aktas, Z. and VanHorn, D. A.
BIBLIOGRAPHY ON LOAD DISTRIBUTION IN BEAM-SLAB HIGHWAY BRIDGES, Fritz Engineering Laboratory Report 349.1, September, 1968.

17. Wegmuller, A. W., Cordoba, G. C., and VanHorn, D. A.
SLAB BEHAVIOR OF A PRESTRESSED CONCRETE BOX-BEAM BRIDGE - HAZLETON BRIDGE, Fritz Engineering Laboratory Report 315A.2, February, 1971.

18. Chen, C. and VanHorn, D. A.
STATIC AND DYNAMIC FLEXURAL BEHAVIOR OF A PRESTRESSED CONCRETE I-BEAM BRIDGE - BARTONSVILLE BRIDGE, Fritz Engineering Laboratory Report 349.2, January, 1971.

19. Timoshenko, S. and Goodier, J. N.
THEORY OF ELASTICITY, McGraw-Hill Book Company, New York, 1951.

20. Bouwkamp, J. G., Brown, C. B., Scheffey, C. F., and Yaghmai S.
BEHAVIOR OF A SINGLE SPAN COMPOSITE GIRDER BRIDGE, Structures and Materials Research, University of California, Berkeley, Department of Civil Engineering, Report SESM-65-5, August, 1965.